TAMPERE UNIVERSITY OF TECHNOLOGY

SAMU KUKKONEN

APPLICATION OF POWER ELECTRONICS IN HYBRID FUEL CELL POWERTRAINS

Master of Science Thesis

Examiner: Professor Teuvo Suntio
Examiner and topic approved in the Faculty of Computing and Electrical Engineering Council meeting on 4 April 2010

ABSTRACT

TAMPERE UNIVERSITY OF TECHNOLOGY
Master of Science Degree Programme in Electrical Engineering
KUKKONEN, SAMU: "Application of Power Electronics in Hybrid Fuel Cell Powertrains"
Master of Science Thesis, 82 pages, 8 Appendix pages
October 2010
Major: Power Electronics of Electrical Drives
Examiner: Professor Teuvo Suntio
Keywords: Fuel cell, hybrid powertrain, power electronics

Growing environmental concerns have led to a huge interest in renewable energy sources. Fuel cells have the potential to be one of these sources. They are very well suited for automotive and working machine applications, where they can replace internal combustion engines.

Unfortunately, the load profiles in such applications contain a large number of high transients including regenerative braking peaks. In order to maximize the fuel cell lifetime and to enable the ability to recover braking energy, the fuel cell has to be paralleled with energy storage systems like batteries and supercapacitors or both. The resulting system is called a hybrid fuel cell powertrain.

A hybrid fuel cell powertrain can be constructed without power electronics but only in special applications. Practical hybrid powertrains require the use of power electronic converters from which DC/DC conversion is perhaps the most important.

The dynamic behaviour of every energy source associated with the powertrain has to be understood in order to design proper DC/DC converters. Especially fuel cells are low-voltage high-current devices requiring the use of high-power DC/DC converters with low input-current ripples. Various topologies have been proposed to fulfil this requirement and the requirements of energy storage systems as well. In addition to the topological issues, the control design of the converters is equally important for assuring stable powertrain operation and sufficient transient dynamics.

The results obtained from the simulations imply that a well-behaving powertrain can be realized, provided that the control loops are designed properly. The results emphasize the need for proper sizing of the powertrain components and the need for choosing correct powertrain configuration with appropriate voltage levels. It can be determined from the results, that even though a powertrain equipped with power electronic converters is more complex than a powertrain without such devices, it has very clear and strong advantages.

PREFACE

This thesis was done at VTT as a part of TopDrive-project. The project's goal has been to develop hybrid fuel cell powertrains intended especially for working machine usage.

Jari Ihonen and Timo Keränen from VTT have worked as instructors of this thesis to whom I would like to express my deepest gratitude not only for their professional impact but also for creating a pleasant working atmosphere. Professor Teuvo Suntio from TUT's Department of Electrical Energy Engineering has worked as the examiner of this thesis and, with his strong professional input, has kept me inspired throughout the writing of thesis.

I would like to thank the whole fuel cells team staff from VTT and the staff of TUT's Department of Electrical Energy Engineering especially from those moments spent around the coffee table from where numerous invaluable ideas were born. Henri Karimäki from VTT staff gets my special thanks for helping me with the reactant starvation experiment.

I would also like to thank my family and friends who have been a constant source of support.

Tampere, October 4, 2010

Samu Kukkonen

TABLE OF CONTENTS

ABBREVIATIONS AND NOTATION

C	Capacitance or double layer capacitor
C_0	Constant capacitance
C_a	Voltage constant part of the supercapacitor capacitance
C_b	The ideal battery voltage source is modeled as this capacitor
C_i	Capacitance representing part of the high frequency behaviour of a supercapacitor
C_o	A capacitance term representing the dynamic behaviour of a battery
$C_{P1,2}$	Capacitors that constitute part of the dynamic supercapacitor leakage behaviour
C_R	Voltage constant part of the supercapacitor capacitance
C_V	Voltage dependent capacitance
d	Instantaneous duty ratio
D	Steady-state duty ratio
$D_\#$	Diode number #
d/dt	Differential operator
d'	Complement of the instantaneous duty ratio
D'	Complement of the steady-state duty ratio
E_{FC}	Theoretical fuel cell open circuit voltage
e_o	Ideal battery open circuit voltage
f	Frequency
F_m	Duty ratio gain
f_s	Switching frequency
G(s)	Transfer function matrix
G_a	Other not specified elements within a loop
G_{cc}	Controller transfer function
G_{ci}	Control-to-input transfer function
G_{co}	Control-to-output transfer function
Gio-o	Forward, input-to-output, line-to-output transfer function or audio-susceptibility
G_{se}	Output-voltage sensing gain
I	Identity matrix
I_{batt}	Battery current
i_C	Instantaneous capacitor current
i_{co}	Control current
I_{FC}	Fuel cell current
I_{FCref}	Fuel cell current reference

$\mathbf{i_{in}}$	Instantaneous input current
$\mathbf{i_{inref}}$	Input current reference
$\mathbf{i_L}$	Instantaneous inductor current
$\mathbf{I_{load}}$	Load current
$\mathbf{i_{out}}$	Instantaneous output current
$\mathbf{i_{sc}}$	Supercapacitor current
K	Controller gain
$\mathbf{K_V}$	This factor describes capacitance C_V dependence on voltage
L	Inductance
L(s)	Loop gain
M(D)	Conversion factor
$\mathbf{M_c}$	Compensation ramp
n	Turns ratio
$\mathbf{P_{out}}$	Output power
$\mathbf{q_x}$	Feedback or feedforward gain
R	Resistance
$\mathbf{R_a}$	A resistance representing the dynamical behaviour of a fuel cell
$\mathbf{R_{bypass}}$	A bypass resistance
$\mathbf{r_C}$	Equivalent capacitor series resistance
$\mathbf{R_{co}}$	A resistance representing dynamic charging behaviour of a battery
$\mathbf{r_D}$	Diode parasitic resistance
$\mathbf{R_{do}}$	A resistance representing dynamic discharging behaviour of a battery
$\mathbf{R_e}$	Resistance in conductors
$\mathbf{R_i}$	Temperature variable resistance
$\mathbf{R_{ic}}$	Battery internal charging resistance
$\mathbf{R_{id}}$	Battery internal discharging resistance
$\mathbf{r_j}$	Junction resistance
$\mathbf{R_L}$	A supercapacitor's leakage resistance
$\mathbf{r_L}$	Inductor equivalent series resistance
$\mathbf{R_{leak}}$	Capacitor leakage resistance
$\mathbf{R_o}$	A resistance term representing the dynamic behaviour of a battery
$\mathbf{R_{ohmic}}$	A resistance representing the ohmic resistance of a fuel cell
$\mathbf{R_p}$	Battery leakage resistance
$\mathbf{R_{P1,2}}$	Dynamic leakage resistances
$\mathbf{R_s}$	Sensing resistance
$\mathbf{R_V}$	Supercapacitor's DC resistance

$\mathbf{s}$	Laplace operator
$\mathbf{S(s)}$	Sensitivity function
$\mathbf{T_{\#}}$	Transistor number #
$\mathbf{T_{oi\text{-}o}}$	Reverse or output-to-input transfer function
$\mathbf{T_s}$	Switching period
$\mathbf{U}$	Supercapacitor DC voltage
$\mathbf{u(s)}$	Input vector in laplace domain
$\mathbf{u(t)}$	Input vector in time domain
$\mathbf{u_{A,B,C}}$	Phase voltages
$\mathbf{u_b}$	Voltage seen from the battery terminals
$\mathbf{U_{batt}}$	Battery voltage
$\mathbf{u_C}$	Instantaneous capacitor voltage
$\mathbf{u_{co}}$	Control voltage
$\mathbf{U_D}$	Diode forward voltage
$\mathbf{U_{DCbus}}$	DC-bus voltage
$\mathbf{U_{FC}}$	Fuel cell voltage
$\mathbf{u_{in}}$	Instantaneous input voltage
$\mathbf{u_L}$	Instantaneous voltage over inductor
$\mathbf{u_{OC}}$	Open circuit battery voltage
$\mathbf{u_{oref}}$	Reference output voltage
$\mathbf{u_{out}}$	Instantaneous output voltage
$\mathbf{U_{sc}}$	Supercapacitor voltage
$\mathbf{X}$	Reactance
$\mathbf{x(t)}$	State-variable vector
$\mathbf{y(s)}$	Output vector
$\mathbf{Y_{in\text{-}o}}$	Input admittance
$\mathbf{Z_L}$	Load impedance
$\mathbf{Z_{o\text{-}c}}$	Closed-loop output impedance
$\mathbf{Zo\text{-}o}$	Open-loop output impedance
$\mathbf{\Delta i_{out}}$	Change in output current
$\mathbf{\Delta U_{act}}$	Activation voltage losses
$\mathbf{\Delta U_{ohmic}}$	Voltage drop due to membrane and electrode resistance
$\mathbf{\Delta u_{out}}$	Change in output voltage
$\mathbf{\Delta U_{trans}}$	Voltage loss due to mass transport losses
$\mathbf{\omega_p}$	Pole frequency in radians
$\mathbf{\omega_z}$	Zero frequency in radians

A hat ($\hat{x}$) over any of the symbols represents perturbed value around the corresponding steady-state value. A dot ($\dot{x}$) over any of the symbols represents derivative of the corresponding symbol.

A	Amperes
AC	Alternating current
AC/AC	A power electronic converter that converts AC to another form of AC
AC/DC	A power electronic converter that converts AC to DC
C	Celsius
DC	Direct current
DC/AC	A power electronic converter that converts DC to AC
DC/DC	A power electronic converter that converts DC to another form of DC
DC-bus	A common electrical node in hybrid powertrains
DoD	Depth of discharge
EMC	Electromagnetic compatibility
EMI	Electromagnetic interference
ESL	Equivalent series inductance
ESR	Equivalent series resistance
ESS	Energy-storage system, a device or devices capable of storing and releasing electrical energy
F	Farads
H	Henrys
Hz	Hertz
MPP	Maximum power point

OVF	Output voltage feedback
Pa	Pascals
PCMC	Peak-current-mode control
PEMFC	Proton exchange membrane fuel cell also known as PEFC, polymer electrolyte fuel cell
PID controller	Proportional-integral-derivative controller
Powertrain	A group of components that generate electrical power
PWM	Pulse width modulation
RHP	Right-hand plane
SoC	State of charge of an ESS. It gives the remaining energy left in the ESS as a percentage of the full charge
SSA	State-space averaging
V	Voltage
VFCO	Voltage-fed current output, a DC/DC converter which input and output is a voltage source.
VFVO	Voltage-fed voltage output, a DC/DC converter which input is a voltage source and output is a current sink.
VMC	Voltage mode control
VRLA	Valve regulated Lead-acid
W	Watts

1. INTRODUCTION

The worry on climate change and environmental concerns have led to a growing interest in renewable energy sources. Among these energy sources are the different types of fuel cells, of which the proton exchange membrane fuel cell (PEMFC) has been shown to be the most promising type in vehicle applications. [1] Studies have shown that the best way to utilize fuel cells in such applications is to use them in conjunction with one or more energy-storage systems (ESS) such as electrochemical batteries and supercapacitors. [2] The resulting system is known as a hybrid fuel cell powertrain. A powertrain like this has many advantages over a plain fuel cell power source but it can also be dynamically quite complex.

A hybrid powertrain can be constructed in such a way that a fuel cell and an ESS are connected passively, i.e. each energy source is directly connected to the same bus. This means that the internal impedances of the different energy sources will dictate the current distribution within the system. This is the simplest way to construct a hybrid fuel cell powertrain, but it has a number of disadvantages. One of them is the inability to control the current distribution, which can be overcome by using cascaded DC/DC converters in conjunction with the energy sources. The implementation of power electronic converters in the powertrain has many advantages but also disadvantages that have to be dealt with.

The purpose of this thesis is to study the construction, dynamic behaviour and utilisation of power electronic converters in hybrid fuel cell powertrains. The advantages and disadvantages of converter implementation are studied. This thesis is a continuation of the Master's thesis of Karimäki [2], which covered directly connected hybrid fuel cell powertrains.

1.1. The Structure of the Thesis

In Chapter 2, hybrid fuel cell powertrains are described. The operation of directly connected powertrains is discussed first before assessing the advantages and problems of a powertrain with converters. In Chapter 3, fuel cells, batteries and supercapacitors are described together with their dynamic behaviour. The most important power electronic converters in hybrid powertrains, their dynamic behaviour and implementation are discussed in Chapter 4. These three chapters constitute the theoretical part of the thesis.

Chapter 5 presents hybrid fuel cell powertrain simulation models and the results obtained from them. In Chapter 6, reactant starvation phenomenon is verified experimentally. Chapter 7 provides the conclusion of this thesis.

2. HYBRID FUEL CELL POWERTRAINS

In this chapter, hybrid fuel cell powertrains are described. Their operating principles are explained and the requirements they present to power electronic converters are investigated. Basic knowledge in the various energy supplying components associated with the hybrid system will be needed in order to understand the operation of the overall powertrain. These components will be discussed briefly in this chapter and in more detail in Chapter 3.

2.1. Fuel Cell and Hybrid Powertrain Component Basics

Fuel cells are devices that convert the chemical energy of hydrogen (or, in some cases, other fuels) into a direct current electrical energy. This conversion resembles the energy conversion inside electrochemical batteries. The difference is that a fuel cell is continuously supplied with new reactants externally. This ensures uninterrupted generation of electricity. Normally fuel cells are incapable of reversing the power flow. The direction of the power flow must always be from the fuel cell into a load. The exception is reversible fuel cells that are used in some special applications.

Batteries are electrochemical energy storage devices converting electricity into a chemical energy and vice versa. Thus, the power flow can be in either direction.
The energy and power densities of a battery depends on the battery type and chemistry. Both densities cannot be maximized at the same time. Therefore, a compromise between these densities must be made depending on the application. [3]

Supercapacitors are devices that store electricity inside an electric field. The operation of a supercapacitor differs from a conventional capacitor in the respect of ion transfer, which gives the supercapacitor a much higher capacity than that of a conventional capacitor. Even so, the energy density of a supercapacitor cannot compete that of batteries but their power density is much higher. [3] By using supercapacitors in conjunction with batteries in a hybrid fuel cell powertrain, the power handling capability of the powertrain can be increased. The supercapacitor has the ability to damp transients because of its low internal impedance.

2.2. Structures and Working Principles of Hybrid Powertrains

Using a plain fuel cell power source in vehicle applications compared to a hybrid fuel cell powertrain has a number of drawbacks. Such as: i) the fuel cell would have to be sized by the peak power demand of the load, which makes the fuel cell large and very

expensive; ii) the fuel cell's lifetime and efficiency would be compromised because of the varying power demand of the load; and iii) a great deal of energy would be lost because braking energy cannot be recovered and stored for future usage. These major drawbacks can be overcome by constructing a hybrid powertrain, i.e. using a fuel cell in conjunction with ESS, which can be batteries, supercapacitors or both. In such a powertrain, the fuel cell itself can be made smaller (i.e. cheaper) by sizing it by the average power demand of the load. Its lifetime can be maximized by operating it at an optimum operating point (fuel cell platinum catalyst deterioration can be minimized by keeping individual cells at low potential (<0.8 V) [4]) and by the load power transient suppression provided by the ESS. This means that the ESS has to handle the transient power and has to be able to store the recovered energy during regenerative braking. [5, 6]

To understand the operation of a hybrid fuel cell powertrain, one should first consider a directly connected system. Such a system is presented in Figure 2.1.

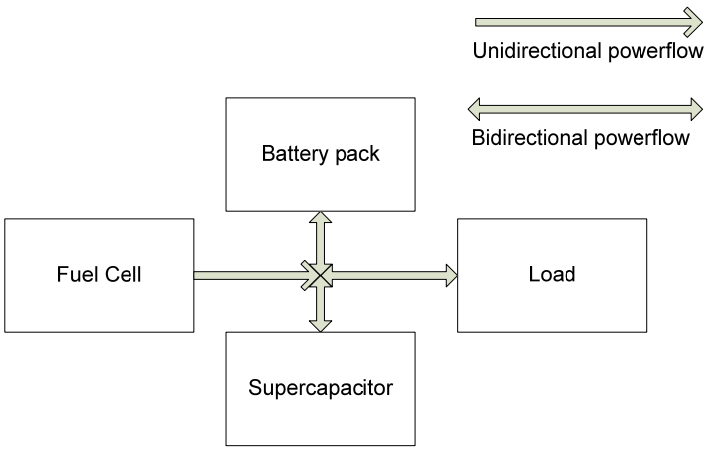

Figure 2.1. *Directly connected three-way hybrid fuel cell powertrain*

The system in Figure 2.1 is known as a three-way hybrid fuel cell powertrain because it has a fuel cell and two ESS. If a hybrid fuel cell powertrain has only one ESS, it is known as a two-way hybrid fuel cell powertrain. [2]

Now let us consider Figure 2.1. The system operates as follows: Because the components are connected directly to the same bus, they operate at the same voltage level, which means that the internal impedances of the various components dictate the current distribution within the system. The supercapacitor has the lowest internal impedance but discharges rapidly. Thus, the supercapacitor can handle the high frequency power transients. The battery has higher internal impedance than the supercapacitor but can sustain high currents for longer periods of time. This means that the battery will take care of low frequency power transients. The fuel cell has the highest internal impedance. Thus, the fuel cell supplies the constant power and charges the battery and the supercapacitor during the low load conditions.

According to [5], to increase fuel cell output power from 10% to 90% can take up to 2 seconds. In addition to this, varying power demand decreases fuel cell lifetime.

A hybrid fuel cell powertrain can tolerate power transients much better than a plain fuel cell system. This is accomplished by using ESS, which improves the dynamic behaviour of the overall system and attenuates fuel cell power transients, increasing its lifetime.

Karimäki [2] has experimentally measured the current distribution in a directly connected three-way hybrid fuel cell powertrain (Figure 2.1.) in his Master's Thesis. Figure 2.2 shows the results when the initial state of charge (SoC) of the battery was 0.7. The figure is presented at this point to demonstrate the current distribution in the directly connected hybrid fuel cell powertrain.

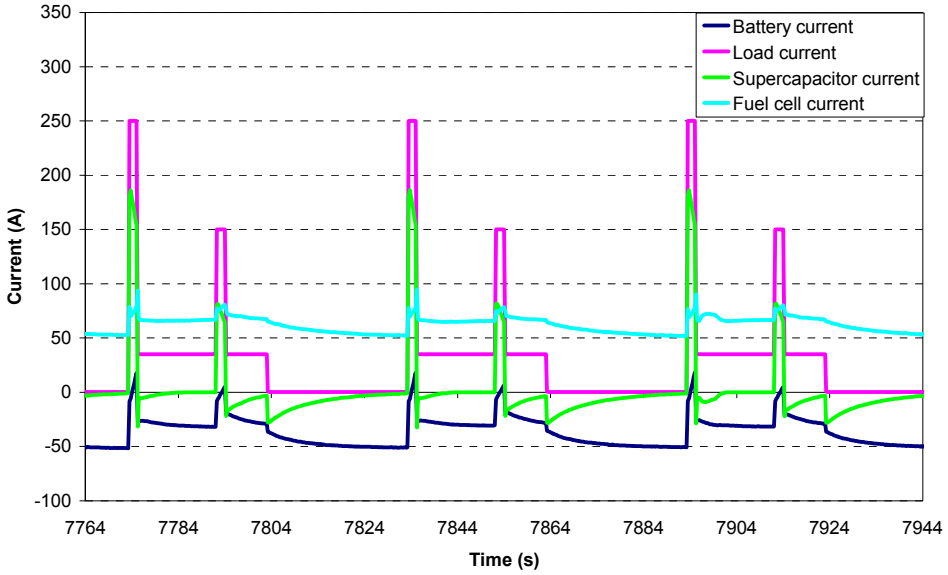

Figure 2.2. *Current distribution in a directly connected three-way hybrid fuel cell powertrain* [2]

According to Figure 2.2, the fuel cell power output is quite constant. The battery and the supercapacitor respond to the power transients. It can be seen that the battery is charged most of the time and the supercapacitor handles load transients almost on its own. The supercapacitor provides very good suppression of the power transients. A hybrid powertrain without a supercapacitor would ultimately lead to a more varying fuel cell output current and decrease in its lifetime. [2]

The problem with the directly connected hybrid powertrain is clearly the fact that the current distribution cannot be controlled and that each component has to operate at the same voltage level. The latter condition can lead to unoptimal component sizing and designs. It also means that the SoC of a supercapacitor cannot be used fully, because the SoC of a supercapacitor is a function of its voltage. The inability to control the current distribution leads to the inability to control the output current of the fuel cell and the charging/discharging processes of the battery and the supercapacitor.

To get rid some of these disadvantages, power electronic converters must be implemented into the hybrid powertrain. Figure 2.3 introduces a system which is the same as in Figure 2.1 but with cascaded converters added. The structure in Figure 2.3 is

known as DC-bus structure, where each converter is an individual converter connected to the same DC-bus.

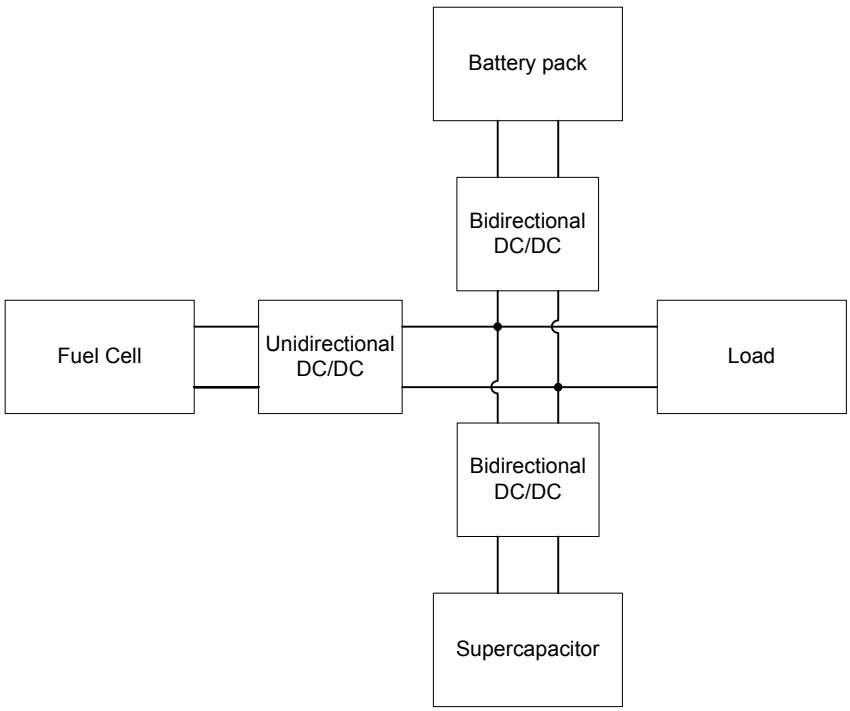

Figure 2.3. *A general depiction of a three-way hybrid fuel cell powertrain with cascaded converters*

Figure 2.3 shows a general three-way hybrid fuel cell powertrain with cascaded power electronic converters. Every energy source or just some of them can be provided with a cascaded converter. There can be a maximum number of three converters in a three-way hybrid powertrain. Between the load and the DC-bus, there may be additional power electronic converters, but we are not interested in them at this point.
The possible converter arrangements for three-way hybrid fuel cell powertrain are listed in Table 1.1.

Table 1.1. *Converter arrangements in three-way hybrid fuel cell powertrain*

Converter configuration number	Fuel cell DC/DC	Battery DC/DC	Supercapacitor DC/DC	Presented in
1				Figure 2.1.
2		x		
3		x	x	
4			x	
5	x			
6	x	x		
7	x	x	x	Figure 2.3.
8	x		x	

The fact is that in vehicle applications power levels are high, which ultimately leads to a high DC-bus voltage requirement such as 650 V in order to keep current levels reasonable. In cases with directly connected powertrains, a high DC-bus voltage creates difficulties in the fuel cell, battery and supercapacitor construction because a high number of individual cells are required to be connected in series. Cascaded DC/DC converters mitigate this problem as the energy source voltages can be set lower than the DC-bus voltage. However, the voltages must not be too low in order to keep converter current ratings realistic.

The three-way hybrid fuel cell powertrain where every energy source is provided with a cascaded DC/DC converter (converter arrangement number 7) is very versatile because the current of every energy source is controllable. However, there are a number of problems, such as:

i) A high number of DC/DC converters may have a noticeable effect on the total powertrain efficiency (single DC/DC converter has an efficiency of around 80 - 95% depending on the operating point and topology used [7]).
ii) There may be controlling difficulties in distributing the load current between the three converters and controlling the DC-bus voltage at the same time.
iii) The fact that there are no directly connected components in the DC-bus may be a problem in terms of controlling the DC-bus voltage. This problem can be mitigated by connecting a battery or supercapacitor directly to the DC-bus.
iv) The system is rather complex and may not be commercially feasible.

The advantage of a directly connected three-way hybrid fuel cell powertrain over a directly connected two-way powertrain is that the supercapacitor has a very good transient suppression capability. By using DC/DC converters, the fuel cell output current can be controlled, its output current rate of change can be limited and it can be protected from reverse powerflow. It follows, that there may not be the need for the supercapacitor if the battery can handle the varying power demand alone. This is especially true with the Li-ion type batteries because they tolerate power transients much better than the Lead-acid batteries. [8, 9] However, regenerative braking may pose difficulties, when the battery is full. Omitting the supercapacitor and providing the fuel cell and the battery with a cascaded DC/DC converter, we get the two-way powertrain arrangement shown in Figure 2.4.

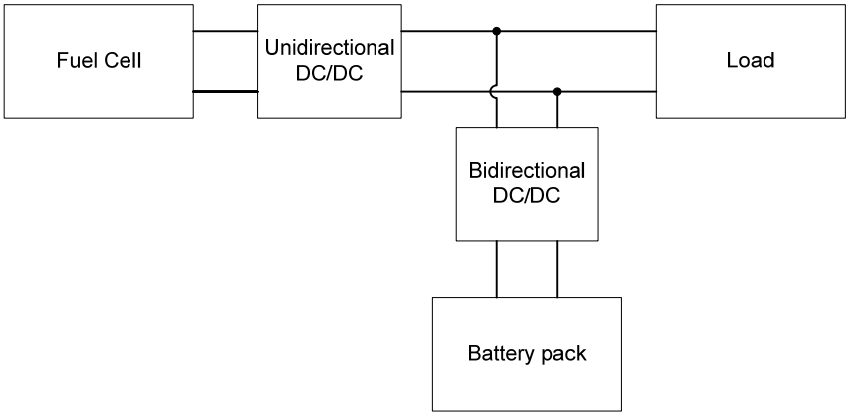

Figure 2.4. *Two-way hybrid fuel cell powertrain*

The powertrain presented in Figure 2.4 is simpler than the three-way hybrid powertrain. The reduced amount of DC/DC converters has a positive effect on the total powertrain efficiency. The converters are also more easily controlled because the load power is divided only between the two converters. This simplicity should also decrease the cost and size of the overall powertrain. However, this powertrain arrangement requires the battery to handle load transients fully if the fuel cell is operated at constant power. For certain battery types this may be a problem. For example, Lead-acid batteries do not tolerate current transients very well. [9] They may require additional filtering, which can be provided by the usage of supercapacitors. The supercapacitor may be connected to the DC-bus with its own DC/DC converter as was done in Figure 2.3, or it may be connected in parallel with the battery as is done in Figure 2.5. In addition to providing transient suppression, the supercapacitor increases the peak-power capability of the ESS. This enables a lower peak-power requirement for the battery, enabling higher energy density battery designs. Moreover, the supercapacitor has very high energy efficiency. This can increase the total charge-discharge efficiency of the parallel battery-supercapacitor connection especially if the battery has low energy efficiency.

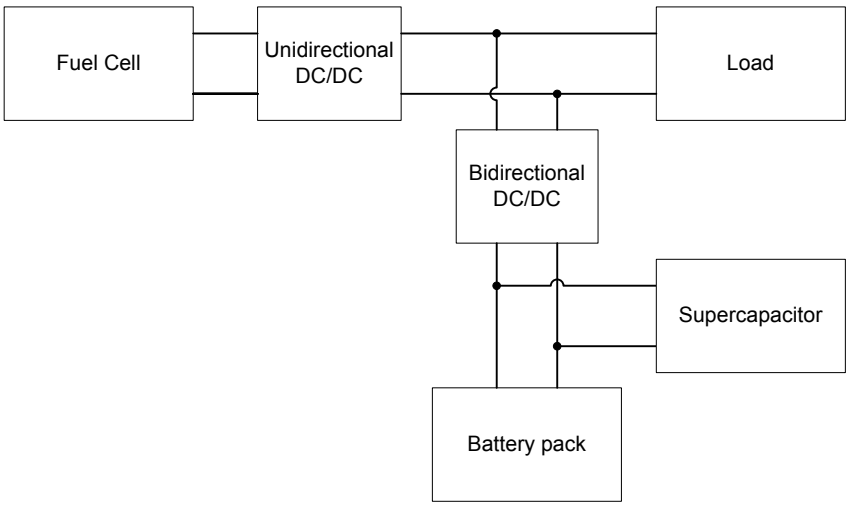

Figure 2.5. *Three-way hybrid fuel cell powertrain*

In Figure 2.5, the battery and the supercapacitor are connected in parallel and they use a single DC/DC converter for DC-bus connection. The supercapacitor provides transient suppression and makes the battery current more constant. The problem with this arrangement is that the SoC of the supercapacitor is not used fully as it is voltage dependent. The powertrains presented in Figures 2.4 and 2.5 are simulated in this thesis.

2.3. Sizing of the Hybrid Powertrain

The reliable operation of a hybrid fuel cell powertrain depends on the correct sizing of the fuel cell and the ESS. The basic principle is that the fuel cell should provide the average power and the ESS should provide the transient power. Therefore, correct energy source sizing depends heavily on the application. For example, the load profile of a forklift is very different from that of a passenger car. On the other hand, the load profile of a car towing a caravan is different than that of a normal car, etc. The load profile determines the average and transient power requirement, i.e. the power handling capability of the fuel cell and the ESS. The characteristics of the load must be, therefore, well known before the correct component sizing can be determined.

In [5], the powertrain sizing of a hybrid fuel cell vehicle is investigated. The goal was to create a hybrid system that minimizes the hydrogen consumption under vehicle driveability constraints. The constraints were: i) gradeability which corresponds to the capability of sustaining 110 km/h on a 5 % slope; and ii) a 0 – 100 km/h acceleration time, which is very important from the consumer point of view in making the fuel cell vehicle attractive. Of these two constraints, the first leads to an average power requirement that specifies the size of the fuel cell, and the second constraint leads to the requirement of the ESS power handling capability. Simulating different driving profiles, the sizing requirements of the different components were plotted as graphs, from which the sufficient sizing of components can be easily determined under different driving conditions.

It is clear that the above findings cannot be directly adapted to the hybrid fuel cell powertrain of a forklift, in which we are interested in this thesis. However, they offer a method in defining the constraints which will eventually define the correct sizing of the hybrid system.

2.4. Dynamic Behaviour of the Hybrid Powertrain

Controlling a directly connected hybrid fuel cell powertrain is relatively simple because the only controlled device is the fuel cell itself. Introducing power electronic converters into the system gives rise to the need to control the electric current in various points in the system. Depending on the load profile, a suitable power management strategy has to be determined to control the converters. The power controller has to decide the correct operating points for the fuel cell and ESS converters. In case of lost control, the powertrain must fail safely.

A directly connected powertrain is inadequate in terms of the ability to control the current distribution. There are many reasons why the current distribution is needed to be controllable. The main reason is to optimize hydrogen consumption while keeping the SoC of the ESS devices within reasonable bounds. [10] Thus, the DC/DC converters will perform two functions in the system: to match the different voltage levels and to control the current distribution within the system. The problem, however, is how to control the converters.

There are basically two types of load profiles: predictable and somewhat or totally unpredictable. [10] Implementing a power management strategy for the predictable loads is naturally more easily optimized compared to the unpredictable load profiles. There are many papers covering power management strategies, such as [10, 11]. According to them, the different power management strategies accomplish two things: regulate the power output of the fuel cell and the ESS. It follows from the slow dynamics of the fuel cell that the required unidirectional converter does not need to be fast, which should make an easier control loop design for the converter. Moreover, the fuel cell current rate of change must be limited in order to maximize fuel cell lifetime. This is easily accomplished with a cascaded DC/DC converter. On the other hand, if the supercapacitor is behind its own cascaded converter, the converter needs to be very fast to maintain the transient suppression capability of the supercapacitor. The converter also needs to be bidirectional with adequate step-up/step-down ratios because the supercapacitor voltage varies widely with the SoC as well as to have a high peak power capability.

A predictable load could be a major asset in controlling the converter associated with the supercapacitor. If the converter cannot be made fast enough, one could predict the changes in the load and the operating mode of the converter could be changed before the actual transient occurs. This would improve the transient response of the converter. The problem is, however, that the magnitude of the load change cannot be accurately determined. For example, if a forklift is raising a container, the beginning of the raising process is easy to determine, but the actual required power is difficult to estimate because the weight of the container is not known.

3. FUEL CELLS, BATTERIES AND SUPERCAPACITORS

In this chapter, the operating principles of fuel cells, batteries and supercapacitors are explained. Their dynamic behaviour is described and the effect of converter ripples on them is investigated.

3.1. Fuel Cells

Fuel cells are devices which convert the chemical energy of hydrogen (or, in some cases, other fuels) into direct current electricity without an actual burning process. This conversion resembles the conversion inside an electrochemical battery. The difference is that a fuel cell is continuously supplied with new reactants externally. This ensures uninterrupted generation of electricity. Fuel cells also differ from secondary batteries in the respect of that they are not able to reverse the power flow (except in some special applications).

In this thesis, we will limit the discussion only to hydrogen supplied fuel cells. The basic reaction inside a fuel cell is as follows:

$$H_2 + \frac{1}{2}O_2 \rightarrow H_2O \tag{3.1}$$

Hydrogen (H_2) is supplied to the anode of the fuel cell and oxygen (O_2) to the cathode. Between the anode and cathode there is an electrolyte which obstructs the mixing of the reactants but provides route for ions. The hydrogen oxidizes, releasing electrons which flow from anode to cathode through an external circuit producing electrical power. The nuclei of hydrogen flow through the electrolyte into the cathode, where the oxygen is reduced to water (H_2O).

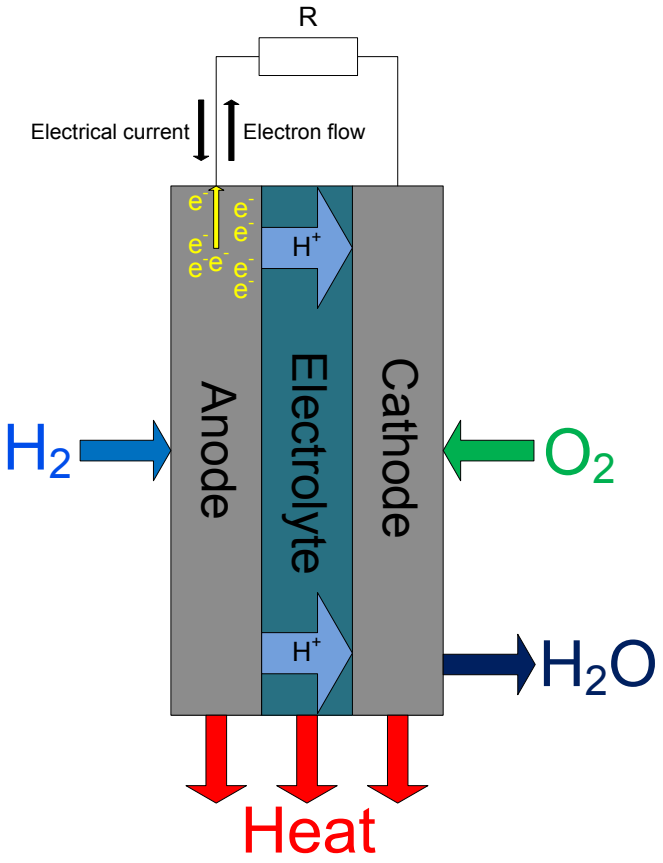

Figure 3.1. *A fuel cell*

There are many different types of fuel cells. They are classified according to the electrolyte name, and their characteristics differ from each other. The main fuel cell types are: polymer exchange membrane fuel cell (PEMFC), alkaline fuel cell (AFC), phosphoric acid fuel cell (PAFC), molten carbonate fuel cell (MCFC) and solid oxide fuel cell (SOFC). The polymer exchange membrane fuel cell has been shown to have many properties required in vehicle applications. [1] As a consequence, further discussions are limited to PEMFC.

PEMFC is a low temperature fuel cell. Its operating temperature is around 60-80 °C, which means short start-up times when compared to higher temperature fuel cell types. The low operating temperature requires a platinum catalyst on the electrodes in order for the reactions to be fast enough. Platinum is an expensive material (approximate average of 55 $/g from August 2009 to August 2010 according to [12]) and forms a large proportion of the whole fuel cell stack cost, though advances in technology have reduced the required amount of platinum needed in a PEMFC. According to [13], the amount of platinum required in a state of the art PEMFC is less than 0.2 g/kW, which at current prices means less than 11 $/kW.

PEMFC is built in such a way that in the middle of the fuel cell is the polymer exchange membrane electrolyte and on the both sides of it are the electrodes, as depicted in Figure 3.1. On the sides of this membrane electrolyte assembly, there are porous gas diffusion layers on the top of the electrodes. Their function is to allow the

reactants to diffuse onto the electrodes. Next to the gas diffusion layers are bipolar plates that provide flow channels for the reactants and cooling liquid. Bipolar plates also serve as the conductors along which electricity is transmitted into the external circuit.

The electrolyte is crucial to the operation of fuel cells. It must provide good ion conductivity for hydrogen ions and it must hinder the mixing of reactants. It must also be durable to last the whole fuel cell lifetime.

Fuel cell lifetime has improved significantly during the recent years. For example, Ballard offers a 12 000-hour or 5-year warranty for their HD6-type fuel cell. [14] There are many factors that affect the lifetime. First of all, the fuel cell should be operated at constant load because the changes in cell voltages will accelerate platinum catalyst deterioration, which permanently decreases the maximum output power. Operational temperature and water balance is also affected by varying load conditions. This can cause tension in the electrolyte membrane and increase the size of the platinum particles, effectively reducing the total area of the catalyst. [2] Also, the fuel cell start-up and shutdown procedures, if not performed correctly, can lead to carbon corrosion and thus affect the lifetime. [15] These are some of the issues that have an effect on the lifetime. Proper control of power electronic converters and devices associated in the operation of the fuel cell (balance of plant (BoP)) can mitigate these problems.

3.1.1. Balance of Plant

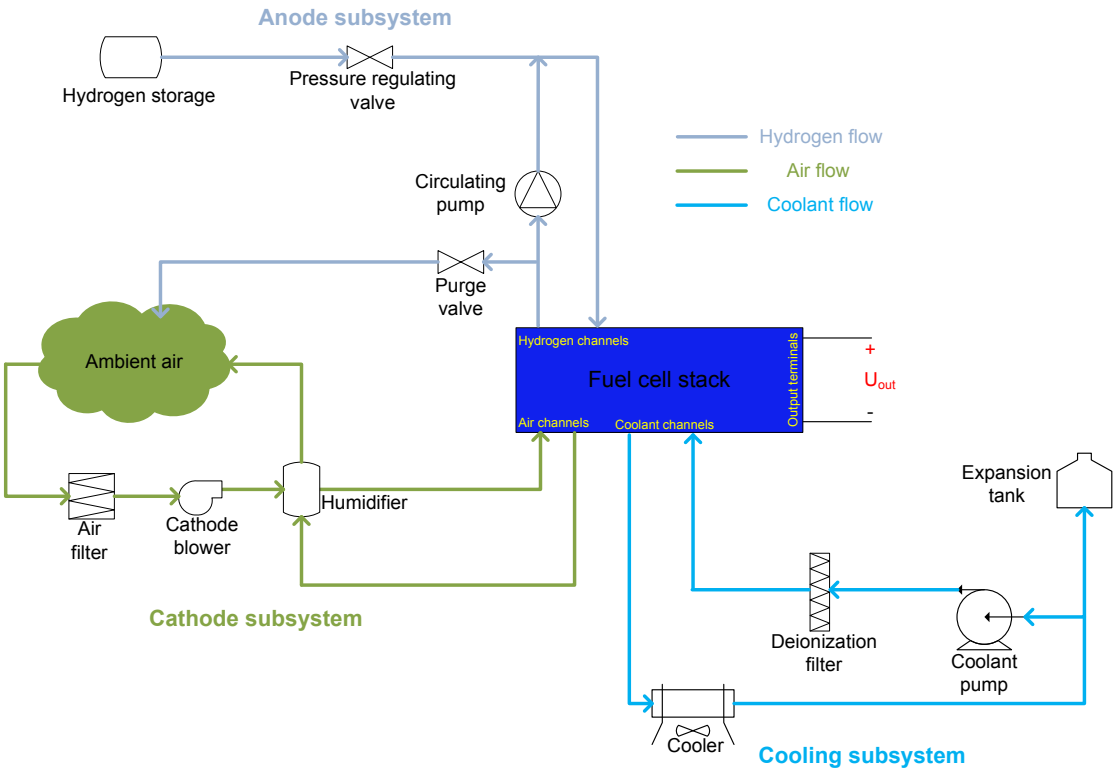

Figure 3.5. Balance of plant

Fuel cell stacks cannot operate on their own. They require additional devices in order to work. These devices provide continuous supply of reactants, coolant flows and maintain the correct water balance inside the fuel cell. These devices are called the balance of plant (BoP) components. Figure 3.5 depicts the main BoP components associated with PEMFC. The various measurements required in a practical system have been omitted from Figure 3.5 for simplicity. The BoP components are controlled as a function of the fuel cell stack output current. This is accomplished by using a control system which is fed with measurements signals from different points of the fuel cell system.

The BoP has an effect on the overall efficiency of the fuel cell system. This is because BoP requires electrical power, the amount of which is dependent on the fuel cell stack output current. For example, the cathode blower is an integral component in controlling fuel cells and can consume hundreds of watts or even kilowatts depending on the size of the fuel cell stack (5 – 15% of the PEMFC power). Most often, the BoP operates at a different voltage level than that of the fuel cell output voltage. In addition, some BoP devices may require DC while others require AC. DC/DC and DC/AC converters can fill these needs.

The BoP electrical power can be supplied from the DC-bus. This most often requires a step-down DC/DC converter to lower the voltage. The DC/DC converter needs to be powerful enough to provide the required power but it must not disturb the delicate measurements and the control system of the BoP. Attention must be paid to the electromagnetic interference (EMI) generated by the converter. The same applies with any converter in the powertrain.

3.1.2. Dynamic Behaviour of PEMFC

Designing power electronic converters for fuel cell applications requires knowledge in the dynamic behaviour of the fuel cells. Fuel cells are voltage sources, but their voltage is strongly dependent on the output current because of their large internal impedance.

The output voltage of a fuel cell depends on many things. First of all, the theoretical open-circuit voltage can be calculated from Gibbs free energy. For a single PEMFC it is in the order of 1.23 V. A fuel cell is therefore a low-voltage, high-current device. Consequently, practical fuel cells are constructed by connecting a multiple number of single fuel cells in series into a fuel cell stack to increase the voltage. [16]

The 1.23 V is the theoretical ideal open-circuit voltage in standard conditions (25 °C and 101.325 kPa). When a load is applied, the voltage starts to drop rapidly as a function of current. This is because of the various losses within the fuel cell. Such as: activation losses, leakage current losses, ohmic losses and mass transport losses. Activation losses are caused by the slow kinetics of the reactants on the electrodes. For the reactions to be fast enough, a certain amount of voltage is required for deviation from the equilibrium. This causes voltage losses at low-current densities. The voltage first falls sharply at low currents and then slightly at higher currents. Leakage current losses, on the other hand, are losses where hydrogen diffuses directly into the cathode through the electrolyte and, therefore, does not take part in generating electricity. This

loss mechanism can be used in determining the fuel cell condition but does not contribute to any voltage drops.

Ohmic losses are caused by the finite conductivity of the fuel cell structure and can be modeled by a simple equivalent series resistor. Ohmic losses are therefore linearly dependent on the fuel cell current. On the other hand, mass transport losses are caused by the reactant pressure reduction at the active area on the electrodes. Reactant concentration on the electrodes decreases when the output current increases. As a consequence, the mass transport losses dominate at high currents. [16]

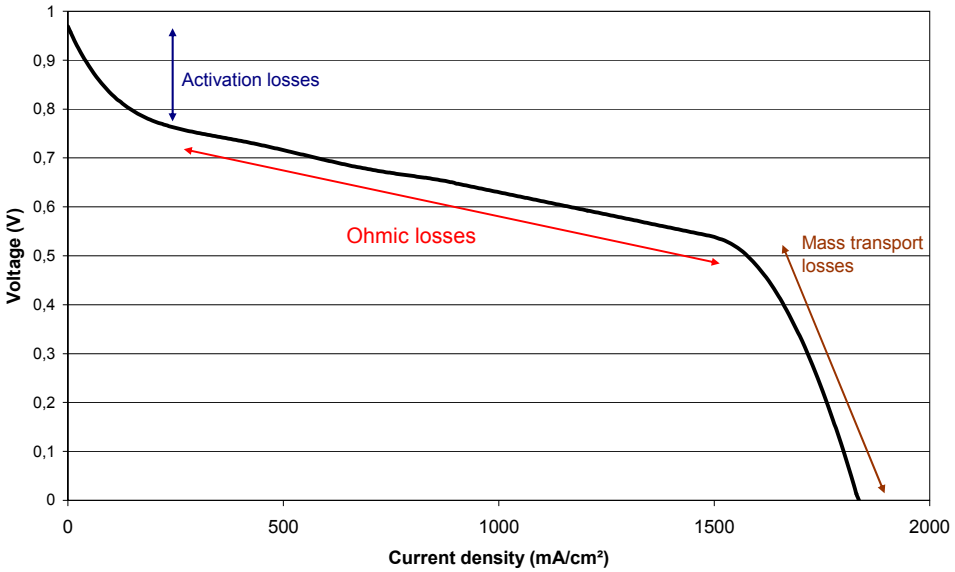

Figure 3.2. *Fuel cell polarization curve* [2]

The current-voltage characteristics of a single PEMFC are shown in Figure 3.2. The figure is drawn to demonstrate the various loss mechanisms and is not based on any measurement data. It can be clearly seen from the figure that the output voltage of a fuel cell is heavily dependent on the current.

Multiplying voltage with current density, a power density curve can be drawn. Such a curve is plotted in Figure 3.3 as a function of current density.

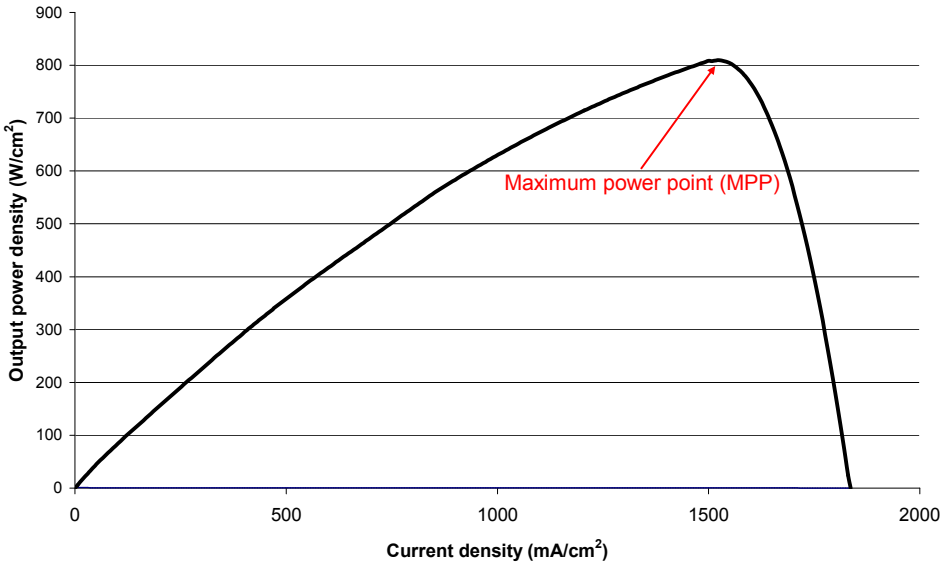

Figure 3.3. *Fuel Cell power density curve*

As can be seen from Figure 3.3, a fuel cell has a maximum power point (MPP) at which it produces the maximum available power. Comparing Figures 3.2 and 3.3, one can determine that a fuel cell produces the maximum available power when the voltage is approximately half the open-circuit voltage. As a consequence, the voltage of a fuel cell varies significantly. Power electronic converters must be able to handle this voltage change.

The efficiency of a fuel cell is dependent on its output current. Figure 3.4 presents the efficiency of a fuel cell stack and the combined efficiency of the fuel cell stack and BoP.

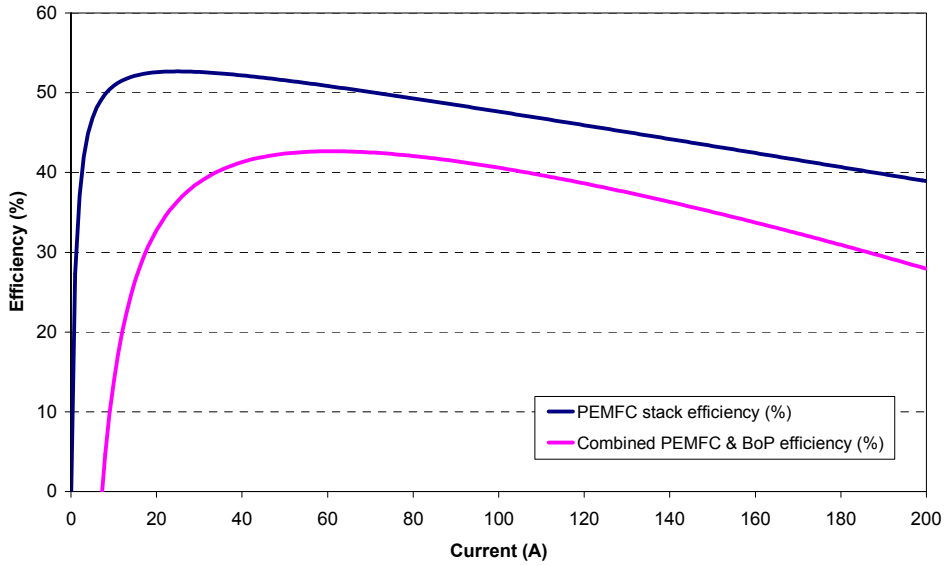

Figure 3.4*. Fuel cell efficiencies* [2]

Figure 3.4 is based on a test data measured from an 8 kW Nedstack P8 fuel cell. The fuel cell stack produces its maximum rated power at approximately 200 A. It can be determined from the figure that the fuel cell operates at its maximum efficiency at very low currents (blue line). However, the efficiency of a fuel cell should be evaluated as a combined efficiency of the BoP and the fuel cell stack (purple line). BoP itself has an efficiency that is also dependent on the output current of the fuel cell stack. The combined efficiency shifts the maximum efficiency of a fuel cell system a little bit more to the higher currents, peaking at around 43% which is typical maximum efficiency for a fuel cell system. For best commercial systems, efficiencies between 55 – 60% are reported. By inspecting the power density curve (Figure 3.3) and the efficiency curve (Figure 3.4), it can be concluded that the maximum power and maximum efficiency cannot be obtained at the same time. A proper operating point can be selected by controlling the cascaded fuel cell DC/DC converter.

In addition to having an effect on the efficiency of a fuel cell stack, the BoP decreases the electrical response of a fuel cell. The reactions inside a fuel cell are fast and can respond to rapid output current transients. However, the reactant supply responds slowly. Transients in the scale of milliseconds are not a problem because there are enough reactant gases stored near the electrodes. On the other hand, transients in the scale of tens of milliseconds are a problem if the reactant supply cannot respond quickly enough to the changed reactant demands. The BoP is, therefore, the reason for the slow dynamics of fuel cells. If a large positive electrical current step is applied at the output of a fuel cell, a phenomenon known as reactant starvation occurs. Its effect is an additional voltage drop before the reactant supply system can respond to the transient. Reactant starvation is particularly dangerous to the fuel cell lifetime and should be, therefore, avoided. A downstream converter must provide a positive ramp-rate limitation for the fuel cell output current. This resolves the reactant starvation issue but decreases the response speed of a fuel cell system even further. It should be noted that the output current of a fuel cell can be decreased as fast as is needed. Only the rapid increase in the output current causes the reactant starvation problem. [1]

3.1.3. PEMFC Impedance Spectrum

From the power electronic converter point of view, it is important to know the impedance spectrum of a fuel cell. This is important because any source interacts with a downstream converter. The interactions and fuel cell ripple attenuation capabilities can be determined from the fuel cell impedance spectrum.

A fuel cell can be modeled by using fundamental electrical components provided that the fuel cell is operated under fixed operating conditions. [17] Such a well-established model is shown in Figure 3.6.

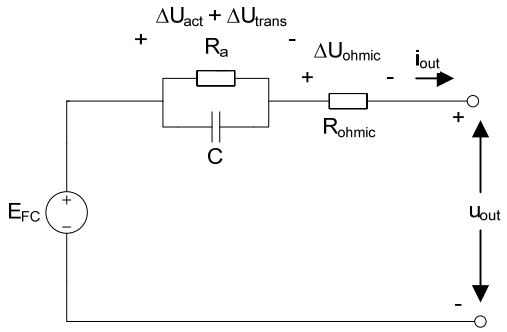

Figure 3.6. *A simplified equivalent electrical model of a fuel cell*

Unfortunately, this model does not take into account the parasitic inductances present in the conductors between a fuel cell and DC/DC converter. It is important to include these inductances in the model because they govern the fuel cell impedance at high frequencies, i.e. at the switching frequencies of a DC/DC converter. The inductance reduces the high frequency filtering capability of a fuel cell and may emphasize the EMI problems.

Parasitic inductance can be modeled by adding a series inductance to the equivalent electrical fuel cell model. This is done for example in [18]. Figure 3.7. shows this improved model.

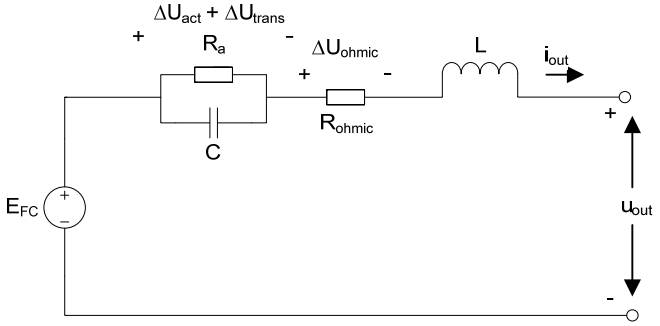

Figure 3.7. *An equivalent fuel cell electrical model including parasitic inductances*

The different terms in Figure 3.7 are as follows:

E_{FC}	= theoretical fuel cell open circuit voltage
ΔU_{act}	= activation losses of the anode and cathode (represented by R_a)
ΔU_{trans}	= mass transport loss term (represented by R_a)
ΔU_{ohmic}	= voltage drop due to the electrodes and membrane resistance (represented by R_{ohmic})
C	= double layer capacitor
L	= total parasitic inductance of conductors
i_{out}	= fuel cell output current
u_{out}	= the actual output voltage of a fuel cell

The capacitance C represents the double layer capacitor in a fuel cell structure and is the key component in the dynamical behaviour of a fuel cell. For a given operating conditions, the model parameters will stay approximately constant. When the operating point changes, the paramaters have to be adjusted to match the new operating point. [17]

A simulated fuel cell impedance spectrum is shown in Figure 3.8 using the following component values given in [17]:

R_a = 1,07 Ω
R_{ohmic} = 1,00 Ω
C = 36 mF
L = 5,0 µH

In [17], the inductance value was used as equivalent series inductance (ESL) of the capacitor to simulate the behaviour of the equivalent circuit. The same amount of inductance is now used as series inductance. It should be noted that Figure 3.8 is drawn merely to demonstrate the behaviour of a fuel cell. One should not pay attention to the actual values on the graph but the shape of the impedance curve.

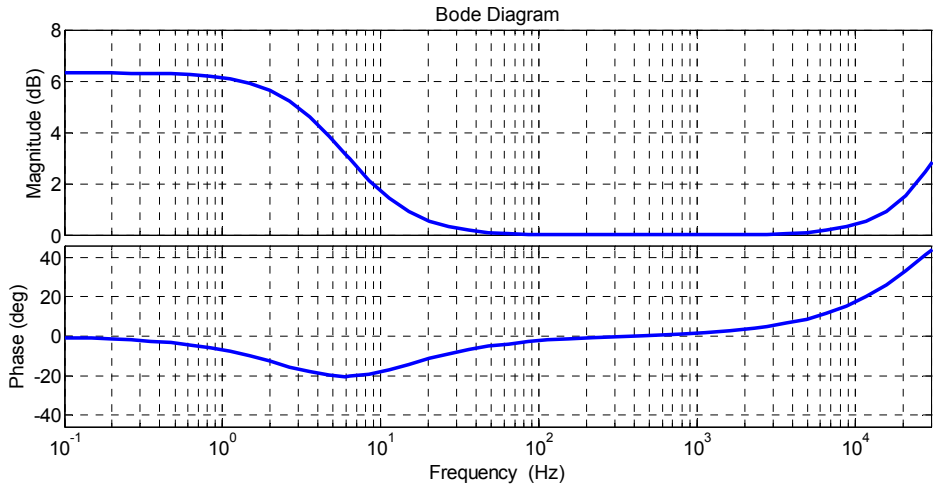

Figure 3.8. *An example fuel cell impedance spectrum*

Figure 3.8 shows clearly that the impedance of a fuel cell becomes inductive in high frequencies. This inductive behaviour is in the switching frequency region of DC/DC converters and may contribute to the EMI problems. Additional EMI filtering may be required. It is interesting to note that the double layer capacitor acts as a short circuit in high frequencies. Therefore any high frequency ripple content will flow through this capacitor and will not theoretically take part in any chemical reactions inside the fuel cell. [19]

3.1.4. Converter Ripple Effects on PEMFC

Power electronic converters perform voltage conversion through switching actions. These actions inherently produce current and voltage ripples. Power electronics designers thus need to know the limits of fuel cell ripple handling capabilities in order to design a converter producing ripples within certain limits. Unfortunately, the effects of converter ripple on fuel cell performance and lifetime are not very well understood. [20] Fortunately, a little progress has been made in the recent years. [19, 21] Two ripple types have been studied: switching frequency ripples and ripples caused by single-phase inverters. Such inverters cause DC-side current ripples having the frequency twice that of the fundamental output current frequency. Thus, the fuel cell tolerance for both low & high frequency ripples needs to be known.

In [4], the effect of potential cycling on a fuel cell performance are studied. The outcome is that the varying voltage of a fuel cell, which a varying power demand causes, increases the platinum particle size and thus decreases the performance of a fuel cell permanently. Unfortunately, these studies are conducted only at very low frequencies where the single cell voltage rate of change is only the order of 10 mV/s.

In [20], it was suggested that varying reactant conditions contribute to the lifetime of fuel cells at least in part. A dynamic model was built and the reactant conditions were simulated with frequencies between 30 Hz and 1250 Hz. This was done to assess the effects caused by single-phase inverter ripples. The preliminary results show that to ensure negligible ripple impact on the fuel cell lifetime, the ripple frequencies need to be above 120 Hz or the peak-to-peak ripple component needs to be 8% that of a DC-component or less. These results were gathered through simulations and were not verified with practical fuel cell systems.

In [19], the interactions of switching frequency ripple currents on fuel cell voltages were studied. A small signal model was developed using impedance spectroscopy. The model was verified with a practical fuel cell connected to a buck converter without filtering. The results were that the high frequency currents flow through the double layer capacitor. This suppresses the high frequency voltage ripples inside the fuel cell. The voltage ripples are therefore determined only by the ohmic resistance and parasitic inductances, as can be seen from Figure 3.7. Unfortunately, the double layer capacitor cannot attenuate low frequency ripples. Therefore the single-phase inverter type ripples will cause more severe voltage fluctuations.

The study in [19] investigated the ripple current effects on the stack voltage, but their impact on fuel cell lifetime was not studied. Theoretically, no charge carrier transfer exists at the double layer capacitor interface. This means that the high frequency ripple should have significantly lower impact on fuel cell lifetime than the low frequency ripples because the high frequency ripples flow through the double layer capacitor. However this study did not indicate how much RMS current the double layer capacitor tolerates. Strains on the capacitor and membrane were not either studied. Similar results are also obtained in [20].

In [21], an experimental system was built to assess the ripple effects on fuel cells. The experiments were made with two 600 W stacks. The first one was run on nominal steady state conditions delivering 250 A for 1000 hours and the second one on dynamic conditions delivering 250 A with 1 kHz +-10 % sinusoidal ripple current for 1000 hours. Measurements were made periodically on both stacks and finally compared at the end of the 1000 hour cycles. The results show that under steady state conditions the fuel cell voltage decayed at the rate of 56 μV/h per cell and under dynamical conditions 61,6 μV/h. In the light of these findings, it seems that the high frequency ripple has only a slight effect on the fuel cell lifetime at least during the first 1000 hour period.

These are the first results concerning ripple effects on the fuel cell lifetime. The conclusion of these findings seems to be that the high frequency ripples have little effect on the fuel cell lifetime. However, the low frequency ripples seem to have a significant effect. Fortunately, solutions have been proposed to mitigate these low frequency ripples [22, 23]. It is, however, difficult to define the actual ripple design boundaries for fuel cells. Clearly, low frequency ripples should be minimized. In [20], it was suggested that the low frequency peak-to-peak ripple component should be less than 8% of the corresponding DC-component. This could be a good starting point for design parameters. On the other hand, it seems that the high frequency ripple content does not have an appreciable effect on the fuel cell lifetime, at least during the first 1000 hours of operation. Longer experiments should be conducted in order to verify that this is valid also for the whole lifetime. There may be no reason to expect that the decay rate will increase after 1000 hours but the current 1000 hour tests are not exactly proving that the decay rate will stay constant either.

3.2. Batteries

Batteries are devices which store electrical energy as chemical energy inside the battery structure. Primary batteries can produce electricity immediately after assembly until the reactants are consumed. After that, the battery is depleted and has to be replaced. Thus, primary batteries have little use in a hybrid fuel cell powertrain.

Secondary batteries can reverse the transfer of energy, i.e. they can convert electrical energy into chemical energy. The direction of electrical current can be in either way. A secondary battery must be recharged after being discharged fully. The properties of secondary batteries as well as primary batteries depend on the battery type. For vehicle applications, there are basically four kinds of secondary battery types that can be used. They are: Lead-acid, nickel-cadmium (NiCd), nickel-metal hydride (NiMH) and lithium-ion (Li-ion). Li-ion technology has advanced a lot during the recent years. They are considered to be the best alternative for vehicle applications. [3] As a consequence, the older NiCd and NiMH types will not be discussed in this thesis. However, being one of the cheapest battery types, Lead-acid can still be considered a

good option in certain vehicular applications where size and weight is not an issue such as forklifts.

Because a single battery cell has a very low voltage, a high number of cells has to be connected in series to raise the voltage into usable level. Using a downstream DC/DC converter in conjunction with the battery, the battery voltage can be set considerably lower than the DC-bus voltage. This makes battery pack design easier.

3.2.1. Lead-Acid Battery

Lead-acid is a very old and matured battery chemistry. It provides low energy density, moderate power density, low cycle life and low energy efficiency when compared to the other battery types. Lead-acid batteries are constructed from pure lead (Pb) anode and lead oxide (PbO_2) cathode immersed in sulphuric acid (H_2SO_4) electrolyte. Lead-acid batteries are available with flooded type electrolyte or as sealed valve regulated Lead-acid (VRLA) batteries where the electrolyte is immobilised in a gel-like structure or in mat micro glass fibre structure. [24] The construction and design of flooded and VRLA batteries are very different but the chemical reactions are the same. The reaction inside a Lead-acid cell during discharging is as follows [24]:

$$Pb + PbO_2 + 2H_2SO_4 \rightarrow 2PbSO_4 + 2H_2O \tag{3.1}$$

Single Lead-acid cell has a theoretical open circuit voltage of 2.1 V. The energy and power density depends on the application because both cannot be maximized at the same time. A Lead-acid cell can achieve 35 Wh/kg energy density with 250 W/kg matched power density [24] [3] or 25 Wh/kg with 390 W/kg [3]. The cycle life of a Lead-acid battery can be as low as 50-500 cycles but higher cycle lives are achievable with special designs. The lifetime of a Lead-acid battery is decreased by repeated deep-cycles as they lead to a crystallization of the lead sulphate on the electrodes. In deep-cycling applications, a special type of lead-acid battery, namely the deep-cycle Lead-acid battery is required. [24]

3.2.2. Li-Ion Battery

Li-ion is the newest, the most expensive and heavily researched battery type. It currently provides the highest energy density and its power density and energy efficiency can be considerably higher than that of a Lead-acid. Li-ion batteries have been used in electronic products for some time. In recent years, the Li-ion battery has gained worldwide attention as a viable battery option also in electric vehicles.

There are a number of different Li-ion chemistries under research and they can be very different from each other. The reactions inside a Li-ion cell depend on the chemistry. The fundamental properties of the most important Li-ion chemistries are presented in Table 3.1 as they were in 2008 [25]:

Table 3.1. *Li-ion chemistries and their properties* [25]

Cathode chemistry	Fundamental Properties
$LiCoO_2$	- Extensively used in electronics products - High storage capacity - Adequate chemical stability - Relatively expensive
$Li(Ni_{0.85}Co_{0.1}Al_{0.05})O_2$	Characteristics are approaching that of $LiCoO_2$ chemistry with lower cost
$Li(Ni_{1/3}Co_{1/3}Mn_{1/3})O_2$	- Less expensive than $Li(Ni_{0.85}Co_{0.1}Al_{0.05})O_2$ - Two possible voltage level of which the higher is around 4.1 V - At higher voltage levels, the cell tends to degrade but has an excellent storage capacity and thus low cost-to-storage-capacity ratio - At lower voltage level, stability is adequate but capacity is substantially reduced and thus cost-to-storage-capacity ratio is higher
$LiMnO_2$	- Very stable - Lower storage capacity than with other chemistries - Lowest cost, which compensates for low capacity
$LiFePO_4$	- Lower cell voltage than with other chemistries - Very stable, safe on overcharge situations - Adequate storage capacity - Adequate cost

A Li-ion cell has a high open circuit voltage, around 3,3 – 4,1 V depending on the chemistry. The high voltage is the main reason for the high capacity of Li-ion cells when compared to other battery types. [25] In 2007, 60 - 70 Wh/kg Li-ion batteries with matched power density of 1500 – 4000 W/kg were available or 100 – 140 Wh/kg with 500 – 1300 W/kg [3]. In 2008, Saft achieved more than 3000 cycle lifetime and Kokam claimed to have achieved 3000 cycles with 80% depth of discharge (DoD) and with a calendar life of around 10 years [25].

Safety has always been a major problem in the Li-ion batteries and is extremely important in vehicular applications. Li-ion battery cells can release tremendous amounts of energy, flammable gases and toxic chemicals if overcharged. [25] Battery management system is most often used in conjunction with Li-ion batteries to prevent the hazardous conditions to materialize. It may be that the safety issue will eventually lead into the usage of the more stable and safer chemistries. A DC/DC converter can play a key role in the management system as it can provide the ability to control the battery current.

3.2.3. Lead-Acid Battery Dynamic Behaviour

In order to understand the interactions between a battery and a DC/DC converter, the battery needs to be modeled with sufficient accuracy. Unfortunately accurate dynamic battery models presented as equivalent electrical models are somewhat rare even though they provide very useful insight into the internal functioning of a battery. This may be because of the difficulty in creating a generic model which takes all factors of a battery into account. Depending on the application, various models have been proposed differing in accuracy. [26]

One common battery model is the so-called Thevenin battery model, shown in Figure 3.9, which is actually fundamentally the same as the fuel cell equivalent model presented earlier with the same problems as discussed previously. [26]

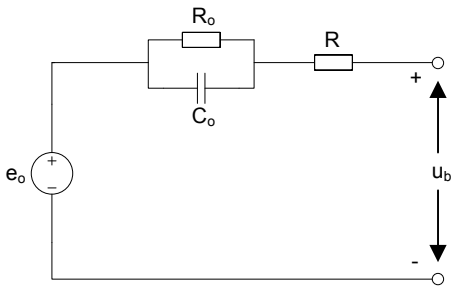

Figure 3.9. *Thevenin battery model*

The equivalent circuit parameters in Figure 3.9 are as follows: the e_o term represents the ideal battery voltage. The C_oR_o-circuit describes the double layer capacitance of the battery and the voltage drop caused by the electrode kinetics and Faradic process under load conditions. Activation losses at low load current and mass transport losses at higher current reduce the ideal internal battery voltage. The resistance R represents the resistance of the electrolyte and battery plates. [26] For improving the high-frequency accuracy, the series inductance has to be added as discussed earlier.

A more accurate way to model a battery is to use the dynamic battery model presented in Figure 3.10.

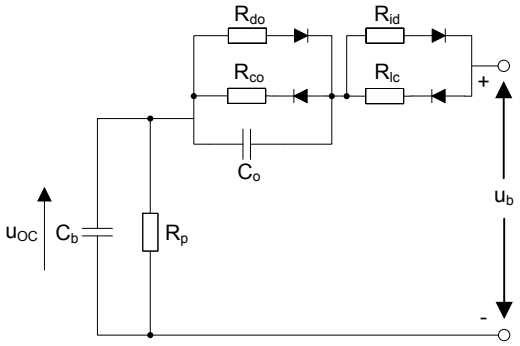

Figure 3.10. *Dynamic battery model*

This model has separate circuits for the charging and discharging processes. The ideal voltage source is modeled as a capacitor C_b. The resistance term R_p takes the self-discharge of the battery into account. The idea behind this model is to use battery measurement data to create functions for the capacitance and resistance terms. Hence, this model will behave more accurately than the previous model, but it is also a bit more complex. [26] The actual process for the derivation of the different terms will not be presented here but can be found from [26]. The model is also validated in [26], and it seems that during discharging the model performs remarkably well. The charging-mode accuracy remains unknown. Because batteries and fuel cells are both electrochemical devices, it is not, therefore, a surprise that their impedance spectrums resemble each other. [27]

3.2.4. Converter Ripple Effects on Batteries

The effect of converter ripples on batteries is a topic that has not been much researched. The key findings are that the high frequency ripples flow through the internal double layer capacitor and therefore may not cause changes in the electrode material. However, the low frequency ripples of single-phase inverters utilize the active material and therefore take part in the chemical reactions. However, research has been made on low frequency ripples mostly during the situations where the battery goes through polarity reversal, i.e. from discharging to charging during the ripple cycles. Contradictory results have been found on low frequency ripple current effects that do not include polarity changes. However, ripple currents may cause additional power losses inside a battery and therefore, increase its temperature and reduce its lifetime. [28] The actual ripple design limits cannot be stated for power electronic converters intended for battery use.

3.3. Supercapacitors

Supercapacitors are improved versions of the well known basic electrical component the capacitor. Capacitors and supercapacitors store energy in an electric field inside the capacitor structure. This process leads to a very high power density and lifetime. However, the conventional capacitor has capacitance too low to store significant amounts of energy. A supercapacitor can surpass this deficiency, keeping most of the good properties of the conventional capacitor.

The conventional capacitors are constructed by means of two overlapped flat plates with dielectric separator in between. The capacitance of a conventional capacitor is determined by the dielectric constant of the separator, the total overlapped area of the plates and the distance of the plates. The physical limitations in terms of voltage withstanding and size limit the obtainable capacitance. [29]

A way to increase the capacitance is to increase the overlapped area of the plates. This can be accomplished by increasing the physical size of the plates or by constructing a sponge-like porous electrolyte. A supercapacitor is constructed in such way that there are two overlapped electrodes, as in a conventional capacitor, but on top

of the electrodes is the porous material suspended within an electrolyte. This effectively increases the total surface area of the electrodes. Between the porous electrodes is a separator to prevent the electrodes from short circuit. The actual energy storing process happens through the action of adsorption and desorption of ions at the interface of electrolyte and electrode. The energy storing process is, therefore, electrochemical without an actual chemical reaction involved. [29, 30] A modern supercapacitor has an energy density around 4 Wh/kg and a power density of 7 kW/kg. The cycle life of a supercapacitor module can be as high as 1 million cycles, which is considerably higher than that of batteries. [31]

Supercapacitors are suited for pulse power applications because a supercapacitor charge/discharge process is very efficient. In hybrid fuel cell powertrain applications, supercapacitors can be used to suppress the rapid load variations, which are harmful for fuel cell lifetime. A supercapacitor can deliver very high short duration current pulses, around 2 kA with a 48.6 V 165 F device [31]. When paralleled with the battery, the supercapacitor peak-power capability can enable the design of a battery with a lower power density which in turn can enable higher energy densities. The high charge/discharge efficiency of the supercapacitor can be used to enhance the total system charge/discharge efficiency.

The maximum operating voltage of a single supercapacitor cell is around 3 V [32]. This means that a great number of cells must be connected in series in order to raise the voltage into usable level. Again, DC/DC converters provide freedom in this, as the actual supercapacitor voltage can be lower than the DC-bus voltage. Special means have to be used when connecting supercapacitor cells in series. Initially, when a series stack of supercapacitors is charged, the voltage distribution between the cells is a function of the cell capacitance. This is because each cell conducts the same amount of current. After the supercapacitor is allowed to hold its charge for some time, the voltage distribution becomes a function of individual cell leakage parallel resistance (leakage current). The leakage resistances determine the voltage distribution of the series stack of supercapacitors and can lead to significant voltage variations between the cells as depicted in Figure 3.9.

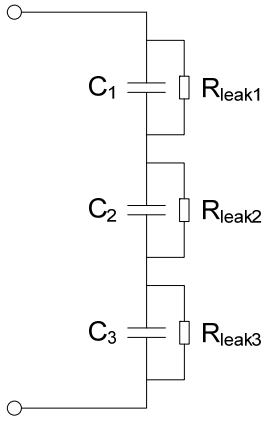

Figure 3.9. *Unbalanced series connection of supercapacitors*

One traditional technique to compensate for this voltage variation is to use bypass resistors as a balancing network as shown in Figure 3.10.

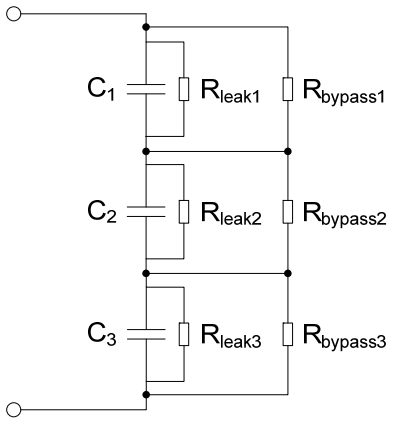

Figure 3.10. *Balanced series connection of supercapacitors*

Let us assume that a single supercapacitor cell has an average leakage current of 10 µA +/- 3 µA. A bypass resistor with 1% tolerance which passes 100 µA would increase the leakage current into 110 µA +/- 4 µA. Thus, the leakage current variation between different cells has dropped from 30% to 3.6%. If the parallel resistances are the same, a cell at a higher voltage discharges more rapidly through the parallel resistance than a cell at lower voltage. This helps to distribute the voltage evenly inside a supercapacitor series stack. The problem with this method is the increased self-discharge. A compromise has to be made between increased self-discharge rate and balancing time. Thus, the faster the balancing action, the greater is the self-discharging rate. For applications with repeated cycles, such as in hybrid powertrains, a traditional resistor balancing method may be a problem due to its limited balancing speed versus the self-discharge rate. For such applications, an active balancing can be used. [33] With an active balancing, lower self-discharge rates and faster balancing can be obtained as well as more sophisticated features such as temperature compensation can be added. [34]

3.3.1. Supercapacitor Dynamic Behaviour

A supercapacitor is a dynamic device. Its capacitance, resistance and reactance are dependent on frequency, voltage and temperature. In this subsection, some of these dependencies are discussed.

When considering the physical phenomena in the double layer interface, a supercapacitor cannot be described by a simple capacitor model. Several models have been proposed but it seems that the most comprehensive model is presented in [35]. This equivalent electric model, based on electrochemical impedance spectroscopy, is presented in Figure 3.11. Table 3.2 explains the different components as explained in [35].

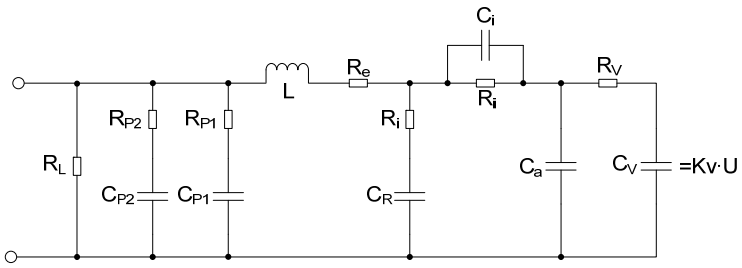

Figure 3.11. *Supercapacitor equivalent electric model* [35]

Table 3.2. *Supercapacitor equivalent electric model components*

C_V, K_V	The capacitance dependence is modeled in these terms. The supercapacitor capacitance is a function of voltage by the relation of $C = C_0 + K_V U$ which is determined experimentally. The Cv reperesents the voltage dependent capacitance and U is the cell DC-voltage.
C_R, C_a	The voltage constant parts of the supercapacitor capacitance. These terms form the C_0 part.
R_V	Constant resistance which equals dc series resistance. R_V and C_V are on placed upstream of the principal capacitance C_a and thus are active only in the low frequency range.
R_i, C_i	R_i is a temperature variable resistance and C_i is used to cancel it in the high frequency range. These terms take into account the electrolyte ionic resistance temperature dependence in the low frequency range.
R_e, L	R_e is the resistance in conductors and L is the internal supercapacitor inductance.
R_L, R_{P2}, C_{P2}, R_{P1}, C_{P1}	These terms describe the leakage current and the internal charge redistribution.

In [35], the values for the different components have been derived for Maxwell 2600 F, 2,5 V, BCAP0010 supercapacitor cell. At the cell voltage of 2.5 Volts and temperature of 20°C the parametres are as shown in Table 3.3.

Table 3.3. *Values for BCAP0010 supercapacitor cell*

Parameters	Values
U	2.5 V
L	25 nH
R_e	0.25 mΩ
$R_{i(20°C)}$	0.22 mΩ
C_i	260 F when f < 15 Hz, 3900/f when f > 15 Hz
R_V	0.5 mΩ
C_R	260 F
Ca	1700 F
K_V	195 F/V
R_L	250 Ω
C_{P1}	65 F
C_{P2}	65 F
R_{P1}	0.6 Ω
R_{P2}	4 Ω

Based on the presented model parameters and the equivalent electric model, BCAP0010 supercapacitor cell resistance, reactance and capacitance can be drawn as a function of frequency. They are presented in Figures 3.12, 3.13 and 3.14, respectively.

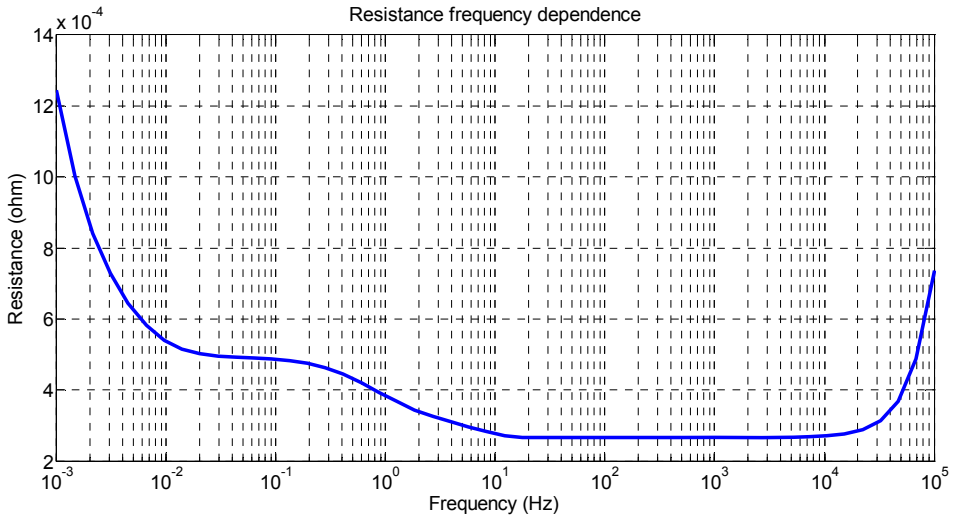

Figure 3.12. *BCAP0010 simulated internal resistance as a function of frequency*

According to Figure 3.12, between 1 and 10 mHz, the resistance consists of the leakage parallel resistance and the resistance in conductors ($R_L + R_e$). Between 10 mHz and 10 Hz, the resistance consists of the conductor resistance R_e and the ionic resistance of the electrolyte R_i. This explains the ESR variation as a function of temperature, because R_i is temperature dependent. Between 10 Hz and 1 kHz, the resistance consists mainly of the conductor resistance R_e. 1 kHz is the frequency in which supercapacitor

manufacturers specify the high frequency AC resistance. After 1 kHz, the supercapacitor's parasitic inductance starts increasing the resistance. [35]

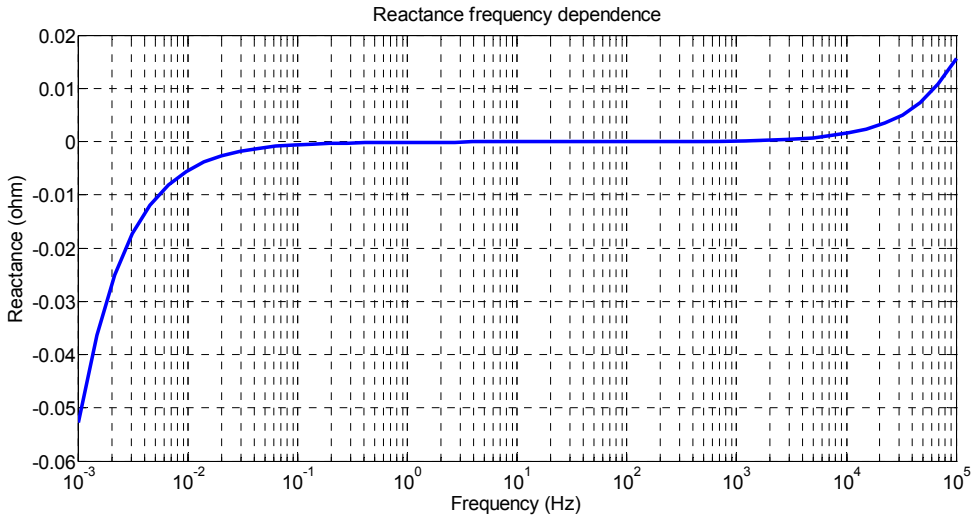

Figure 3.13. *BCAP0010 simulated internal reactance as a function of frequency*

According to Figure 3.13, the BCAP0010 has a resonance frequency around 60 Hz. Below this frequency, the supercapacitor's behaviour is capacitive and above it, inductive. When the supercapacitor inductance L and reactance X is known, the capacitance can be calculated by using (3.2). [35] Based on this equation, the capacitance frequency dependency can be presented as shown in Figure 3.14.

$$C = \frac{1}{2\pi f(2\pi f L - X)} \tag{3.2}$$

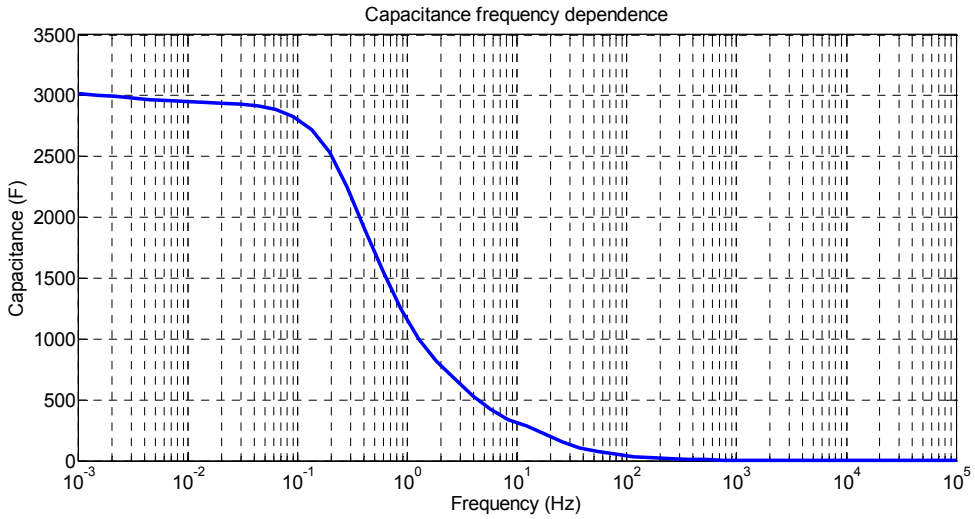

Figure 3.14. *BCAP0010 simulated capacitance as a function of frequency*

According to Figure 3.14, the capacitance is heavily frequency dependent, rapidly dropping towards zero as the frequency increases. The capacitance is at maximum in very low frequencies. This is because the ions need time to reach the electrode surface.

As frequency increases, the ions cannot follow the applied electric field, causing capacitance to drop rapidly as the frequency increases. [35] In addition, the capacitance is voltage dependent. This dependence can be modeled by the equation $C = C_0 + 2K_v U$ where C_0 is the constant capacitance and K_V is the slope of the capacitance change as a function of voltage U. The coefficient 2 is because this equation represents the differential capacitance. This yields a linearized approximation of the capacitance as a function of voltage. [35] Using the values given in Table 3.3, we get Figure 3.15 which presents simulated capacitance at 1 mHz as a function of voltage.

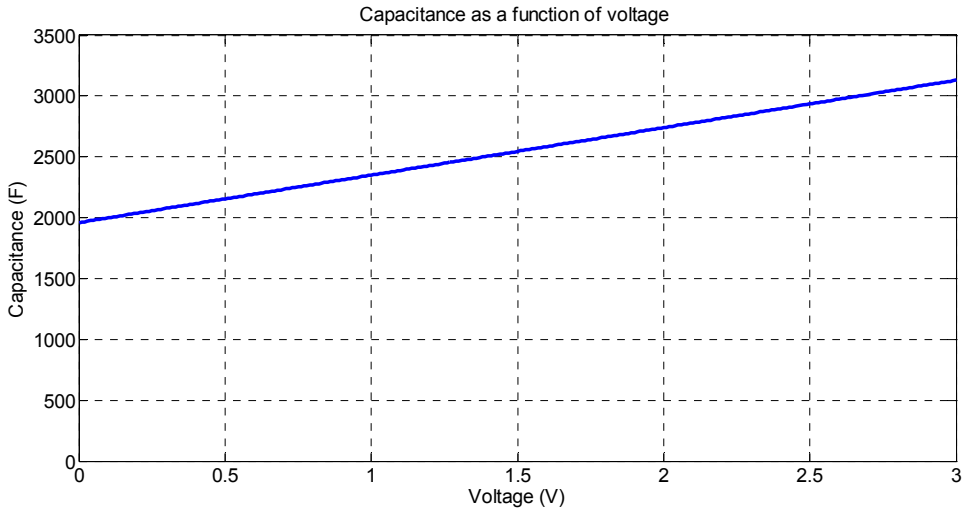

Figure 3.15. *BCAP0010 simulated capacitance as a function of voltage*

According to Figure 3.15, we can clearly see that the capacitance is quite strongly affected by the voltage across the supercapacitor. The energy stored in a capacitor is defined as $E = \frac{1}{2} C U^2$. In the case of supercapacitors, this method can yield erroneous results if the capacitance is assumed constant. For example, let us assume that the BCAP0010 cell is first charged to nominal voltage of 2.5 V and then discharged to half of the nominal voltage 1.25 V. The SoC is defined as a percentage of remaining energy divided by the full charged energy. If constant capacitance found at 2.5 V is used, this method would yield:

$$SoC = 100\% - \frac{E_{1.25V}}{E_{2.5V}} \cdot 100\% = 100\% \frac{-0.5 \cdot 2935F \cdot 2{,}5V^2 - 0.5 \cdot 2935F \cdot 1.25V^2}{0.5 \cdot 2935F \cdot 2.5V^2} \cdot 100\% = 25\%$$

Thus, the supercapacitor has released 75% of its energy and only 25% remains. Using the correct capacitance values of corresponding voltages we get:

$$SoC = 100\% - \frac{E_{1.25V}}{E_{2.5V}} \cdot 100\% = 100\% \frac{-0.5 \cdot 2935F \cdot 2.5V^2 - 0.5 \cdot 2448F \cdot 1.25V^2}{0.5 \cdot 2935F \cdot 2.5V^2} \cdot 100\% = 20.85\%$$

The correct SoC is thus 20.85%. Comparing the SoC calculation with ideal capacitance and SoC calculation with the capacitance variations included, there is almost a 20% difference between the two results. If an accurate indication of SoC is required, the capacitance variation as a function of voltage has to be taken into account.

3.3.2. Converter Ripple Effects on Supercapacitors

As discussed earlier, a supercapacitor is a device whose ESR is higher than that of a traditional capacitor. The capacitance is also frequency dependent, rapidly dropping towards zero at very low frequencies. The behaviour of a supercapacitor is inductive at the switching frequencies of DC/DC converters. These issues lead to the fact that supercapacitors may not have enough voltage ripple attenuating capability and thus can cause EMI problems. On the other hand, any ripple current flowing through a supercapacitor will cause additional power losses in the ESR, heating the supercapacitor. This is very harmful in respect to the supercapacitor lifetimes because in general, a 10 ºC increase in the temperature will drop the lifetime of a supercapacitor in half. [36] Therefore, the level of input-current ripple of the associated converter has to be carefully considered in order not to reduce the lifetime of the supercapacitor. A solution has been proposed to this problem in [36]. On the other hand, attention has to be paid on the limited voltage ripple attenuation capabilities of supercapacitors. The effect of the supercapacitor dynamics has to be analyzed in respect to these two problems.

4. POWER ELECTRONIC CONVERTERS

In this chapter, various power electronic converters will be described. Different kinds of topologies will be discussed as well as the advantages and disadvantages associated with them. Dynamic, EMC and ripple issues are also investigated.

The powertrain and individual component requirements for the converters are repeated here for convenience:

Hybrid fuel cell powertrain requirements for the converters:

- The ability to control the output current of the fuel cell
- The ability to control the SoCs of the ESS
- Matching of different voltages
- DC-bus voltage control

Component requirements:

- Ramp-rate limitation for the fuel cell output current
- Low fuel cell current ripples (at least at the low frequencies)
- Maximum allowable current & voltage of the energy sources

The power electronic converters in automotive and working machine applications should also be reliable, lightweight, compact in size and highly efficient. [7]

4.1. Power Electronics Basics

Power electronics is a field which concentrates on the conversion of electrical power from one form into another. The subfields of power electronics are DC/DC, AC/DC, DC/AC and AC/AC conversions. Power electronic converters can be used to convert DC into another form of DC or AC into DC, or another form of AC. All of these are accomplished through the usage of semiconductor devices.

Power electronic converters are not ideal devices. Their operation relies on the switching action of semiconductor devices. This process always causes power losses in the parasitic resistances and switching processes of the various components. The operating range of a converter is limited, which ultimately requires the converter to be designed for the specific application. The internal control system of a converter is delicate, and poses the converter to instability if not properly designed. The properties of a converter, as well as the properties of the devices connected to it, all have an impact on the behaviour of the converter. Therefore, the dynamic nature of a converter and its

interactions with the devices connected to it must be understood in order to design a proper converter.

In this thesis, we are most interested in DC/DC conversion, as this form of a conversion is used in different points of the hybrid powertrain. In addition to this, DC/AC conversion is also used, especially when converting the DC-bus voltage into AC for the drive motor or for certain BoP devices like a cathode blower and cooling fans.

4.1.1. DC/DC Converter Basics

A DC/DC converter is a device that is typically used to convert the input voltage into a different kind of output voltage. This is accomplished by using semiconductor switches and memory elements, i.e. inductors and capacitors. An inductor is a peculiar device because the voltage over it is defined by the current rate of change. This means that by chopping the inductor current, higher or lower voltages can be produced from the input voltage, depending on the configuration. In order to produce a steady enough output voltage, capacitors must be used at the output of a converter.

A DC/DC converter is a device that can be either voltage fed or current fed. The output of a DC/DC converter, on the other hand, is either voltage or current output type, respectively. These eventually yield four different configurations which are the basis for the dynamic analysis of a converter. They are described in Figure 4.1.

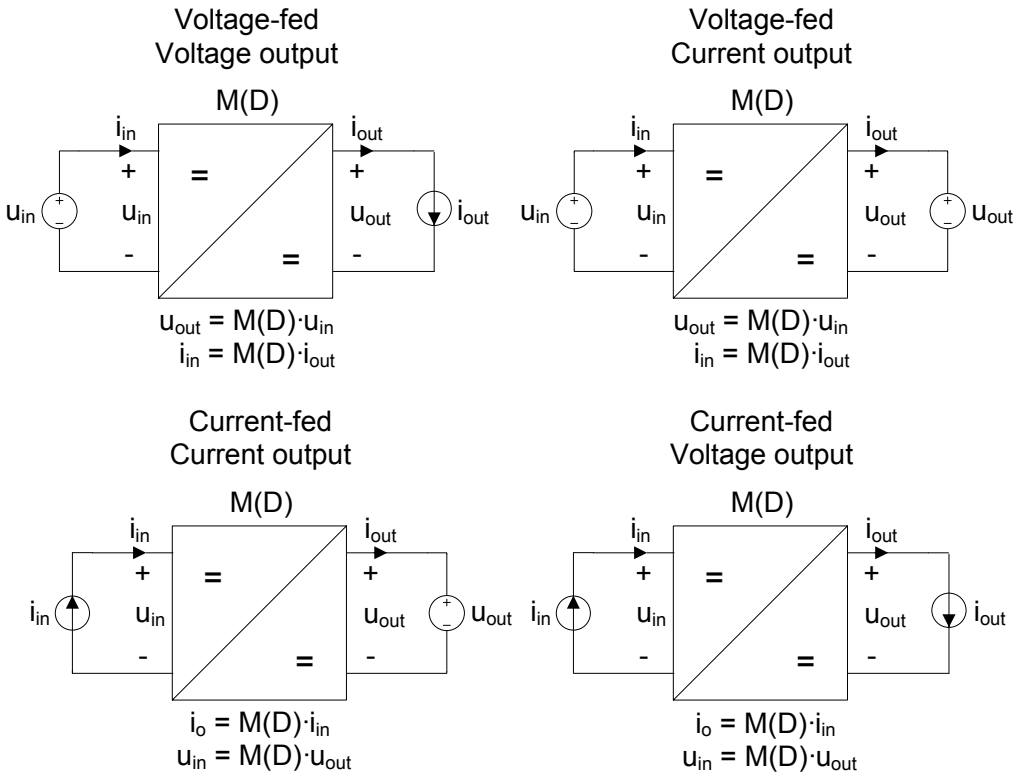

Figure 4.1. *DC/DC converter arrangements*

An ideal voltage source is a source whose voltage cannot be controlled. Only the output current of an ideal voltage source is controllable. The same applies with an ideal current source: its current cannot be controlled, but the voltage over it is controllable. The type of the source and load must be recognized, as they have an impact on the dynamics of a converter. In this thesis, we are dealing with voltage-fed voltage output (VFVO) and voltage-fed current output (VFCO) converters. In VFVO converters, input current and output voltage are controllable, and in VFCO converters, input current and output current are controllable, respectively.

If a converter is analyzed by using resistance as a load, as is often the case, a control loop design error may occur because the resistive loading has an effect on the dynamic behaviour of the converter. Purely resistive loading in practical applications is quite rare. For example, in this thesis, we are dealing with load types that are either nearly ideal voltage sources (the ESS) or the inputs of other converters which are current sinks. If resistive loading is used, the converter's dynamic behaviour should first be analyzed by the connections presented in Figure 4.1 and then the effect of resistive loading should be assessed. In Subsection 4.4, the dynamic analysis of a VFVO boost converter is described first because VFVO configuration is perhaps the most common. After that, VFCO configuration is investigated.

As a summary, the implementation of DC/DC converters presents two key issues that have to be considered: i) a suitable topology has to be selected and implemented; and ii) proper control strategies have to be developed for the converters. Any topology used can be handicapped by the inefficient design of the control loops.

4.2. Basic DC/DC Converter Topologies

In this subsection, the basic DC/DC converter topologies are described. They are known as buck, boost and buck-boost converters and are the simplest practical circuits that can perform step-down (buck), step-up (boost) and step-down/step-up (buck-boost) conversions. Figure 4.2 presents these converters with corresponding ideal conversion ratio dependences. Parasitic elements have been omitted for simplicity.

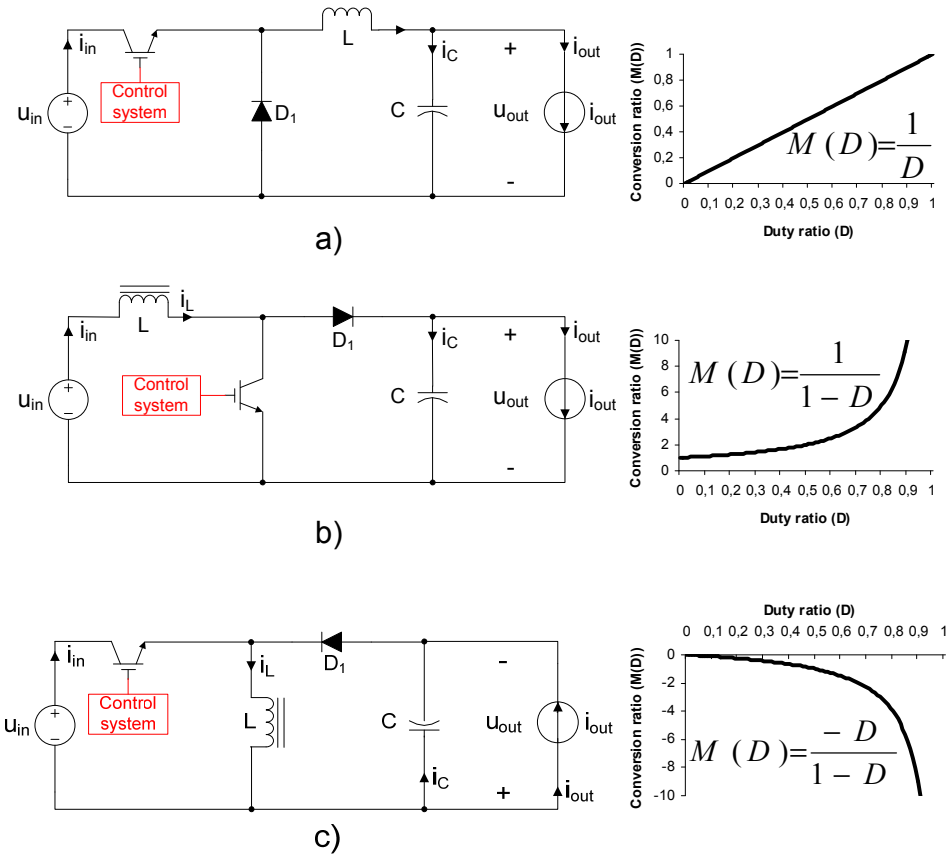

Figure 4.2. *a) buck, b) boost and c) buck-boost converters*

A DC/DC converter works in such way that by using a semiconductor switch, an inductor is periodically charged and discharged. The absolute values of inductor voltage integrals over time are equal during the charging and discharging periods under steady state conditions. This means that if the charging and discharging periods are of unequal lengths, the voltages over the inductor during those periods are also unequal. This characteristic enables the step-up and step-down functions of DC/DC converters. By changing the duty ratio of the transistor switch, the conversion ratio is changed. Duty ratio is defined as the ratio of transistor on time and the whole switching period. A DC/DC converter can operate at open loop, where the duty ratio is set without an actual feedback, or it can be controlled with one or more feedback signals. Figure 4.4 shows the waveforms of a boost converter from which the operation of the corresponding converter can be easily understood.

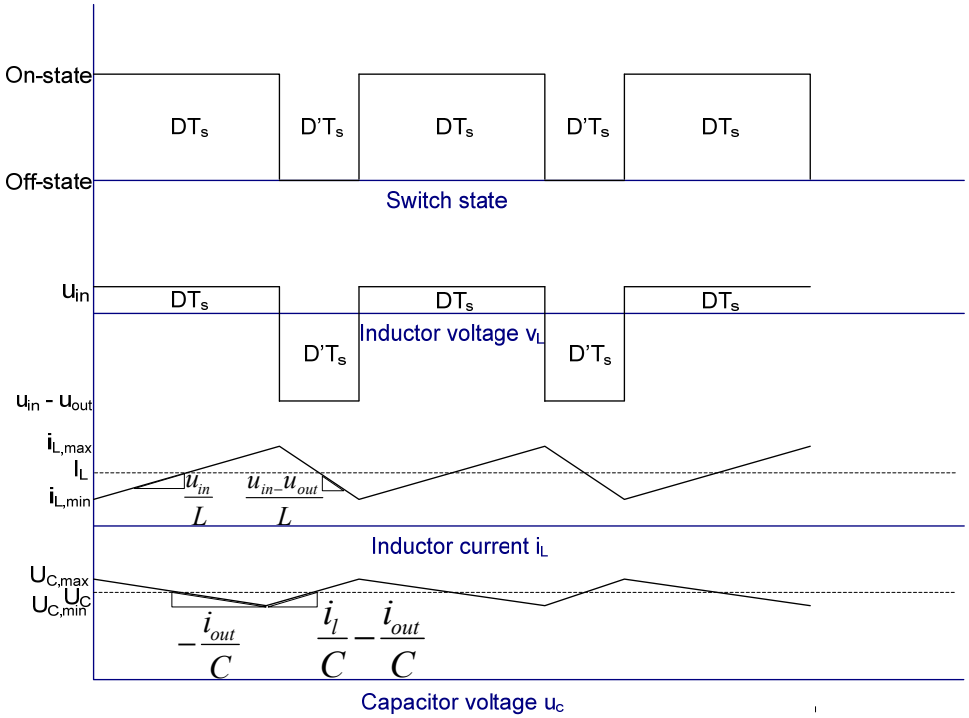

Figure 4.4. *Boost converter waveforms*

As can be determined from Figure 4.4, there are some ripples in the inductor current and capacitor voltage. The inductor current is equal to the input current and the capacitor voltage is the same as the output voltage. The size of the ripples depends on the switching frequency, the size of the inductor and output capacitor as well as from the output power. The input current waveforms depend on the converter type. For a boost converter, the input current is the same as the inductor current but for buck and buck-boost converters, the input current is pulsating and needs to be filtered in order to meet EMI requirements.

From the basic DC/DC converters, the boost converter is perhaps the most often used in the fuel cell applications because a fuel cell is a low voltage high-current device. Step-up conversion is usually needed to match the fuel cell voltage with the DC-bus voltage. However, there are some problems with a simple boost converter in high power applications. The key problem is with the inductor. It is challenging to design a proper high inductance, high current inductor required in high power applications. The other problem is with the high input ripple current, which is directly defined by the amount of the inductance. Therefore, low ripple levels may be challenging to obtain with a simple boost converter. [1] Also, the very high input current can have a considerable effect on the efficiency of a boost converter when compared to more sophisticated topologies. In an addition to these, the weight and volume of a boost converter is not as good as with the more sophisticated topologies, [7] though, being a simple circuit, the reliability of a boost converter can be very high.

The problems with a boost converter in high power applications have led to an interest in finding better step-up topologies for fuel cell applications. From these

topologies, the most important ones are presented in Subsection 4.3. However, as the boost converter is a simple converter, it offers a good starting point. Therefore, a boost converter is dynamically analysed in this thesis and used in the powertrain simulations.

Buck converters can be used in supplying the BoP power. The operation and characteristics of a buck converter are quite the same as with boost converter. However, input current ripple is much higher than that of a boost converter. Buck-boost is a topology very rarely used in the fuel cell applications. A buck-boost could be used if the output voltage of a fuel cell and the DC-bus voltage are expected to be equal at some operating points. However, the inverting nature of a buck-boost output voltage can be a disadvantage. Non-inverting buck-boost topologies are also available but their power stage is more complex reducing efficiency and reliability.

4.3. Sophisticated DC/DC Converter Topologies

In this subsection, some of the sophisticated converters proposed for fuel cells are introduced. Bidirectional converters for ESS are also discussed. There is a large number of different topologies and variations proposed for powertrain applications. Therefore, to limit the discussion on the converters to a reasonable scope, only the most important topologies are treated. Some of the other topologies are compared for example in [37].

4.3.1. Interleaved Boost Converter

The interleaved boost converter is a topology that improves the performance of a single boost converter by connecting a number of boost converters in parallel. Such a converter is presented in Figure 4.5 and is of three-phase type because of its three boost converter legs.

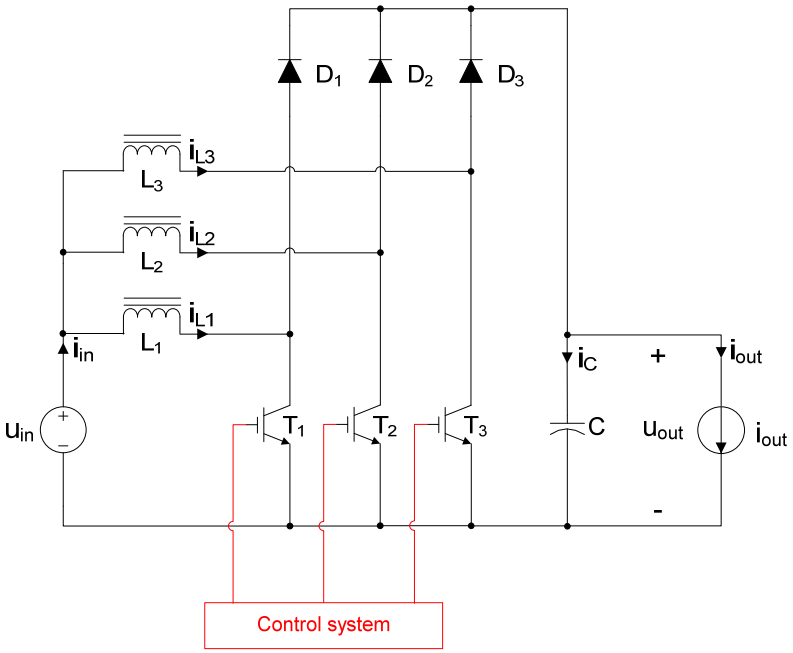

Figure 4.5. *Three-phase interleaved boost converter*

The three-phase interleaved boost converter can operate either synchronously or in interleave mode. In the latter mode, the transistor switches have a phase difference between them. [38] We will only discuss the interleave mode because it has a number of advantages when compared to the synchronous mode.

The operation of a three-phase interleaved boost converter is relatively simple. The circuit consists of three parallel boost converters which are controlled in such a way that there is a phase difference of $2\pi/N$ between the switching cycles of the three switches where N is the number of converter legs. This effectively reduces the input current ripple as the ripple is the sum of the three phase-shifted inductor currents. The interleaved topology distributes the input current between multiple inductors and therefore resistive losses are smaller and efficiency is higher. Also, the individual inductances can be made smaller which enables easier inductor design. [38] The lower power losses and easier inductor design lead to reduced volume and weight of the converter. [7] The advantages and disadvantages of the interleaved converter when compared to traditional boost converter can be summarized as follows [7, 38]:

+ The size of passive components is reduced enabling easier inductor design and smaller and lighter converter
+ Ripple is reduced both at the input and output
+ Ripple frequency is increased, enabling easier EMI filtering
+ The converter can be made modular, increasing reliability and power
+ Current stresses are reduced
+ Due to lower current stresses, higher efficiency and easier thermal management is obtained
- Added complexity

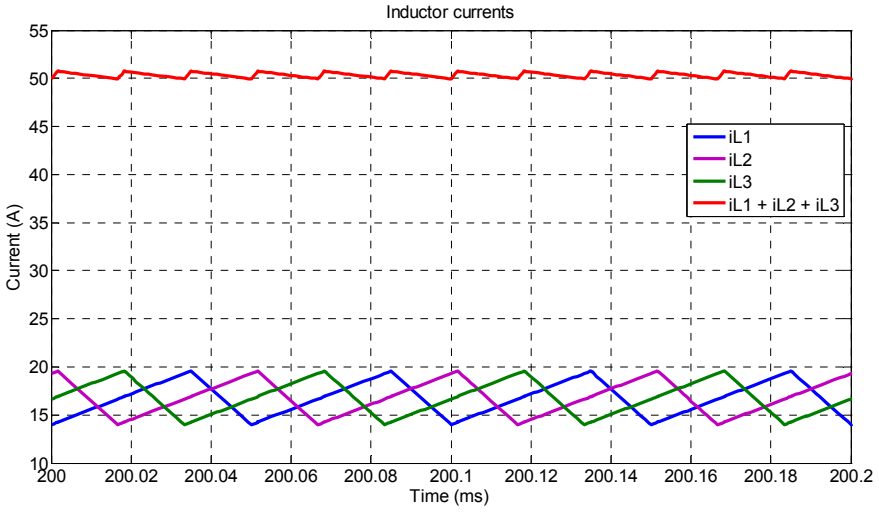

Figure 4.6. *Example of the inductor & input currents*

Figure 4.6 presents an example of the inductor and input currents of the three-phase interleaved boost converter. As can be seen, the input current, which is the sum of the individual inductor currents, is nearly DC with very low ripple content whereas the individual inductor currents contain very high amounts of high frequency ripple. It is also interesting to notice that the ripple frequency of input current is higher than the individual ripples of inductor currents. This means that the input current can be more easily filtered if additional filtering is required.

The three separate converter legs can be analyzed as single boost converters with individual control loops. It is important to implement the phase difference in the PWM modulators and in case of current mode control the reference current signal needs to be divided for the separate converters.

4.3.2. Bidirectional Converter

A bidirectional converter is a converter that can interchange its powerflow. Such a converter is presented in Figure 4.7.

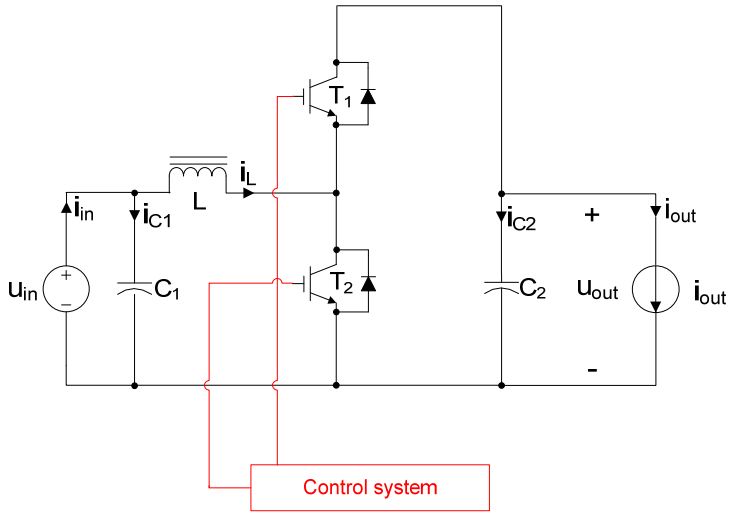

Figure 4.7. *B*idirectional converter

The converter operates as follows: When a PWM signal is applied to the gate of transistor T_1, the converter will operate as a buck converter delivering power from u_{out} to u_{in}. On the other hand, if a PWM signal is applied to transistor T_2, the converter will act as a boost converter delivering power from u_{in} to u_{out}. Thus $u_{in} < u_{out}$ is required. The converter can be analyzed as a buck converter in one direction and as a boost converter in the other direction. Separate control loops have to be designed for both converters. For this, buck and boost dynamic analyses can be used.

The advantages and disadvantages of this type of a converter are the same as with buck and boost converter. However, this type of a converter can be improved by the same interleaving technique as was used in the three-phase interleaved boost converter. [39] Such a three-phase interleaved bidirectional converter is described in Figure 4.8.

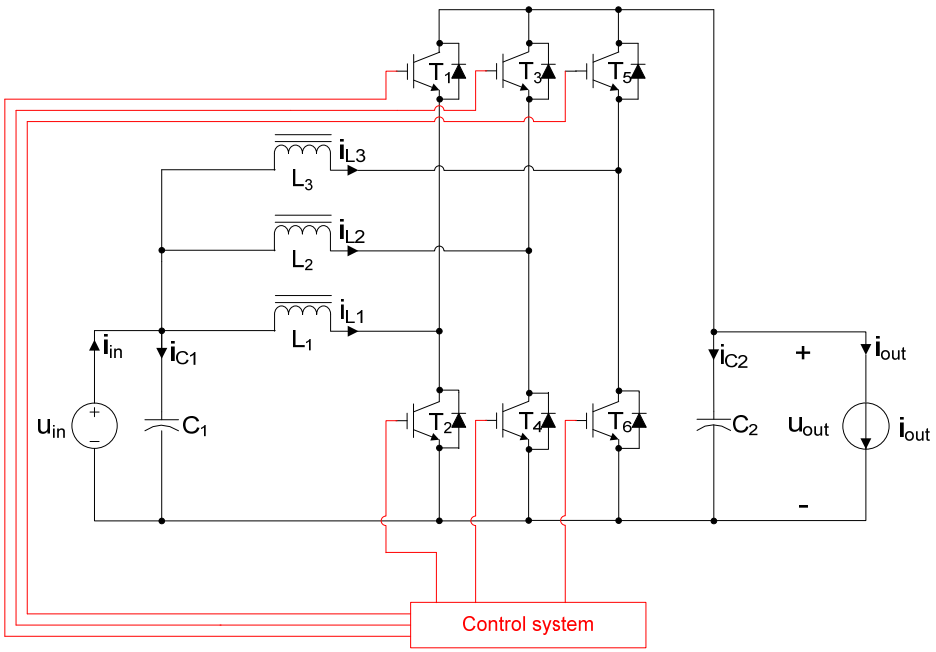

Figure 4.8. *Three-phase interleaved bidirectional converter*

As can be seen from Figure 4.8, the three-phase interleaved bidirectional converter resembles the three-phase interleaved boost converter in Figure 4.5. However, the number of active switches has now increased to six.

4.3.3. Full-Bridge Converter

The full-bridge converter is a converter topology that has been widely researched in fuel cell applications. [7, 40, 41] Figure 4.9 shows such a converter. There are half-bridge and push-pull variations of this converter as well but the former presents twice the current stresses on the switches when compared to full-bridge converter and the latter presents twice the voltage stresses. In addition to these, the push-pull converter requires a centre tapped transformer, which creates difficulties in high power designs. [41] These are the reasons that half-bridge and push-pull converters are not discussed in this thesis.

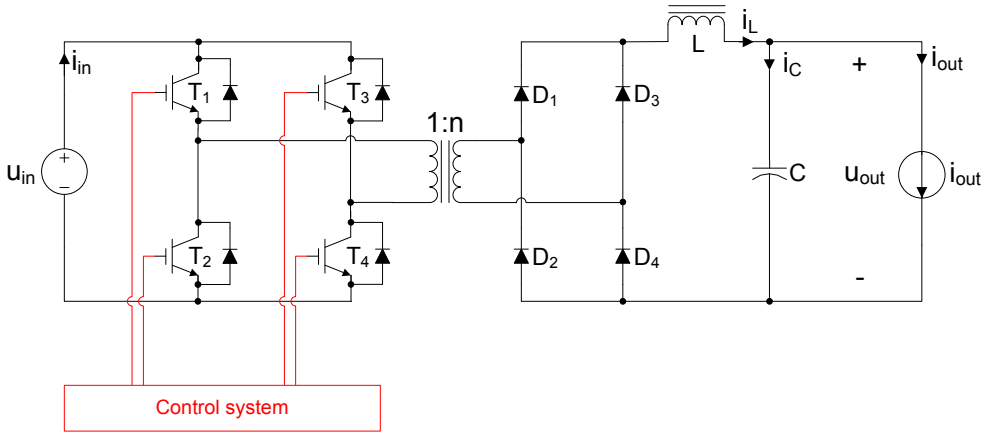

Figure 4.9. *Full-bridge converter*

According to Figure 4.9, a full-bridge converter consists of an inverter, a high frequency transformer, a rectifier, and output filtering. The converter is basically a buck converter with turns ratio. A large voltage gain is obtainable with appropriate turns ratio. The efficiency of a full-bridge converter can easily be over 90% [7]. Other full-bridge advantages include [37]:

+ Galvanic isolation
+ Reduced switching losses if soft switching strategies are implemented
+ Low input and output current and voltage ripples

The disadvantages with full-bridge converters are the added complexity when compared to the traditional buck converter and the requirement for a high frequency transformer, which is a bulky component easily making the converter large and heavy [7].

There is a possibility to construct a bidirectional converter using two full-bridges. Such a converter would be suitable for the ESS. Especially where high voltage conversion ratios are needed. Figure 4.10 describes the bidirectional full-bridge converter.

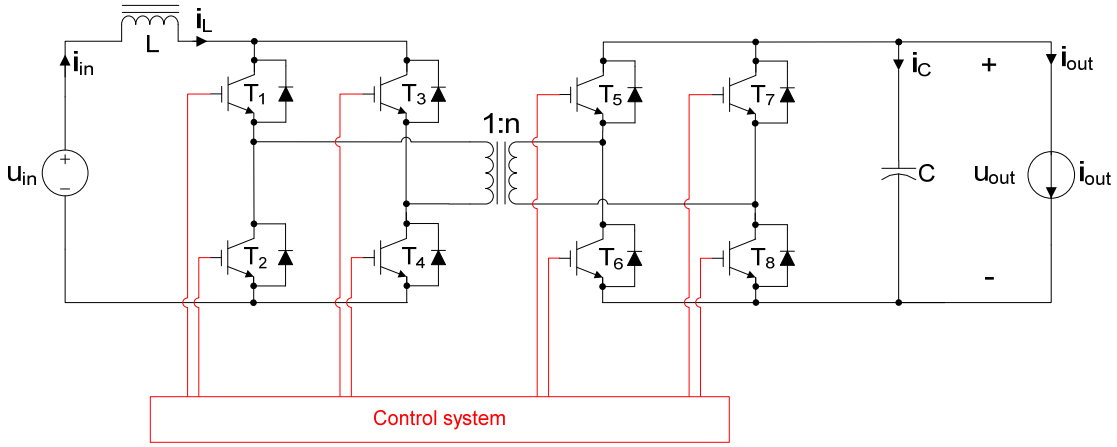

Figure 4.10. *Bidirectional full-bridge converter*

The bidirectional full-bridge converter is basically a buck converter in one direction and a boost converter to the other direction. It is very well suited for high power applications with large voltage conversion ratios.

4.4. Boost Converter Dynamical Behaviour

In this section, a boost converter is analyzed and its dynamic behaviour is investigated. VFVO and VFCO arrangements are analyzed as well as are the load effects. The dynamic analyses are based on Dynamic Profile of Switched-Mode Converter [42] by Teuvo Suntio. For further information, the reader is encouraged to read this book.

The derivation of the dynamic equations for the boost converter is a lenghty process and presented in detail in Appendix 1. The outcome of this derivation is the transfer function matrix G(s). For VFVO converters, this matrix consists of transfer functions denoted by superscript 'v' forming a G-parameter set and for VFCO converters, it consists of Y-parameters denoted by superscript 'i'. These matrices are presented in (4.1) and (4.2), respectively.

$$G(s)=\begin{bmatrix} Y^{v}_{in-o} & T^{v}_{oi-o} & G^{v}_{ci} \\ G^{v}_{io-o} & -Z^{v}_{o-o} & G^{v}_{co} \end{bmatrix} \tag{4.1}$$

$$G(s)=\begin{bmatrix} Y^{i}_{in-o} & T^{i}_{oi-o} & G^{i}_{ci} \\ G^{i}_{io-o} & -Y^{i}_{o-o} & G^{i}_{co} \end{bmatrix} \tag{4.2}$$

where

Y_{in-o} = input admittance
T_{oi-o} = reverse or output-to-input transfer function
G_{ci} = control-to-input transfer function
G_{io-o} = forward, input-to-output, line-to-output transfer function or audio-susceptibility
Z_{o-o} = output impedance
Y_{o-o} = output admittance
G_{co} = control-to-output transfer function

The matrices describe the input-to-output dynamics of a converter. When analyzed carefully, the behaviour of a converter can be understood. Although, the matrices in (4.1) and (4.2) look similar, the actual values of the parameters can be significantly different. These transfer function matrices describe the frequency domain input-output relationships, as can be seen from (4.3).

$$y(s) = G(s)u(s) = \left[C(sI - A)^{-1}B + D\right]u(s) \tag{4.3}$$

where y(s) is the output vector and u(s) is the input vector.

For output feedback converters, the control-to-output transfer function is the key in analyzing the stability of a converter. Most often the converter is operated with a negative feedback from the output. For an output voltage feedback (OVF) voltage-mode control (VMC) converter, this yields a loop gain as:

$$L(s)= G_{se}G_{cc}G_{a}G_{co} \tag{4.4}$$

where G_{se} is the output-voltage sensing gain, G_{cc} is the controller transfer function, G_a is all the other dynamic elements within the loop and G_{co} is the control-to-output transfer

function. The loop gain forms a sensitivity function, which is an integral part in the dynamic behaviour of a converter:

$$S(s) = \frac{1}{1 + L(s)} \tag{4.5}$$

The converter is unstable if L(s) becomes -1. Adequate gain and phase margins must be provided in order that the converter is stable. The margins are obtained by shaping the loop gain with a PID controller, which affects the shape of the loop gain through G_{cc}. The design practice is that first the G_{co} is drawn and then the loop-gain is shaped with G_{cc}. The key is to choose a correct operating point when using this method. If the controller is designed at a wrong operating point, the converter may become unstable when the operating point changes.

The effect of the sensitivity function to converter dynamics can be demonstrated by the following equation:

$$\Delta u_{out} = Z_{o-c}\Delta i_{out}(s) = \frac{Z_{o-o}}{1 + L(s)}\Delta i_{out}(s) \tag{4.6}$$

where $Z_{o\text{-}o}$ is the open-loop output impedance and $Z_{o\text{-}c}$ is the closed-loop output impedance of a converter. The sensitivity function decreases the output impedance of a converter. The closed loop impedance, at the crossover frequency, causes an initial voltage dip when a current transient is applied at the output. The settling time and behaviour are affected by the closed loop impedance at frequencies below the crossover frequency. This means that a converter cannot react instantly and that its response speed is determined by the loop gain. The loop gain is not constant but changes in conjunction with the operating point of a converter. The loop gain and the issues affecting it are investigated in this section.

4.4.1. Boost Converter under Output Feedback Voltage Mode Control

In this subsection, the VFVO boost converter with OVF VMC will be analyzed. Figure 4.11 presents the boost converter with a control loop added.

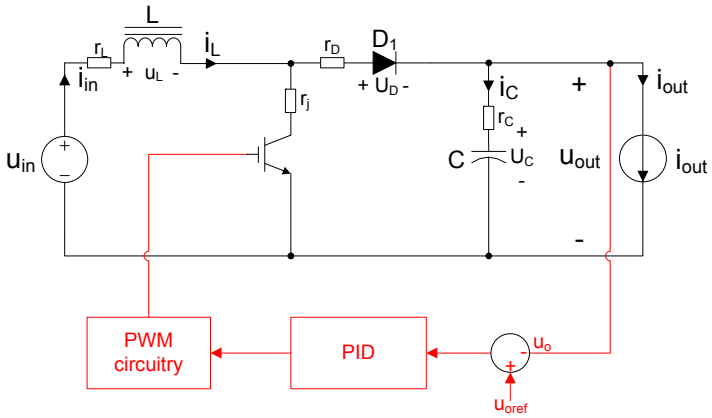

Figure 4.11. *Boost converter under OVF VMC*

In order to analyze the VMC boost converter, the values of the different components must be known. We will use the following arbitrarily chosen parameters to demonstrate the dynamic behaviour of a boost converter under VMC. The parameters have been chosen with a moderate power fuel cell application in mind.

f_s = 20 kHz
L = 400 µH
C = 800 µF
r_L = 20 mΩ
r_C = 40 mΩ
r_D = 15 mΩ
r_j = 10 mΩ
u_D = 1.5 V
U_{inmin} = 160 V
U_{out} = 650 V
P_{out} = 10 kW

The duty ratio D is the only variable whose value is unknown. It can be found by setting the derivatives of the average state space equations (A1.22-A1.23) to zero and replacing the total values of the variables with the corresponding steady state values. This yields (4.7) from which the duty ratio D can be solved algebraically.

$$U_{out} = \frac{U_{in}}{D'} - U_D - \frac{(r_L + Dr_j + D'r_D + DD'r_C)}{D'^2} I_{out} \qquad (4.7)$$

Evaluating the duty-ratio and then Gco from Equation A1.34, a control-to-output bode plot can be drawn. A boost converter has a right-hand plane (RHP) zero which sets a limit for the maximum obtainable control bandwidth. The zero frequency is at lowest when the input voltage is at minimum and the output power at maximum. Therefore, the

controller transfer function has to be designed at minimum input voltage. The control-to-output bode plot is plotted at the low input voltage in Figure 4.12.

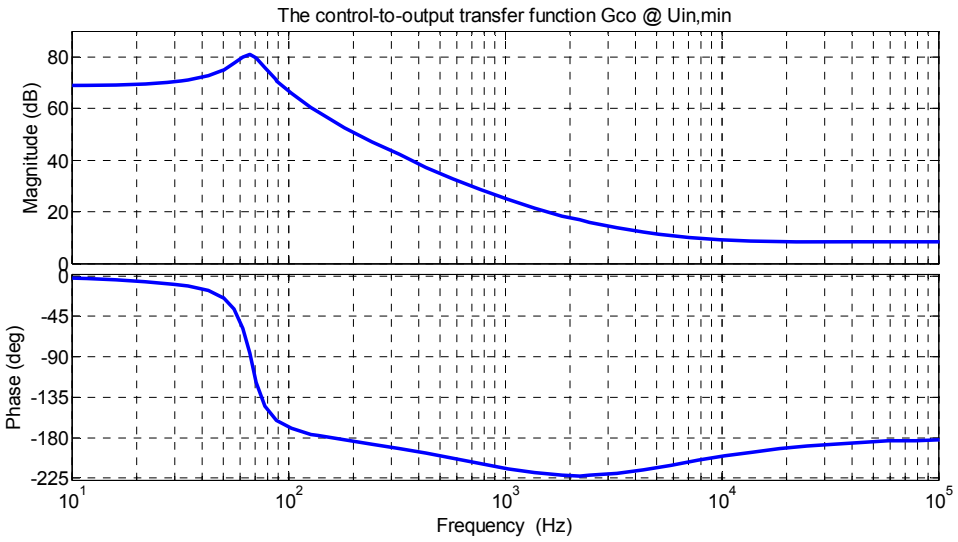

Figure 4.12. *VMC boost Gco bode plot at low input voltage*

Based on Figure 4.12, the converter has RHP-zero at approximately 1 kHz. Next, the Gco bode plot is used in PID-controller (Gcc) design. The loop gain is defined as:

$$L(s) = G_{se} G_{cc} G_a G_{co} \tag{4.8}$$

from which the sensor gain (G_{se}) is equal to 1 in our case and G_a is 1/3 because of the modulator gain. The PID-controller transfer function (Gcc) is defined as:

$$G_{cc} = K \frac{(1 + s/\omega_{z1})(1 + s/\omega_{z2})}{s(1 + s/\omega_{p1})(1 + s/\omega_{p2})} \tag{4.9}$$

where K is the controller gain, ω_{z1} and ω_{z2} are the zero frequencies in radians and ω_{p1} and ω_{p2} are the pole frequencies in radians associated with the controller.

The goal is to set the Gcc in so that the loop gain has a minimum of 6 dB gain margin and 45° phase margin. Because PID has a pole in the origin, the phase of the G_{cc} starts from -90°. This means that the first zero of the controller has to be placed before the LC-resonance frequency and a second zero close enough to the first zero to get an adequate phase boost before the LC-resonance. The first pole is placed after the second zero to decrease the high frequency gain. The second pole is placed at a half of the switching frequency to make the controller proper. Thus we will use the following parameters:

$$\omega_{z1,2} = 0.5 \frac{D'}{\sqrt{LC}} \tag{4.10}$$

$$\omega_{p1} = 30\omega_{z1} \tag{4.11}$$

$$\omega_{p2} = \frac{2\pi f_s}{2} \tag{4.12}$$

The controller gain K is chosen in such a way that sufficient gain and phase margins are obtained. With the value K = 0.5 the margins are adequate. Equating the loop gain with the given values, we get a loop gain presented in Figure 4.13.

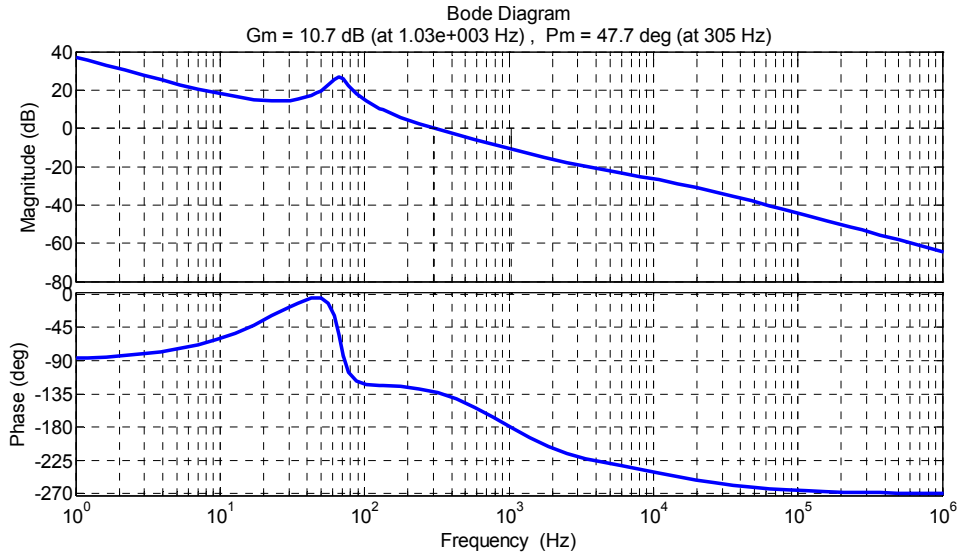

Figure 4.13. *VMC boost converter loop gain L(s)*

From Figure 4.13, a gain margin of 10.7 dB and phase margin of 47.7° can be determined. Together with the shape of the magnitude and phase plots, it can be concluded that the converter should be stable. The stability is demonstrated by a simulation in Figure 4.14 where the voltage reference is 650 V, input voltage is 160 V and a current transient from 20% to 100% of nominal current is applied at the output.

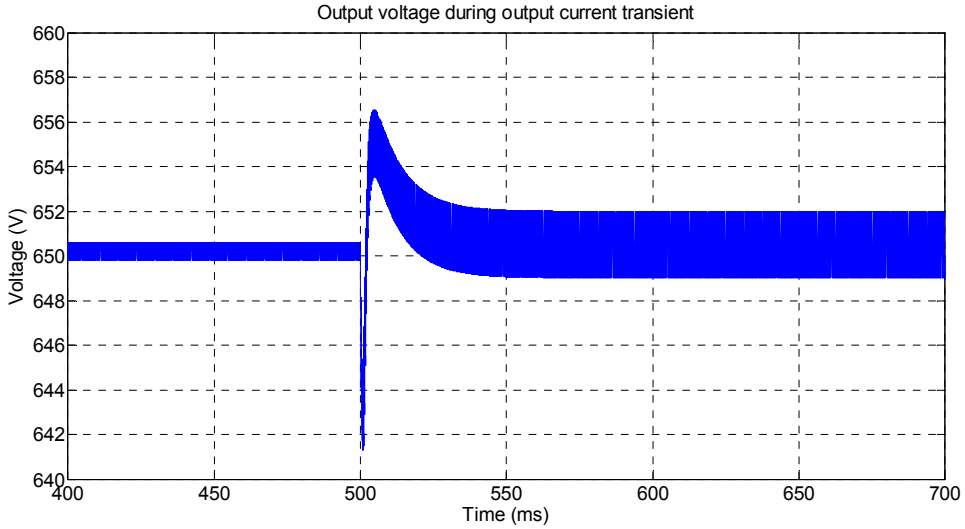

Figure 4.14. *Output voltage during output current transient*

We can conclude from Figure 4.14 that the converter responds to the current transient quite well when kept in mind the control bandwidth and margins obtained.

4.4.2. Boost Converter under OVF PCMC

In this subsection, the peak-current mode control (PCMC) scheme will be described. PCMC requires an internal inductor current control loop as well as a current sensor for the inductor current. The idea behind PCMC is that the duty ratio is generated by comparing inductor current to the control current that is generated by outer voltage control loop.

PCMC was invented in 1970s and has gained a lot of popularity because of the positive effects it has on converter dynamics. It provides a partial or total damping of the LC-resonance and thus creates first order-like transfer functions. Other features include increased input-noise attenuation, pulse-by-pulse current limiting and ease in paralleling converters due to common current reference. The disadvantage of PCMC is duty cycle limitation to the maximum of 0.5, but the problem can be solved with artificial compensation ramp.

Figure 4.15 shows the same boost converter as in the previous subsection but with an OVF PCMC control scheme implemented.

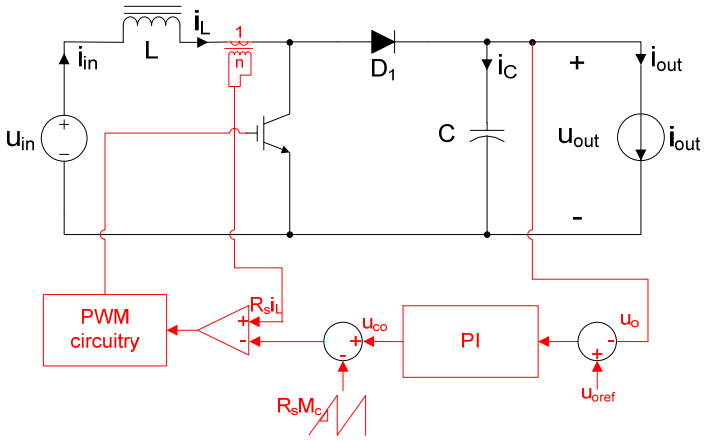

Figure 4.15. *OVF PCMC boost converter*

The outer loop is an output voltage control loop, which generates a control voltage u_{co} for the PCMC loop. From this control voltage, a time dependent compensation ramp is subtracted and the result is then fed to the negative terminal of an operational amplifier (if analog circuitry is used). Inductor current sensor senses the inductor current and returns a voltage value which is the product of the equivalent sensing resistor R_s and the inductor current. This product is then fed to the positive terminal of the operational amplifier. The actual values on the positive and negative terminal of the operational amplifier define the state of operational amplifier output. This forms the duty ratio. The process of this is better understood from Figure 4.16.

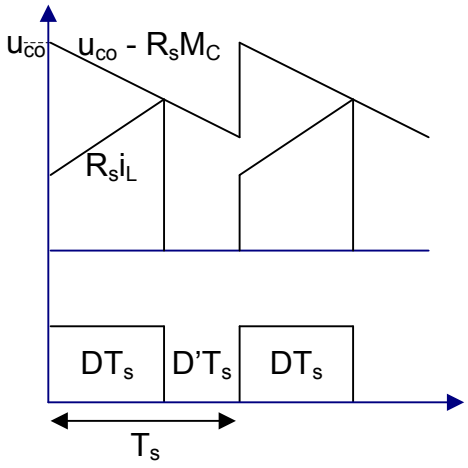

Figure 4.16. *The operation of PCMC*

Because of the inductor current feedback, the dynamics of a converter will change. Therefore, the state space representations will also change. The PCMC state space can be obtained from the model in Figure 4.15 or by adapting the VMC state space (equations A1.31-A1.32). We will use the latter method. To adapt the VMC state space, we must rewrite the perturbed duty ratio $\hat{d}$ with the new dependence corresponding to the PCMC mode. This dependence is known as duty ratio constraints and for second-order converters is given as:

$$\hat{d} = F_m(\hat{i}_{co} - q_c\hat{i}_L - q_o\hat{u}_c - q_i\hat{u}_{in} - q_{io}\hat{i}_o) \tag{4.13}$$

where F_m is the duty ratio gain and q-terms are feedforward or feedback gains from the defined variable. At this point, it is too troublesome to derive the actual symbolic equations for the different terms. For a boost converter the resulting terms are:

$$F_m = \frac{1}{T_s(M_c + \frac{(D'-D)(U_{out}+U_D+(r_D+Dr_C-r_j)I_L)}{2L})} \tag{4.14}$$

$$q_c = 1+\frac{DD'T_s}{2L}(r_D+r_C-r_j) \tag{4.15}$$

$$q_o = \frac{DD'T_s}{2L} \tag{4.16}$$

$$q_i = 0 \tag{4.17}$$

$$q_{io} = -\frac{DD'T_s}{2L}r_C \tag{4.18}$$

$$M_c = \frac{U_{out}+U_D+(r_D+Dr_C-r_j)I_L}{2L} \tag{4.19}$$

Substituting the previous equations to the VMC small signal state space (Equations A1.31-A1.32) and stating that $U1 = (U_{out} + U_D + (r_D + Dr_C - r_j)I_L$, we get the PCMC small signal state space:

$$\begin{bmatrix} \frac{d\hat{i}_L}{dt} \\ \frac{d\hat{u}_C}{dt} \end{bmatrix} = \begin{bmatrix} -\frac{r_L + Dr_j + D'(r_D + r_C) + F_m U1\ q_c}{L} & -\frac{D' + F_m U1 q_o}{L} \\ \frac{D' + F_m I_L q_c}{C} & \frac{F_m I_L q_o}{C} \end{bmatrix} \begin{bmatrix} \hat{i}_L \\ \hat{u}_C \end{bmatrix} + \begin{bmatrix} \frac{1}{L} & \frac{D' r_C - F_m U1 q_{io}}{L} & \frac{F_m U1}{L} \\ 0 & -\frac{1 - F_m I_L q_{io}}{C} & -\frac{F_m I_L}{C} \end{bmatrix} \begin{bmatrix} \hat{u}_{in} \\ \hat{i}_{out} \\ \hat{i}_{co} \end{bmatrix} \tag{4.20}$$

$$\begin{bmatrix} \hat{i}_{in} \\ \hat{u}_{out} \end{bmatrix} = \begin{bmatrix} 1 & 0 \\ D' r_C + F_m q_c r_C I_L & 1 + F_m q_o r_C I_L \end{bmatrix} \begin{bmatrix} \hat{i}_L \\ \hat{u}_C \end{bmatrix} + \begin{bmatrix} 0 & 0 & 0 \\ 0 & -r_C + F_m q_{io} r_C I_L & -F_m r_C I_L \end{bmatrix} \begin{bmatrix} \hat{u}_{in} \\ \hat{i}_{out} \\ \hat{i}_{co} \end{bmatrix} \tag{4.21}$$

Using (4.3), we get the PCMC transfer function matrix. Being too complicated, it is not derived at this point, but the process is the same as with the VMC state space.

Next the G_{co} of the PCMC mode is plotted at minimum input voltage, because then the RHP-zero is at lowest value.

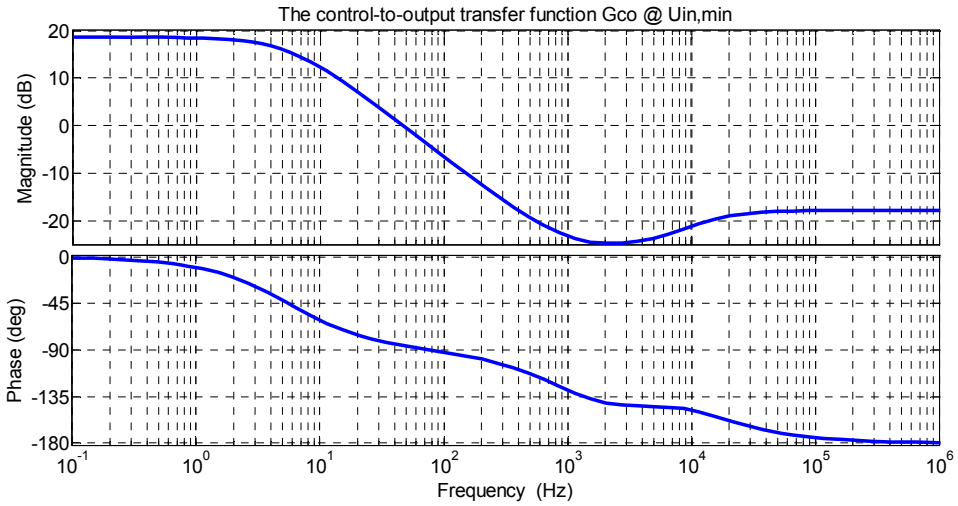

Figure 4.17. *PCMC boost Gco bode plot with low input voltage*

Comparing the PCMC Gco bode plot (Figure 4.17) to the VMC Gco bode plot (Figure 4.12), we can determine that the LC-resonance has been damped, and thus it may be expected that higher control bandwidth/margins are obtainable. Although the RHP-zero is still present as can be determined.

Because of the LC-resonance damping provided by PCMC, a PI-controller is sufficient in obtaining enough gain and phase margins. The loop gain is defined the same way as in VMC mode, but the G_a term is now:

$$G_a = \frac{1}{R_s} \tag{4.22}$$

where Rs is the equivalent current sensing resistor which in our case is selected to be 8 mΩ. The PI-controller transfer function is defined as:

$$G_{cc} = K\frac{(1+s/\omega_z)}{s(1+s/\omega_p)} \tag{4.23}$$

Using the following controller parameters, sufficient margins and control bandwidth are obtained.

$$\omega_z = 0.5\frac{D'}{\sqrt{LC}} \tag{4.24}$$

$$\omega_p = \frac{2\pi f_s}{8} \tag{4.25}$$

$$K = 18 \tag{4.26}$$

Using the previous equations, we get the PCMC loop gain shown in Figure 4.18.

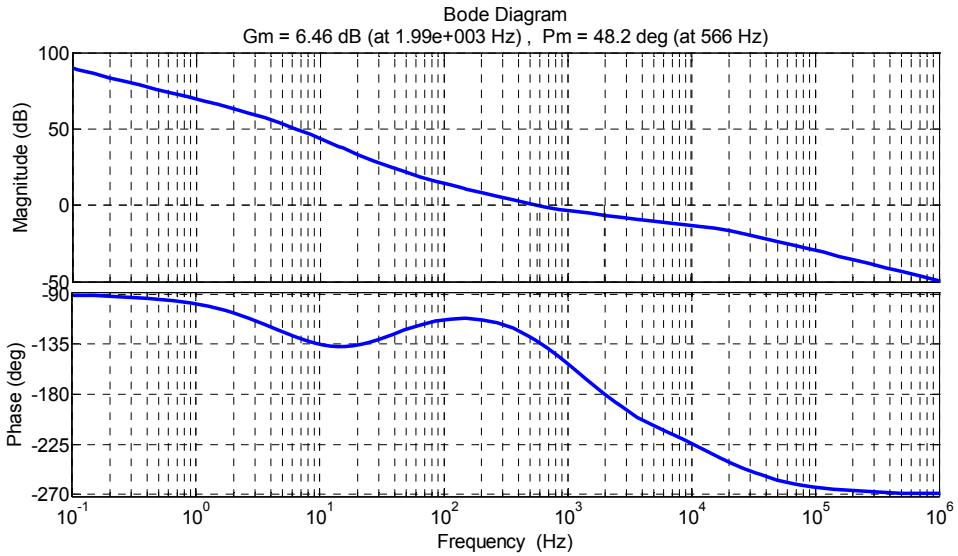

Figure 4.18. *Output voltage feedback PCMC loop gain*

Comparing the PCMC loop gain Figure 4.18 with the VMC loop gain Figure 4.13, we can determine that there is marginal improvement in the control bandwidth, which is now 566 Hz in contrast to VMC's 305 Hz.

The behaviour of the OVF PCMC converter is demonstrated in Figure 4.16, where the voltage reference is 650 V, input voltage is 160 V and a current transient from 20% to 100% of nominal current is applied at the output.

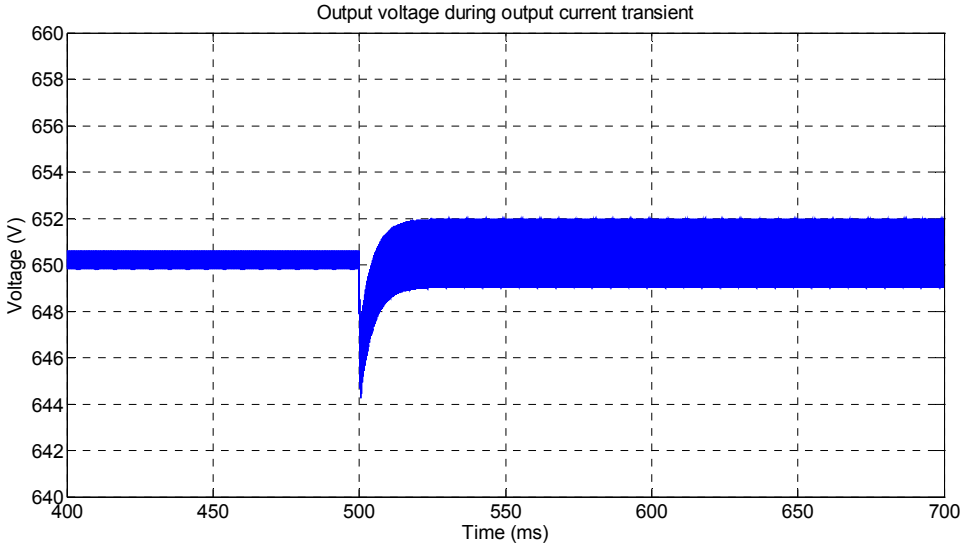

Figure 4.19. *OVF PCMC output voltage during output current transient*

Comparing the OVF VMC and PCMC output voltages during the current transients (Figures 4.14 and 4.19), we conclude that the PCMC mode responds slightly better to the current transient when compared to the VMC mode. The initial voltage dip in PCMC mode is a bit lower. Also, PCMC mode responds more quickly to the transient without any peaking and ringing as can be seen. As a summary, PCMC mode offers some advantages at the expense of added complexity.

4.4.3. Load Interactions

Up to this point, the discussion has been limited to VFVO converters with ideal current sink loading. However, there is a problem if the load is non-ideal i.e. the impedance of the current sink is not infinite. The load interactions presented by non-ideal loading have a considerable effect on the dynamics of a converter. We will not discuss the load interactions fully, only as much as is required to understand the problem. The load interactions are perhaps best understood by considering how they affect the loop gain. The load affects the loop gain of OVF VFVO converter as follows:

$$L(s)^{v-L} = \frac{L(s)^{v}}{1+\frac{Z_{o-o}{}^{v}}{Z_{L}}} \tag{4.27}$$

where the $L(s)^{v}$ is the unaffected loop gain, $Z_{o\text{-}o}$ is the unaffected converter open-loop impedance, Z_L is the load impedance and $L(s)^{v\text{-}L}$ is the load affected loop gain. We can

conclude from the equation that if the load impedance is high, the loop gain is left unaffected but if the load impedance is considerably lower than the open-loop impedance of the converter, the loop gain will decrease drastically. The actual effect presented by the load impedance to the loop gain depends on the magnitude of the converter's open-loop impedance. If it is made smaller, the loading effect on the loop gain is equally smaller.

In our application, we have high capacity batteries and supercapacitors. The bidirectional converters work as step-down converters when charging the ESS. This means that the load of the step-down side of the bidirectional converters is a very low impedance voltage source. On the other hand, if for example, a supercapacitor is connected passively to the DC-bus and a battery through a bidirectional converter, when stepping-up the capacitor voltage, the boost side of the converter will see the supercapacitor as a very low impedance voltage source.

Let us consider, for example, a setup where a converter is charging a supercapacitor and the converter is designed as a VFVO with OVF PCMC. The supercapacitor DC resistance is, say, 12 mΩ. We will approximate the loading effect in such a way that we will suppose that the supercapacitor impedance will stay constant at 12 mΩ regardless of frequency. We will plot the affected loop gain of the OVF PCMC converter. For that purpose, we will take the unaffected output impedance from the transfer function matrix, use the unaffected loop gain that was plotted and, together with the 12 mΩ impedance and (4.27), we can plot the affected loop gain in Figure 4.20:

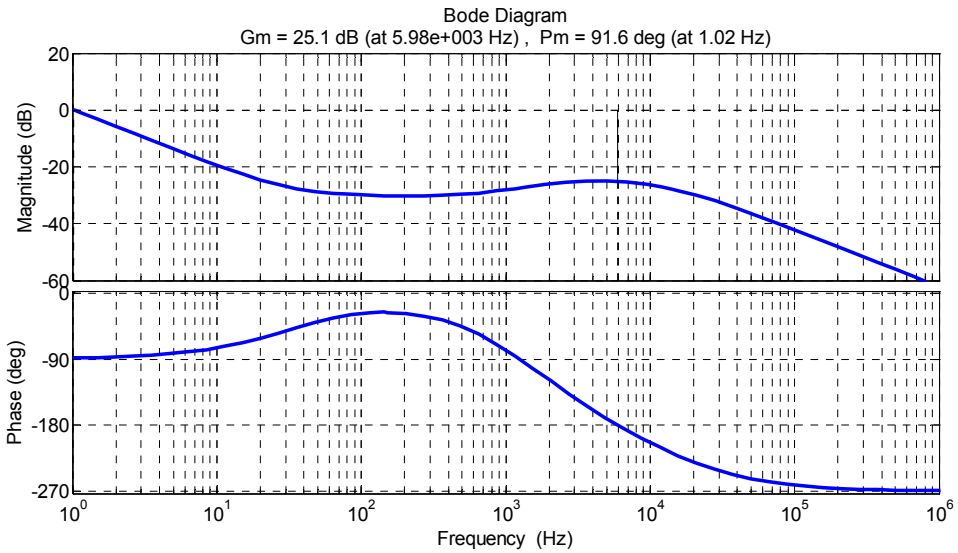

Figure 4.20. *Affected loop gain of OVF PCMC boost converter*

According to Figure 4.20 and comparing it with the unaffected bode plot Figure 4.18, we can conclude that the control bandwidth has been reduced to a drastically low value of approximately 1 Hz. The behaviour of the converter resembles an open-loop converter. With a 1 Hz control bandwidth, a converter follows reference values very slowly.

4.4.4. Voltage-Fed Current Output Converters

In this subsection, VFCO converters are studied. A VFCO configuration is depicted in Figure 4.21.

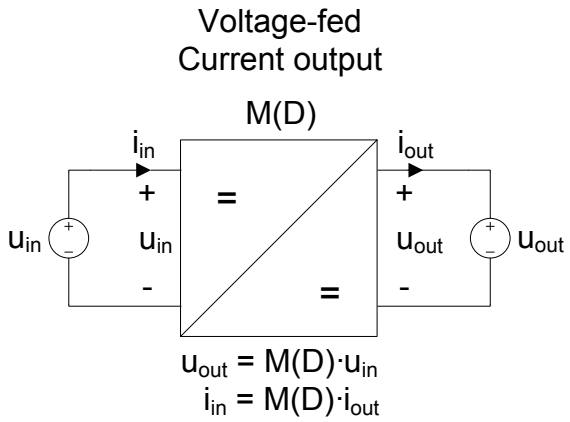

Figure 4.21. *Voltage-fed current output converter*

It was seen in the last subsection that the loading effect reduces the capabilities of voltage output type converters if low impedance loads are used. A solution to this is to use the converters in such applications as current output converters. VFCO converters are particularly important in our case because batteries and supercapacitors present low impedance loading.

For current output converters, the characteristic dynamic parameters are called the Y-parameters, which can be conviniently obtained by converting the voltage output transfer function matrix with the following equation:

$$G(s)=\begin{bmatrix} Y^{i}_{in-o} & T^{i}_{oi-o} & G^{i}_{ci} \\ G^{i}_{io-o} & -Y^{i}_{o-o} & G^{i}_{co} \end{bmatrix}=\begin{bmatrix} Y^{v}_{in-o}+\dfrac{G^{v}_{io-o}T^{v}_{oi-o}}{Z^{v}_{o-o}} & -\dfrac{T^{v}_{oi-o}}{Z^{v}_{o-o}} & G^{v}_{ci}+\dfrac{G^{v}_{co}T^{v}_{oi-o}}{Z^{v}_{o-o}} \\ \dfrac{G^{v}_{io-o}}{Z^{v}_{o-o}} & -\dfrac{1}{Z^{v}_{o-o}} & \dfrac{G^{v}_{co}}{Z^{v}_{o-o}} \end{bmatrix} \tag{4.28}$$

In (4.28), the superscript ‘i’ denotes a current output converter and the superscript ‘v’ denotes a voltage output converter. It can be concluded from the equation that the dynamic parameters will change when the output type changes.

The control-to-input parameter G_{ci} is a key parameter when designing an input current controlled converter. Such a converter has advantages in hybrid powertrains because the energy source current is easily controlled. However, the converter type has to be carefully recognized (basically VFVO or VFCO) before the control loops can be designed properly.

4.5. Power Electronics in Hybrid Fuel Cell Powertrain

It was shown in the previous subsections that the converter types have to be recognized and dynamic behaviour of the converters must be understood in order to implement proper converters into the powertrain. In this subsection, DC/DC converters are designed for simulation purposes and their implementation into the powertrain is described. Figure 4.22 presents a three-way hybrid fuel cell powertrain with a power controller controlling the converters. The various measurement signals required by the power controller have been omitted from the figure. The simulation models differ from the figure in the respect of having only two converters.

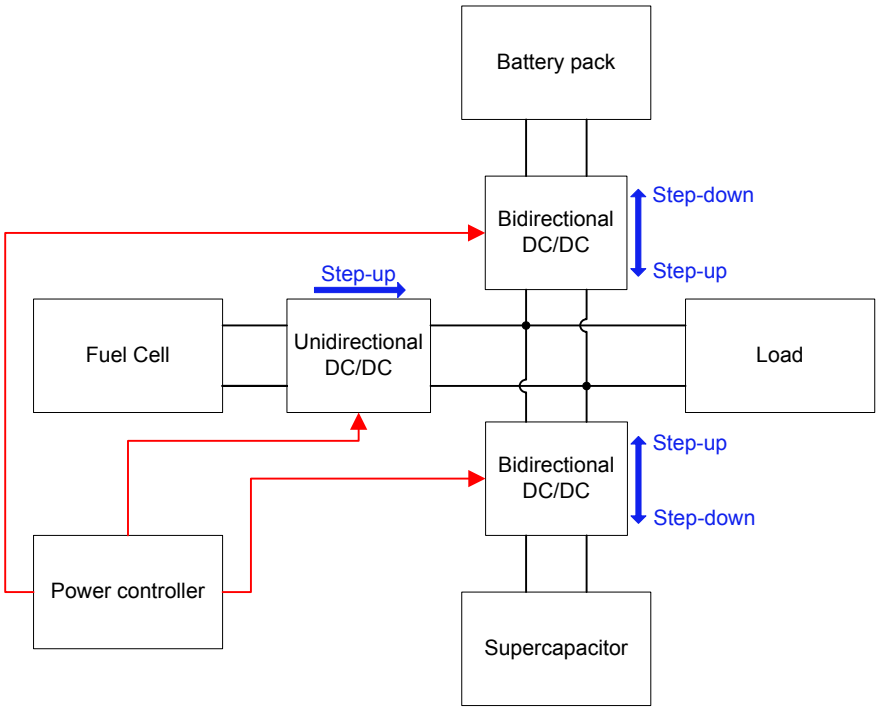

Figure 4.22. *Hybrid fuel cell powertrain with a power controller*

In the powertrain of Figure 4.22, a power controller controls all of the DC/DC converters. It is important to design stable and fast enough internal control loops in order to get them respond quickly enough to reference signals supplied by the power controller. A suitable power management strategy needs to be implemented into the power controller in order to distribute the current properly in the powertrain and to manage the SoCs of the ESS. The power controller has to do all of this based on the measurement signals fed to it. In an addition to SoC control, the power controller needs to operate the fuel cell with steady enough current to maximize its lifetime. The transient load power should be distributed between the battery and the supercapacitor. The most severe transients should be provided by the supercapacitor. Also, the DC-bus voltage is needed to be kept in certain limits at all the time. There has to be always at least one converter which controls the DC-bus voltage. In an addition to this, the currents and voltages of the different energy sources are needed to be kept within certain limits.

It is important to recognize the converter types in order to design proper internal control loops for them. In the case of Figure 4.22, every energy source is behind a DC/DC converter. The load includes a DC/AC converter which converters the DC voltage into suitable AC voltage for the motor. Thus, the outputs of the DC/DC converters, when looking into the DC-bus, have current sinks as loads because power electronic converter inputs are current sinks. The converters need to be modeled as VFVO type converters. On the other hand, if there are passively connected batteries or supercapacitors in the DC-bus, they change the converter types into VFCO type converters. The bidirectional converters are always VFCO types when they are charging the ESS.

In the simulations, the internal control loops are current control loops with feedbacks from the energy source side. This has the advantage of easy limiting of the energy source currents.

Unfortunately, simple current control loops are not enough in practical applications. If the power controller were to fail, there would be nothing to protect the DC-bus or the energy sources from hazardous voltages and currents. The individual converters are needed to have individual voltage and current limiting for safety. A cascaded internal voltage loop would protect hazardous voltages from forming. However, in this thesis, only simple current control loops are used. The purpose of the simulations is to gather data on how powertrains work with converters, not to build a fully feasible powertrain solution.

4.5.1. The Fuel Cell Converter

The voltage of the fuel cell used in the simulations is lower than the DC-bus voltage. In an addition to this, the powerflow of a fuel cell is unidirectional. Therefore, a boost converter is used. Figure 4.23 presents the fuel cell boost converter with the required control loop.

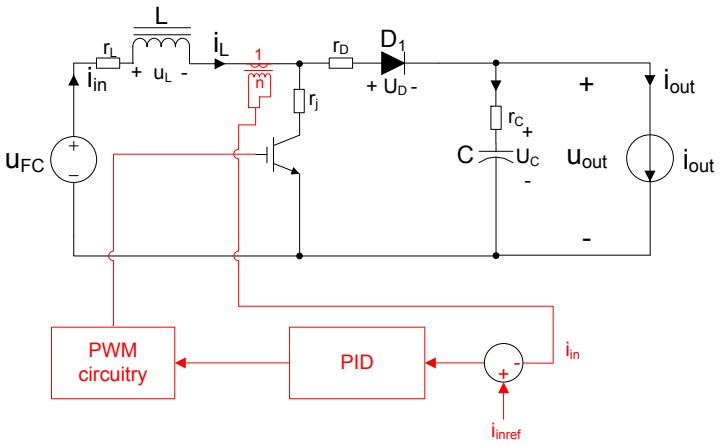

Figure 4.23. *The fuel cell boost converter*

The fuel cell used in the simulations is constructed from two series connected Nedstack P8 fuel cell models. The series connection has the electrical characteristics presented in Table 4.1.

Table 4.1. *Fuel cell characteristics*

U_{FC}	I_{FCmax}	P_{outmax}
70 – 128 V	250 A	16 kW

In the simulations, the DC-bus voltage is set to 350 Volts in order to obtain a reasonable conversion ratio. We will also use the following ripple design boundaries: the input current peak-to-peak ripple is allowed to be 20 % from the average input current and output voltage peak-to-peak ripple is allowed to be 5 % from average output voltage. From these requirements, we will use a boost converter with values presented in Table 4.2.

Table 4.2. *Fuel cell converter values*

f_s	20 kHz
L	400 µH
C	800 µF
r_L	5 mΩ
r_C	5 mΩ
r_D	10 mΩ
r_j	10 mΩ
u_D	1,5 V

It may be obvious that this kind of a boost converter may be hard to realize in practice. It could be easier to use multiple smaller boost converters in parallel. Nevertheless, single converters are used in simulations.

The fuel cell converter control loop is designed the same way as in Subsection 4.4.1. The difference is, however, that this time, we are using input current control. Thus, the control loop has to be designed using control-to-input G_{ci} transfer function. The actual derivation of the control loop will not be presented but the results are:

$$G_{cc} = K\frac{9.97\cdot 10^{-6}s^2 + 0.006315s + 1}{1.675\cdot 10^{-9}s^3 + 0.0001212s^2 + s} \tag{4.29}$$

$$K=6.05 \tag{4.30}$$

where Gcc is the controller transfer function and K is the controller gain.

4.5.2. The ESS Converters

The powerflow of the ESS can be in either direction. This means that a bidirectional converter, depicted in Figure 4.24, is required.

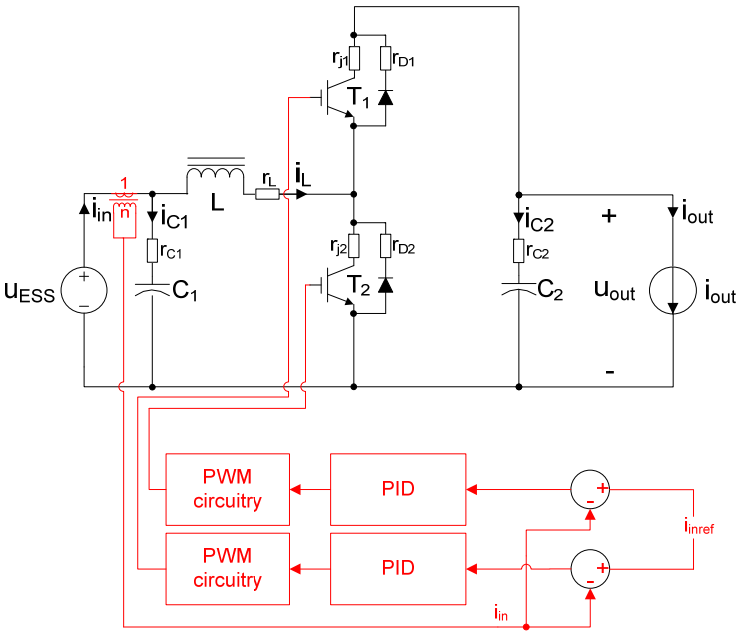

Figure 4.24. *The ESS bidirectional converter*

The battery used in the simulations is constructed from Energeco Lead-acid battery models and the supercapacitor used is constructed from two Maxwell 165 F 48.6 V supercapacitor models connected in series. The battery's electrical characteristics are presented in Table 4.3 and the supercapacitor series connection in Table 4.4, respectively.

Table 4.3. *Battery characteristics*

U_{batt}	$I_{battmax}$	P_{outmax}
70 – 100 V	200 A	20 kW

Table 4.4. *Supercapacitor characteristics*

U_{sc}	$I_{scpulse}$	$P_{outpulse}$
48 – 96 V	800 A	50 kW

The supercapacitor voltage is quite low compared to the DC-bus voltage and the peak-current capability of the supercapacitor is very high. A converter with high enough conversion ratio and peak-current capability may be hard to realize in practice.

We will again use a DC-bus voltage of 350 Volts and the same ripple design boundaries as with the fuel cell converter (i.e. input current peak-to-peak ripple is the maximum of 20 % of the input average current and output voltage peak-to-peak ripple is the maximum of 5 % from the average output voltage). These requirements lead to a bidirectional converter with the values given in Table 4.5. The same kind of converter is used for both battery and supercapacitor.

Table 4.5. *ESS converter values*

f_s	20 kHz
L	400 µH
$C_{1,2}$	800 µF
r_L	5 mΩ
$r_{C1,2}$	5 mΩ
$r_{D1,2}$	10 mΩ
$r_{j1,2}$	10 mΩ
$u_{D1,2}$	1,5 V

As can be concluded from Table 4.5, the parameters are the same as with the fuel cell converter, only that there is an additional capacitor at the ESS side. The bidirectional converter operates in buck mode when charging the ESS and in boost mode when stepping up the voltage to the DC-bus. The energy-source-side current-mode control requires output current mode control in buck mode and input current mode control in boost mode. The respective transfer functions for the control loop design are G_{co} and G_{ci}. In an addition to this, a logic is required to choose a proper operating direction depending on the measured current value and current reference.

We will use the same control system parameters for the boost side of the converter as with the fuel cell converter expect for the controller gain which is now set to 5. However the buck side control parameters have to be derived from buck dynamic analysis. The actual analysis is omitted but the procedures are the same as with a boost converter. The actual control system parameters for the buck side of the converter are:

$$G_{cc} = K\frac{0.0032s^2 + 0.1131s + 1}{9{,}003 \cdot 10^{-7}s^3 + 0.05658s^2 + s} \tag{4.31}$$

$$K = 100 \tag{4.32}$$

The converters and parameters presented in this section will be used in Chapter 5 for hybrid fuel cell powertrain simulations.

4.6. EMC and Ripple Considerations

The switching nature of power electronic converters inherently generates high current and voltage rate of changes which are a source of electromagnetic interference (EMI). The definition of EMI includes unwanted conducted current and voltage ripples as well as unwanted electromagnetic radiation produced by the high rate of changes. EMI may have a serious effect on the different kinds of delicate measurements and control systems used in the powertrain. It may disturb the operation of these systems if not taken into account in the design of the overall powertrain.

There are a number of different standards which set a limit for EMI generated by an electronic equipment. The compliance is marked with a CE marking. However, a CE marking on a converter does not gurantee the absence of EMI problems. In an addition to this, the sum of CE markings is not equal to CE i.e. a number of EMI compliant sources may generate too much EMI when used in the same system.

Electromagnetic compatibility (EMC) is the absence of EMI. The problems caused by the EMI require the following three aspects: i) the generator of EMI; ii) the transmission path of EMI; and iii) the victim. Therefore, there are three options to ensure EMC: to reduce the amount of EMI generated, to cut-off the EMI transimission path or to make the victim more EMI tolerable. It may be possible that every one of these options have to be used in order to construct a system with proper EMC.

The EMC is a wide topic in itself and unfortunately any further discussion is beyond the scope of this thesis.

4.7. DC/AC Inverters

DC/AC inverters are devices which convert DC into AC with wanted amplitude and frequency. In hybrid fuel cell powertrain applications, they are typically used to convert the DC-bus voltage into a suitable AC voltage for the drive motor. In an addition to this, the BoP requires DC/AC inverters to supply fans and blowers.

There are many types of DC/AC inverters. Only the most important ones are described here. There are equally as many DC/AC control schemes and we will only discuss the pulse width modulation scheme because it produces sinusodial output voltages with minimum output filtering. Figure 4.25 presents a single-phase full-bridge inverter.

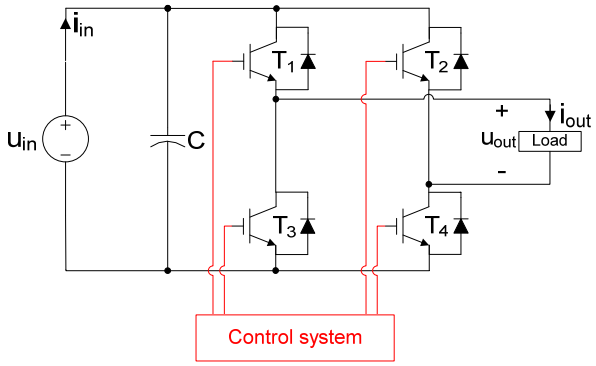

Figure 4.25. *Single-phase full-bridge inverter*

The single-phase inverter is operated by driving the transistors T1-T4. The load is connected to either the positive voltage u_{in} or its inverse $-u_{in}$. The output voltage u_{out} therefore consist of the input voltage with either polarity. By utlizing PWM and high enough switching frequency, the switches are controlled in such a way that an approximate sinusoidal output voltage is formed from the two voltage states. The output is not exactly sinusoidal but it contains harmonic components in addition to the

fundamental desired frequency. These harmonics can be filtered by using inductors and capacitors between the load and the inverter.

The nature of single-phase inverters is that when the harmonic frequencies are filtered, the output voltage is sinusoidal which effectively means pulsating output power. This effectively makes the inverter input current i_{in} pulsating as well. Therefore, in an addition to the switching frequency ripples, the input current i_{in} contains current ripple which frequency is twice that of the fundamental output voltage frequency. The frequency of this ripple is known to be low enough to cause fuel cell degradation if the ripple flows through a fuel cell. Fortunately, solutions have been proposed to cancel out this problem. For example, in [43] the problem is mitigated by controlling a DC/DC converter feeding a DC/AC converter in such a way that the DC/DC converter provides only the DC-component for the inverter. This effectively filters the low frequency ripples from the fuel cell.

Three-phase inverters are devices which are used to deliver power to drive motors in hybrid applications. Such a converter is presented in Figure 4.26.

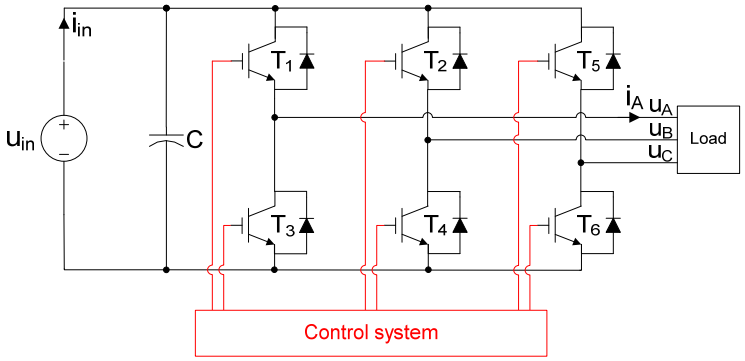

Figure 4.26. *Three-phase inverter*

Basically a three-phase inverter operates the same way as its single-phase equivalent. The sinusoidal voltages are accomplished by PWM and additional filtering. However, the difference is that the output is three phase which means that the power output is constant. Therefore, the input current is effectively constant if not including high frequency switching ripples. Thus, the three-phase converter produces the harmful low frequency ripples only during assymetric loading which should only happen during the fault conditions. This means that the low frequency ripple current problem does not exist with three-phase inverters. Three-phase inverters produce only the switching frequency ripples to the DC-side.

5. MODELING OF THE HYBRID POWERTRAIN & POWER ELECTRONICS IN SIMULINK

In this chapter, two different hybrid fuel cell powertrain configurations are simulated. The purpose of the simulations is to gain understanding from the operation of powertrains equipped with DC/DC converters.

The powertrains are modeled in Simulink environment. The converters are modeled using fundamental electrical components found from Simscape library. This enables easy and accurate modeling but the resulting model is heavy and time consuming to compute. The energy source models used are the same models used by Karimäki [2] with minor modifications. Unfortunately, it was not possible to validate the powertrain models during the writing of this thesis. The accuracy of the models is therefore, not known.

5.1. Introduction to the Modeling

The two simulated powertrains are described in Figures 5.1 and 5.2.

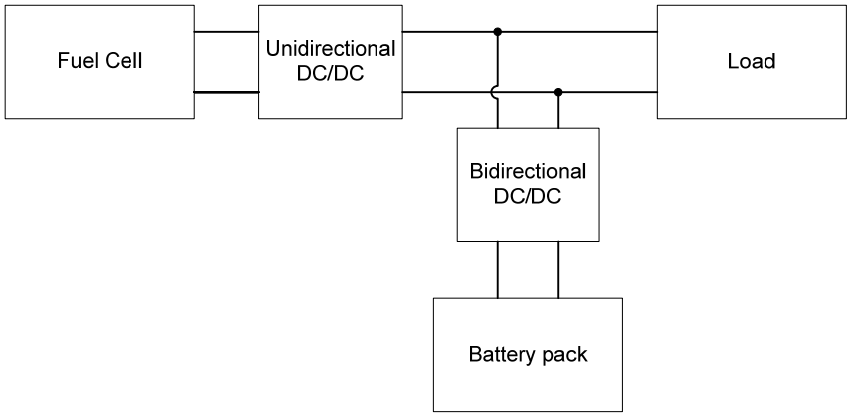

Figure 5.1. *Two-way hybrid fuel cell powertrain*

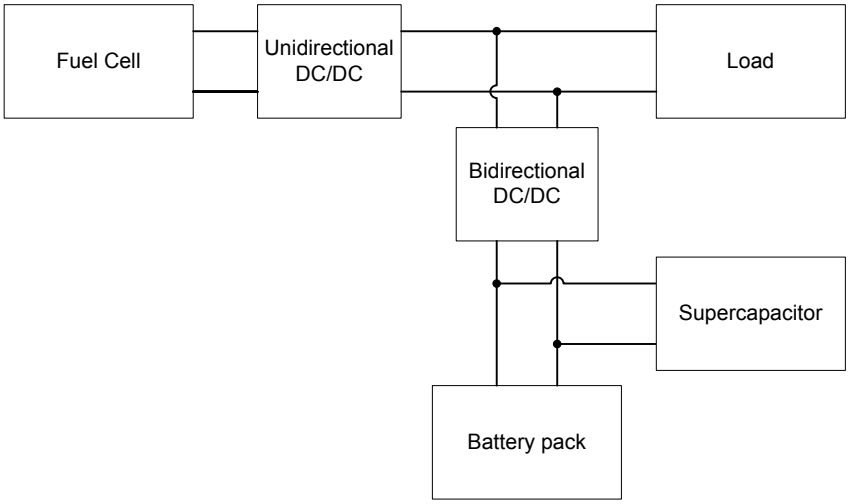

Figure 5.2. *Three-way hybrid fuel cell powertrain*

The powertrains presented in Figures 5.1 and 5.2 are operated in such a way that the fuel cell DC/DC converter is given a constant 200 A input current reference when the load current is above 0 A. When the load current becomes negative (during regenerative braking) the input reference for the fuel cell converter is given by the relation:

$$I_{FCref} = 200A + \frac{U_{DCbus}}{U_{FC}} I_{load} \tag{5.1}$$

where
I_{FCref} is the input reference current for the fuel cell converter
U_{DCbus} is the DC-bus voltage
U_{FC} is the fuel cell voltage
I_{load} is the load current

This decreases the fuel cell output current proportional to regenerative load current I_{load}. This is done because the bidirectional DC/DC converter has an ESS side current limit of 250 A and thus cannot accommodate both fuel cell current and regenerative current at the same time. In an addition to this, a ramp-rate limitation is implemented into the fuel cell converter. The converter can change the fuel cell current at the maximum positive rate of 80 A/s and at unlimited negative rate. This is done to solve the reactant starvation problem.

The bidirectional converter controls the DC-bus voltage which is set to 350 V. It should be noted that there is no management strategy implemented for the battery/supercapacitor SoC. It depends on the average fuel cell and load power difference whether the battery/supercapacitor is being charged or discharged.

The voltages and currents are measured both from the DC-bus side and the input sides of the converters. The model also calculates the SoCs of the battery and supercapacitor. The load is a constant current sink which value is given in a table

representing a drive cycle of a forklift. In an addition to the blocks presented in Figures 5.1 and 5.2, there is an additional 10 mF electrolytic capacitor connected to the DC-bus.

The unidirectional and bidirectional converters were designed in Subsections 4.5.1 and 4.5.2 and have been implemented to the model by using Simscape fundamental electrical components.

5.2. The Models

The simulink model for a two-way hybrid fuel cell powertrain is described in Figure 5.3. The same but larger figure can be found from Appendix 2.

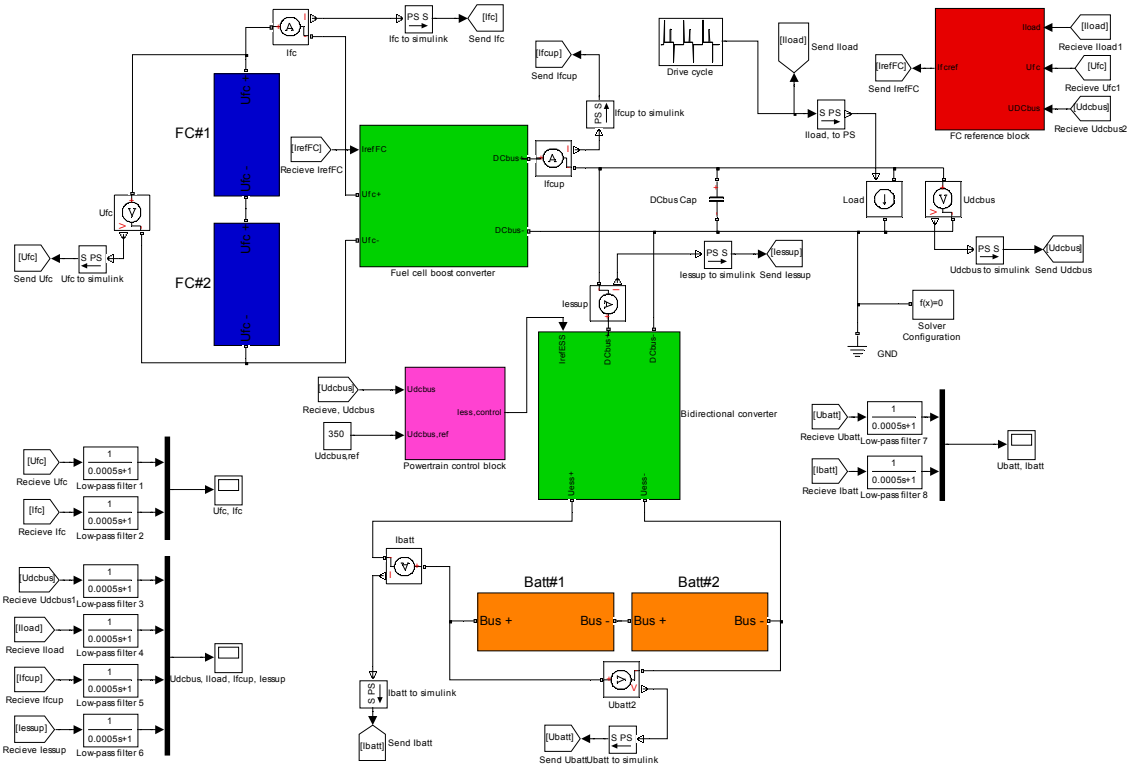

Figure 5.3. *Two-way hybrid fuel cell powertrain model*

The model in Figure 5.3 is the same arrangement as in Figure 5.1 but with measurements and other blocks added. These blocks include: i) the PI-block which controls the DC-bus voltage by controlling the bidirectional converter (the pink block); ii) fuel cell reference current block which gives the reference current for the fuel cell converter (the red block); iii) drive cycle block which gives a repeating 60 second drive cycle for the current sink acting as load; and iv) all the other blocks like measurements and scopes.

The three-way hybrid fuel cell powertrain simulink model is described in Figure 5.4 and can also be found from Appendix 3.

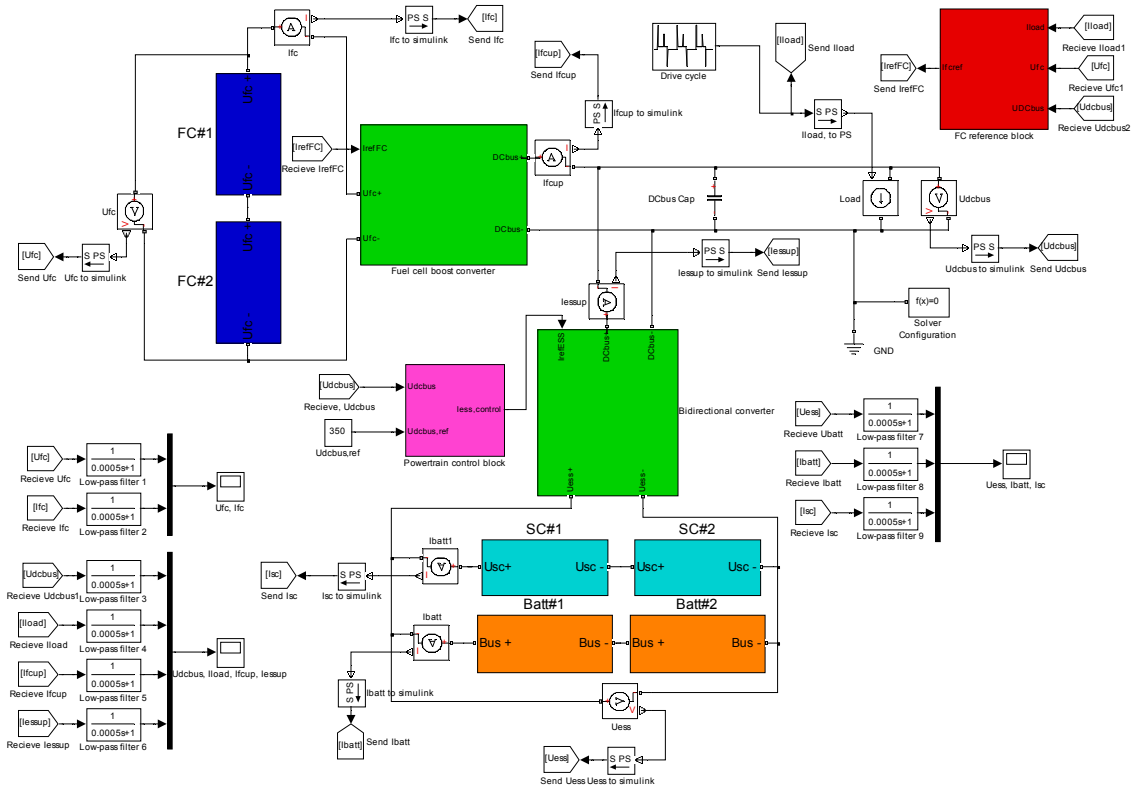

Figure 5.4. *Three-way hybrid fuel cell powertrain model*

The three-way model is the same as the two-way model except for the supercapacitor series connection that has been connected in parallel with the battery pack. There are also individual current measurements for the battery and supercapacitor current.

Due to the very short simulation step-time, long simulations cannot be performed without extra measures because of large amount of data points created. Thus every measured signal is low-pass filtered with a time constant of 50 µs and then sampled with 1 ms sample time. This removes the switching waveforms of the converters but preserves the lower frequency changes in the system in which we are interested in this thesis. In fact, the AC-accuracy of the energy sources is limited so there would be no reason to simulate switching waveforms.

5.2.1. Fuel Cell, Battery and Supercapacitor Models

The fuel cell and battery models are the same models as in [2] with minor modifications. Figure 5.5 shows the fuel cell model.

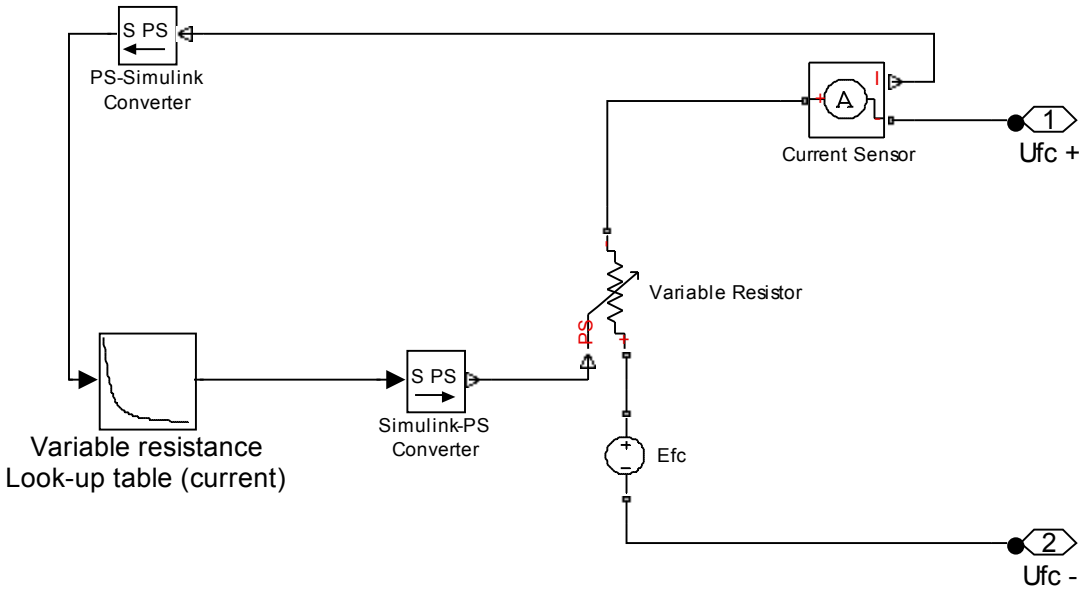

Figure 5.5. *The fuel cell model*

The fuel cell model is based on the IV-graph measured from Nedstack P8 fuel cell stack. From this IV-graph, a variable resistance term was calculated, which is placed in series with the open-circuit voltage source E_{fc}. This way a sufficient DC-accuracy is obtained, but the model fails in AC because it does not include the double layer capacitance behaviour of the fuel cell. The powertrain model incorporates two of these fuel cell models in series. The series connection can deliver approximately 16 kW of power and has approximate voltage and current ranges of 70 – 128 V and 0 – 250 A.

The battery model used in the powertrain is shown in Figure 5.6.

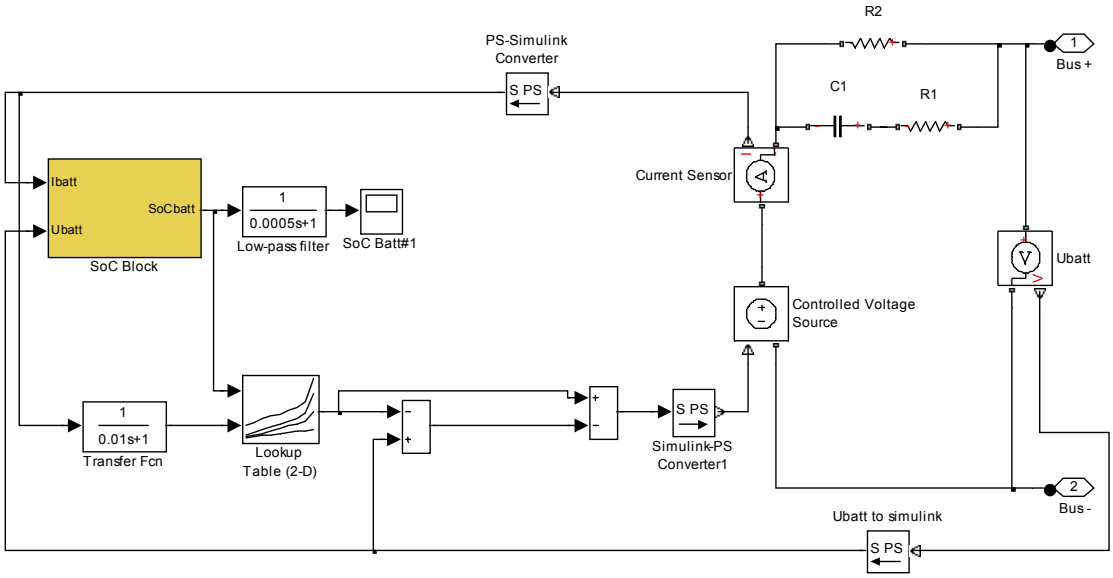

Figure 5.6. *The battery model*

The battery model is based on a battery pack constructed from 20 pieces of Batteriunion 300 Ah Lead-acid cells. The battery pack voltage is approximately 40 V depending on the SoC and loading. The model includes a variable voltage source which is controlled by a 2-dimensional look-up table which gives the voltage as a function of SoC and charging current. This look-up table is based on the data given by the manufacturer. The resistances R_1 and R_2 and capacitance C_1 represent the dynamic behaviour of the battery and have been fitted from measurement data. The SoC block calculates the SoC of the battery. [2] The DC-accuracy was validated in [2] and was found to be adequate. AC-accuracy remains unknown but should be better than with the fuel cell model because the battery double layer capacitance has been included in the model.

The powertrain model incorporates two series connected battery models. The battery current is limited to 250 A by the bidirectional converter. The power capability of the battery is therefore limited to around 20 – 25 kW depending on the SoC. The battery has to handle the surplus power from the DC-bus during regenerative braking. Therefore, the fuel cell output power must be decreased in order to the battery to be able to sink all the regenerative power.

The supercapacitor model used in the three-way model is given in Figure 5.7.

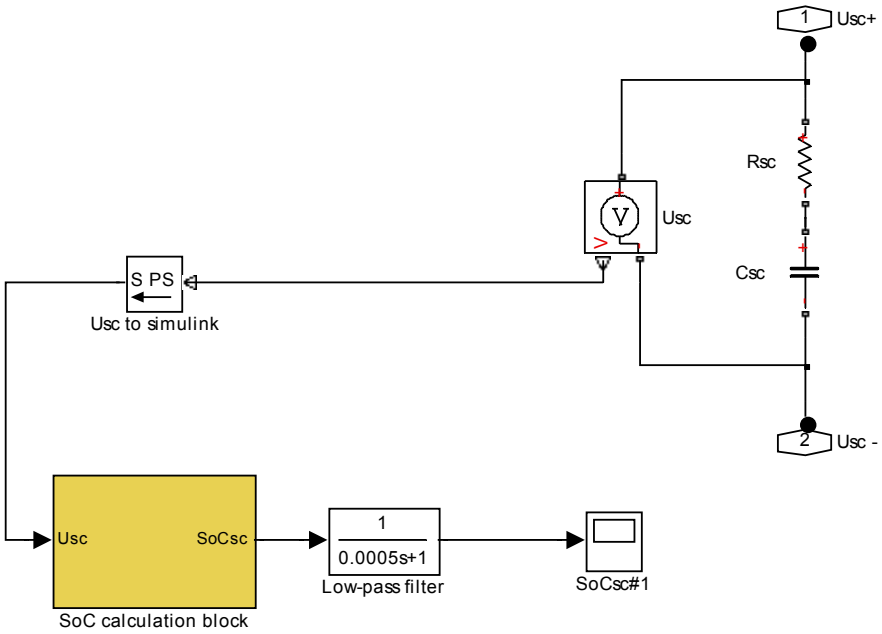

Figure 5.7. *The supercapacitor model*

The supercapacitor model is based on the Maxwell BMOD0165 supercapacitor pack which has the rated voltage and capacitance of 48.6 V and 165 F. The model is a simple ideal 165 F capacitor in series with a resistance constituting of the internal DC-resistance of the supercapacitor and wiring resistances. Clearly, the model is valid only at low frequencies. The SoC block calculates the supercapacitor SoC from its energy relation $\frac{1}{2}CU^2$ and comparing it to the full charged energy. Constant capacitance and the maximum voltage of 48.6 V are assumed.

5.2.2. The DC/DC Converter Models

The bidirectional DC/DC converter is shown in Figure 5.8. The unidirectional converter is not described here as it is basically the same as the bidirectional converter with only the boost side implemented.

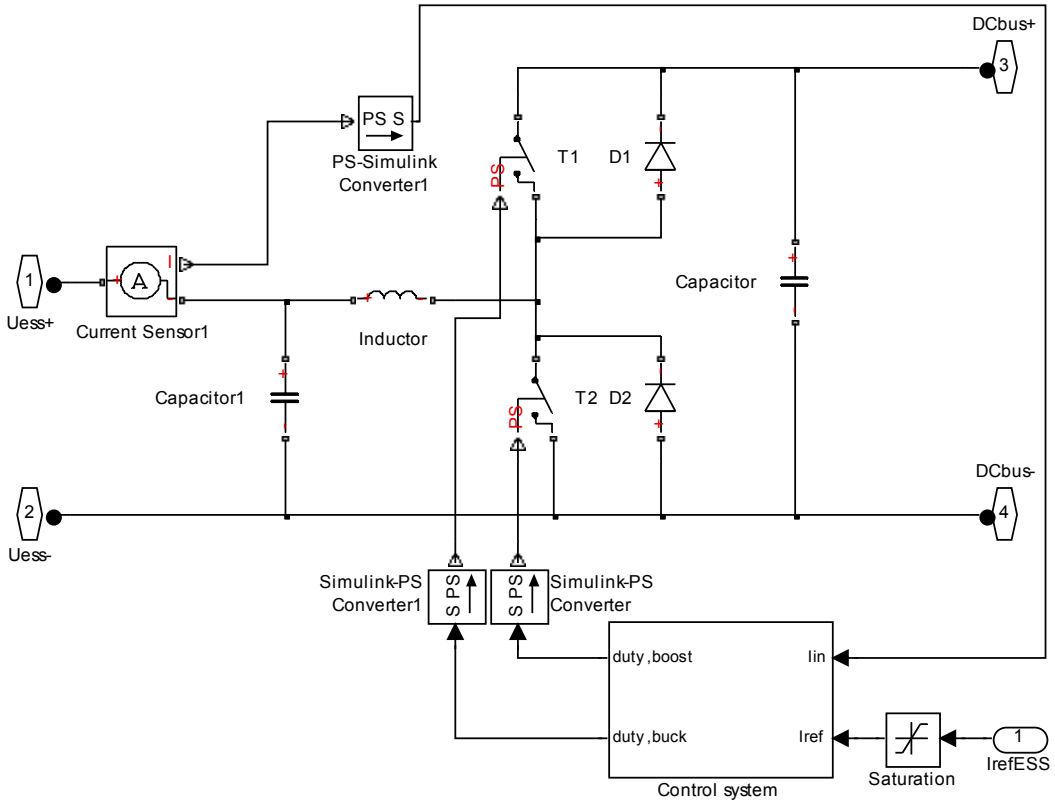

Figure 5.8. *The bidirectional converter model*

The converter is modeled by using electrical components with corresponding parasitics included. The switching model requires the use of a very short simulation step yielding time consuming simulations, but also accurate responses. The corresponding control system is shown in Figure 5.9.

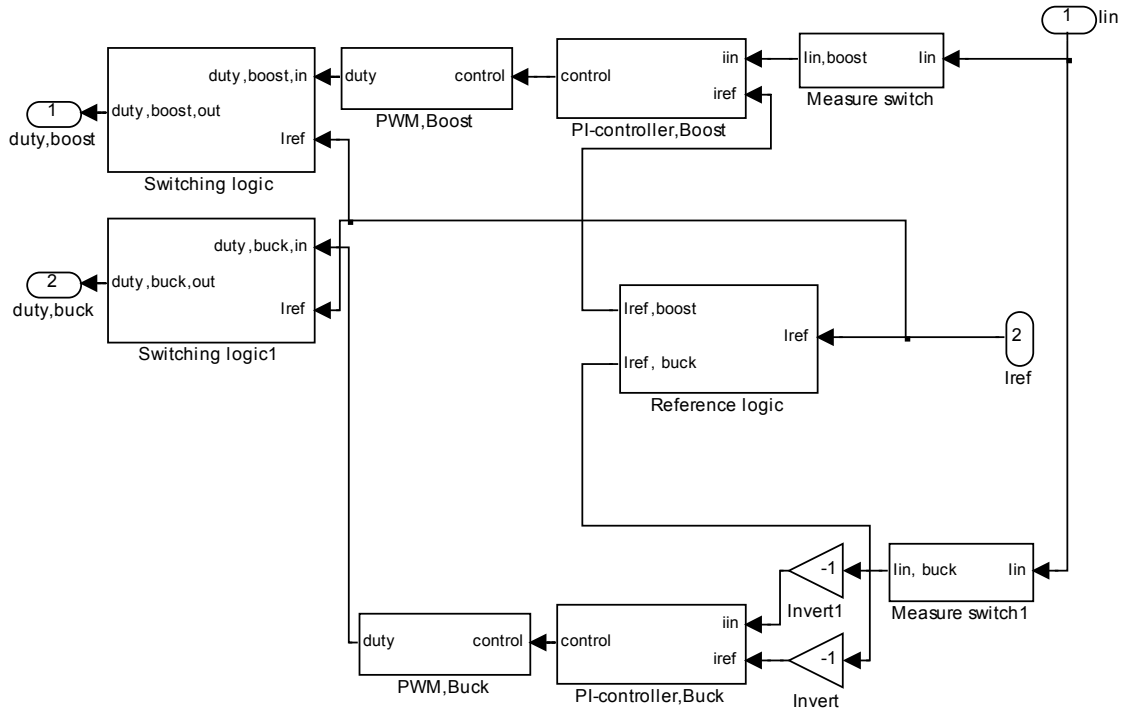

Figure 5.9. *Control system for the bidirectional converter*

Because the converter is bidirectional, the control block has to decide in which way to operate the converter based on the reference and measured current. If reference current is higher than zero, the boost side converter is fed with a PWM signal and the buck side is turned off. The same happens with measurement signal: if the measured current is higher than zero then the boost side control system is fed with the corresponding measured signal and buck side is fed a constant zero in order to solve controller windup problem when the converter changes direction. When the reference and measured current is below zero, the converter is operated in the buck-mode, respectively. The switching frequency of the converters is 20 kHz.

5.2.3. The Drive Cycle

The drive cycle used in the simulations is presented in Figure 5.10.

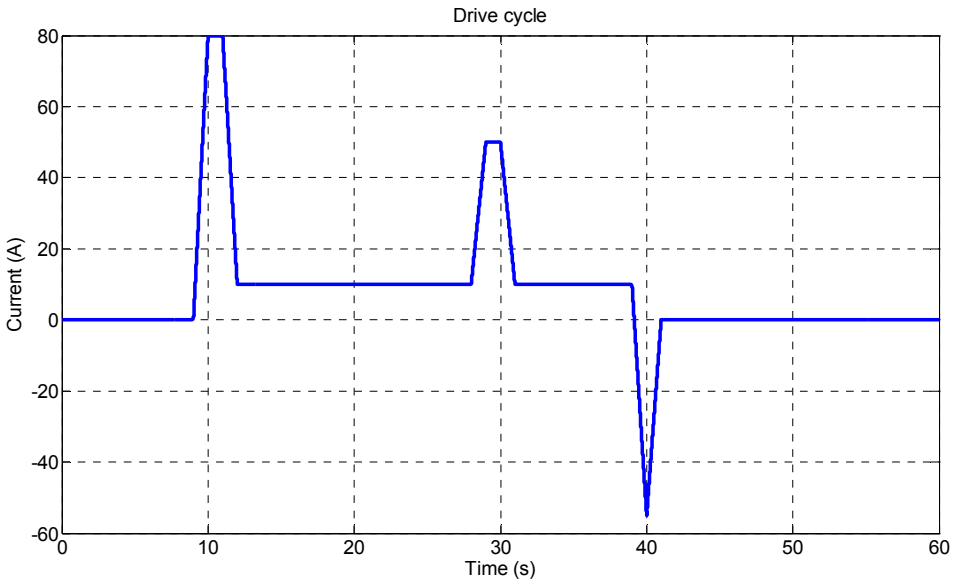

Figure 5.10. *Drive cycle*

The drive cycle is loosely based on a load profile of a forklift but mostly it has been crafted to invoke the properties of the modeled powertrains. The negative peak on the drive cycle is a regenerative braking peak at which time the load delivers power to the DC-bus. Remembering that the DC-bus voltage is nominal 350 V, the highest positive load peak is 28 kW and negative -19.25 kW.

5.3. Results

This subsection describes the results obtained both from the two-way and three-way configurations using the specified drive cycle. The results on the two- and three-way powertrains are divided in their own respective subsections.

5.3.1. Results for the Two-Way Hybrid Fuel Cell Powertrain

Figure 5.11 describes the voltages and currents obtained from the DC-bus.

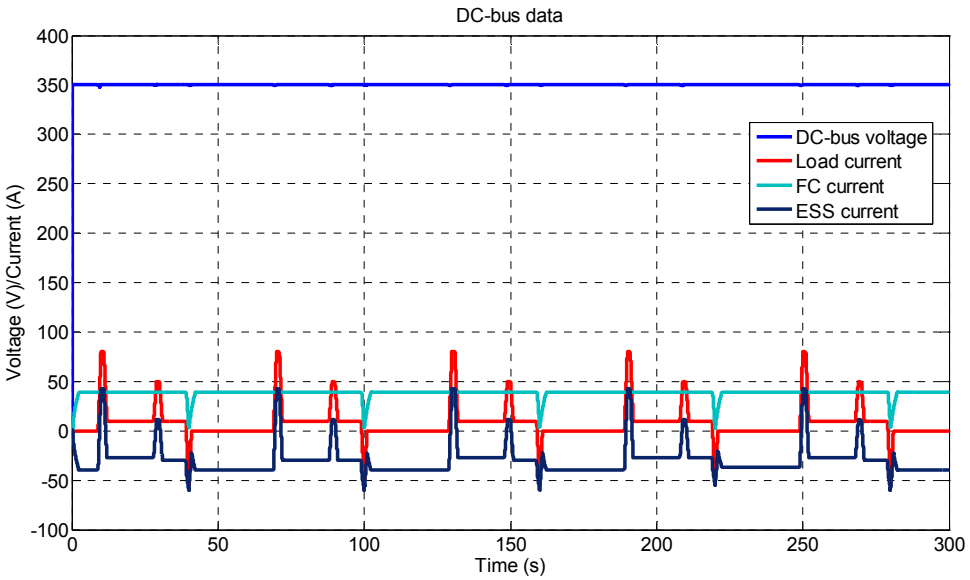

Figure 5.11. *DC-bus results*

As can be concluded from Figure 5.11, the DC-bus voltage remains nominal 350 V with only minor perturbations regardless of load current. The fuel cell current is steady DC when the load current is above or equal to zero. During regenerative braking, it is decreased and increased afterwards in a controlled way. The powertrain works extremely well.

Figure 5.12 describes the DC-bus values from the first cycle i.e. the first 60 seconds of the simulation.

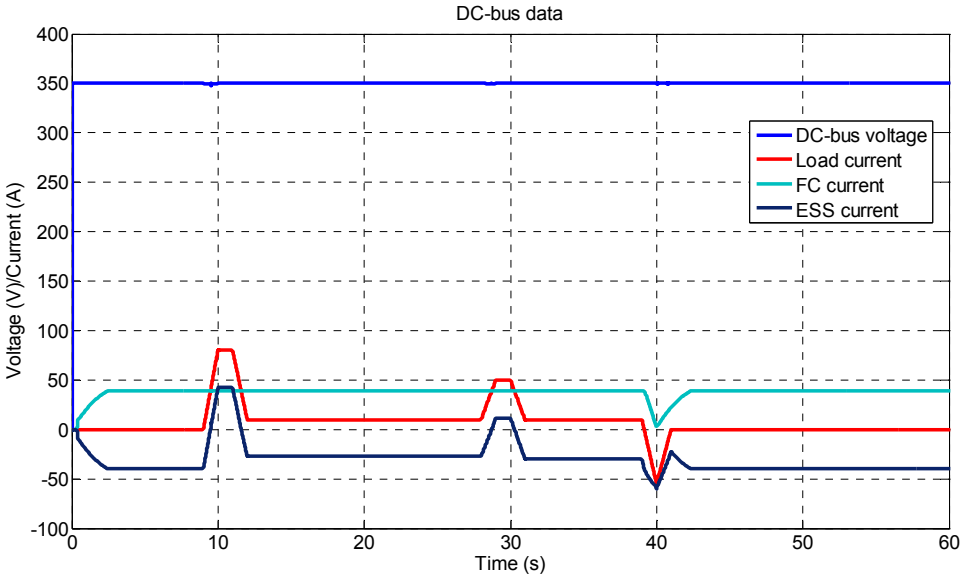

Figure 5.12. *DC-bus results from the first 60 seconds of simulation*

The steadiness of the DC-bus voltage and fuel cell current can be seen in Figure 5.12. At the beginning of the simulation, the DC-bus voltage seems to rise very sharply from

zero to 350 V. This is because the initial value for the DC-bus capacitor is 350 V but the low-pass filters assume zero as an initial value. This causes the sharp rise. Another interesting thing to notice is that the 80 A/s positive ramp rate limitation for the fuel cell current does not linearly raise the fuel cell current at the DC-bus side because the output power of a fuel cell is not linearly dependent in current. The same reasoning applies when the fuel cell current is decreased during regenerative braking.

Figure 5.13 describes the values obtained from the fuel cell terminals.

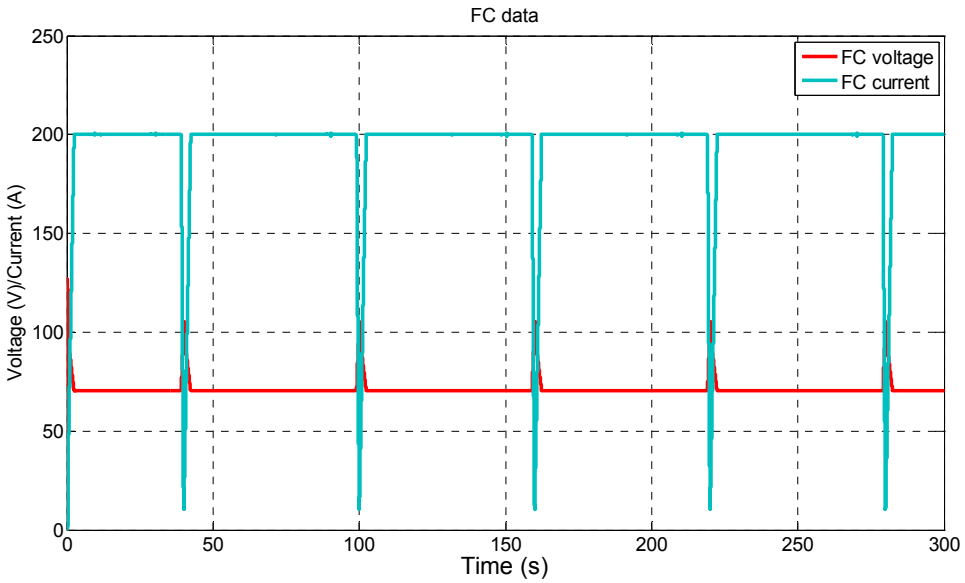

Figure 5.13. *Fuel cell results*

Figure 5.13 reveals that there are slight perturbations in the fuel cell current at times when the bidirectional converter is changing direction. The change in direction has a slight effect on the DC-bus voltage also. The bidirectional converter has slowness in changing the direction. This may be because the converter has to climb through DCM. Whether or not this is a real issue or a simulation deficiency cannot be verified without an actual setup.

Figure 5.14 describes the battery voltage and current.

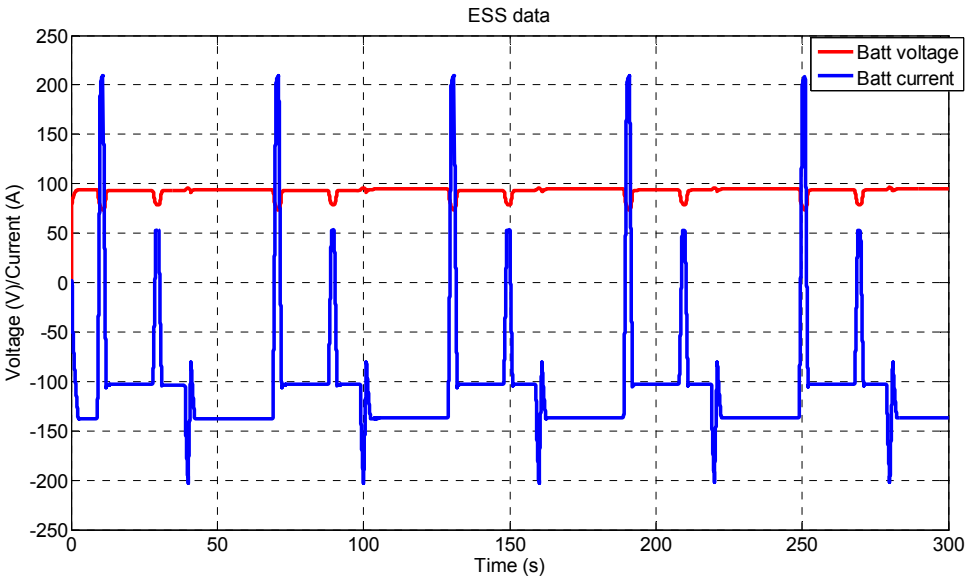

Figure 5.14. *ESS results*

As can be concluded from Figure 5.14, the battery handles basically all transients except during regenerative braking when the fuel cell current is also decreased. The battery current is changing approximately between -200 A and 200 A. In the three-way powertrain, the battery current transients are much smaller.

Figure 5.15 describes the battery state-of-charge.

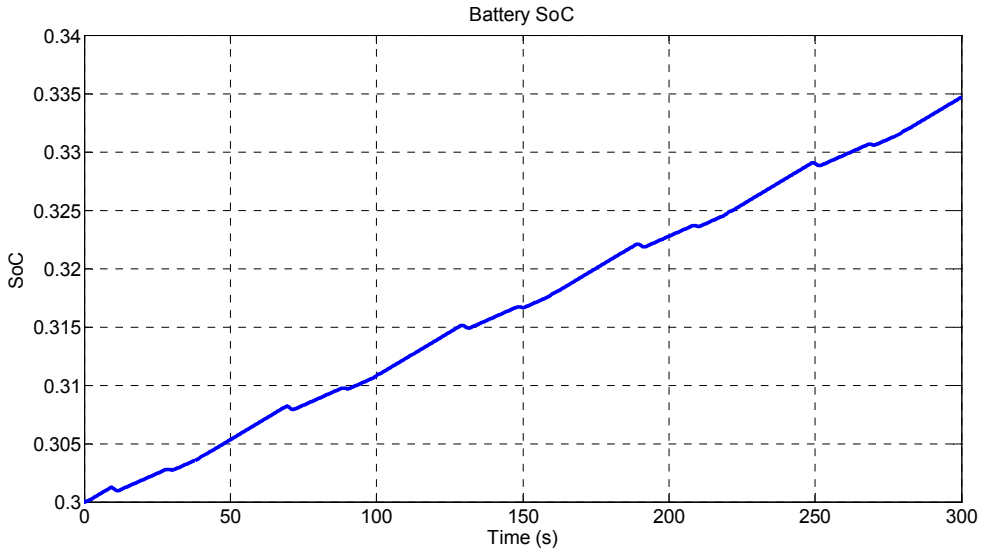

Figure 5.15. *Battery SoC*

Any DC-bus surplus or deficit power is either sinked or supplied by the battery. Figure 5.15 shows that there is a surplus amount of power generated by the fuel cell and the battery SoC changes from 30 % into approximate 33.5 % during the 300 seconds of simulation. A practical powertrain requires a control scheme to control the battery SoC.

5.3.2. Results for the Three-Way Hybrid Fuel Cell Powertrain

This subsection describes the results obtained from the three-way hybrid fuel cell powertrain. Figure 5.16 describes voltages and currents obtained from the DC-bus.

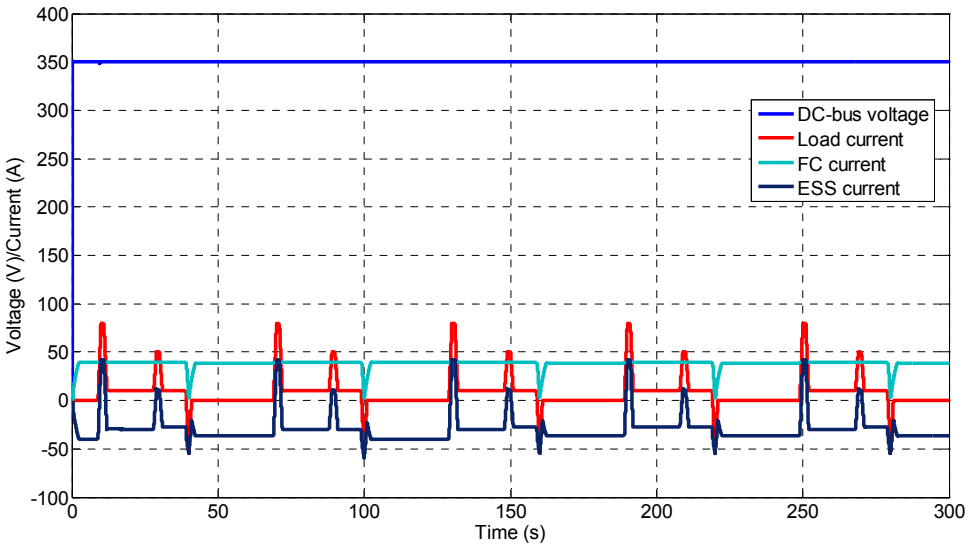

Figure 5.16. *DC-bus results*

The DC-bus voltage and currents are basically the same as with the two-way configuration. Figure 5.17 describes the first 60 seconds of the simulation more in detail.

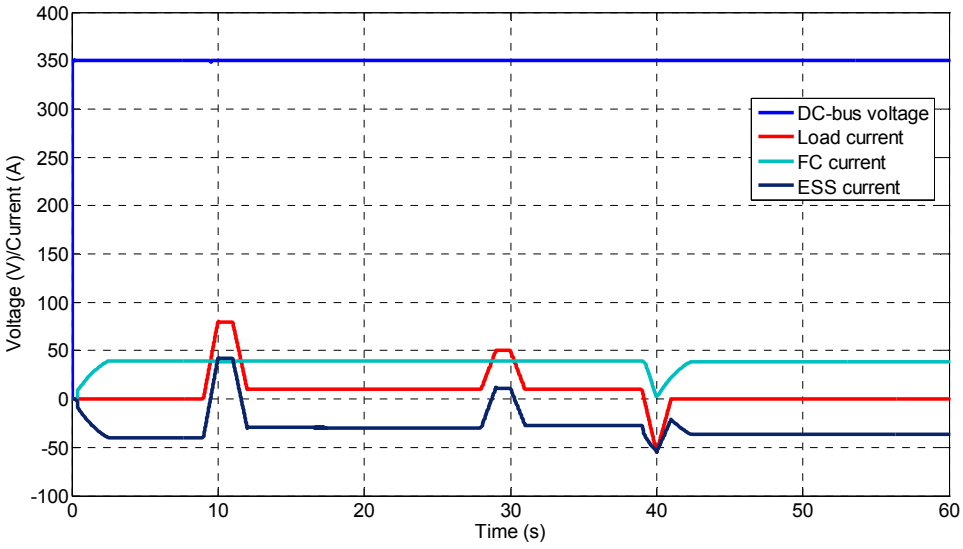

Figure 5.17. *DC-bus results from the first 60 seconds of simulation*

Comparing Figure 5.17 with Figure 5.12, we can conclude that the addition of the supercapacitor in parallel with the battery has nearly no effect at all on the values in the DC-bus.

Figure 5.18 describes the values obtained from the fuel cell terminals.

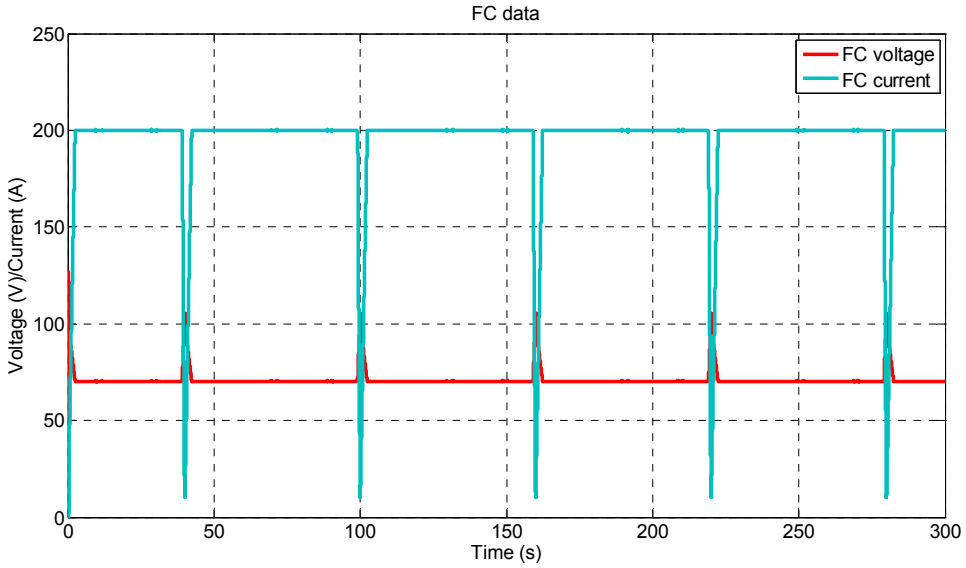

Figure 5.18. *Fuel cell results*

Comparing Figures 5.18 and 5.13, we can conclude that there is little difference between the two results.

Figure 5.19 describes the results obtained from the battery and supercapacitor terminals.

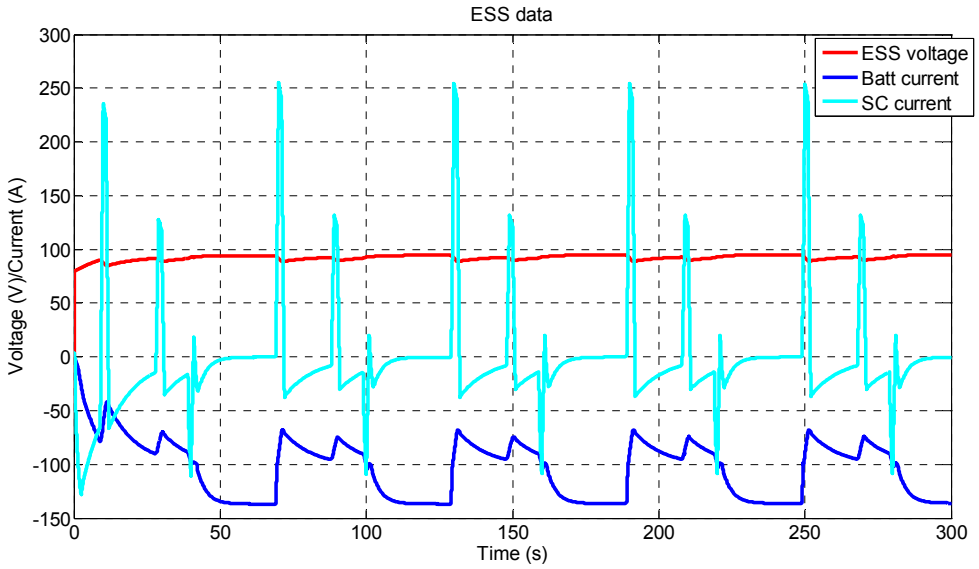

Figure 5.19. *ESS results*

Comparing Figures 5.19 and 5.14, we can conclude that there is a major difference between the two results. In the three-way powertrain case, the supercapacitor handles a great portion of the transients smoothing the battery current and ESS voltage. This may have a positive effect on the battery lifetime as well as may increase the charge/discharge efficiency in general, because supercapacitors are more efficient than batteries in their charge/discharge cycles. The current is clearly distributed according to the impedances of the battery and supercapacitor.

Figure 5.20 describes the battery SoC.

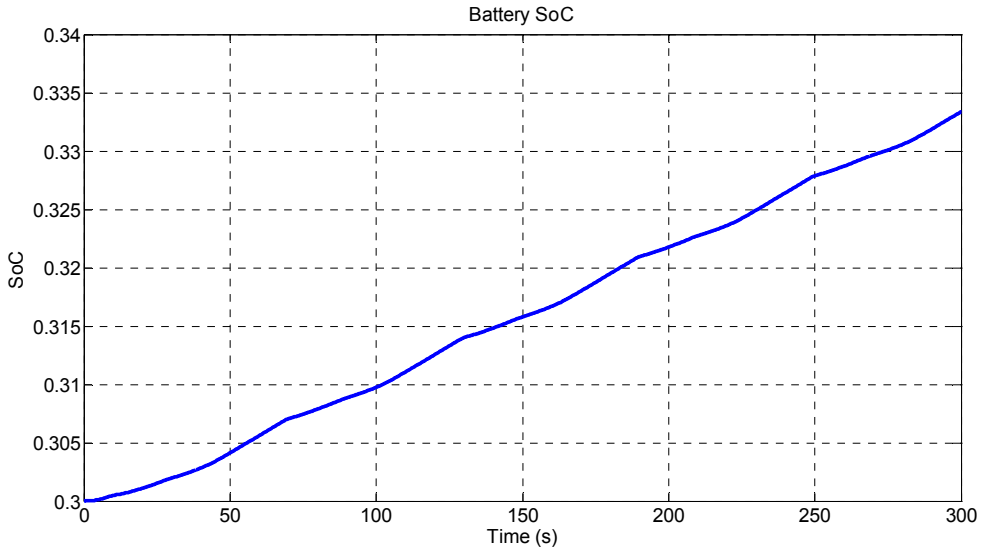

Figure 5.20. *Battery SoC*

According to Figure 5.20, the battery SoC increases from 30 % to approximate 33.5 % during the 300 seconds of simulation. The increase in SoC is the same as in the two-way hybrid fuel cell powertrain discussed previously.

Figure 5.21 describes the supercapacitor SoC.

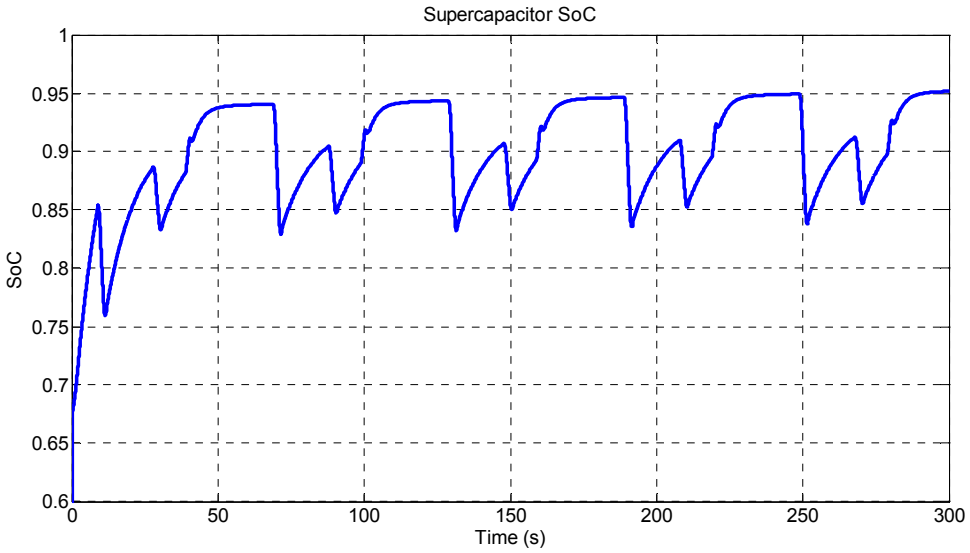

Figure 5.21. *Supercapacitor SoC*

According to Figures 5.20 and 5.21, the balance in currents between the battery and supercapacitor is obtained during the first drive cycle. After the first drive cycle, approximately 10 % of the supercapacitor's SoC is being used during the drive cycles. If the supercapacitor SoC is to be used more fully, the supercapacitor needs to be connected behind its own cascaded DC/DC converter but causes additional issues that have to be dealt with.

5.4. Discussion on the Results

The simulated powertrains work extremely well. The DC-bus voltage stays at nominal 350 V at all the time with only minor deviations. The fuel cell current is almost pure DC (not counting the converter ripples) and is decreased and increased during regenerative braking in a controlled way. However, it was not possible to validate the models and therefore, the accuracy of the models is unknown.

The fuel cell can deliver approximately 16 kW of power whereas the ESS is capable of supplying or sinking approximately 23 kW (depending on the SoC) of power limited by the bidirectional converter 250 A input current limit. The overall powertrain can, therefore, supply the total of 16 kW + 23 kW = 39 kW of power and sink the maximum of 23 kW if the fuel cell current is kept at zero. On the other hand, if the fuel cell supplies 16 kW of power, it limits the powertrain power sinking capability into 23 kW – 16 kW = 7 kW which is quite a low value. This is the reason why the fuel cell current needs to be decreased during regenerative braking.

The powertrain power levels are quite low when compared to the current levels. The 250 A input current is a very high value. A practical converter with this high input current can be hard to realize. In an addition to this, high currents usually cause high losses and require thick cables and heavy components. It can be concluded that the voltage levels of the energy sources are too low. Increasing the voltage levels will

increase power levels and/or drop the current levels into more reasonable values. For example, the present Toyota Prius battery has a voltage of 202 V. [44]

In the light of these findings, it is very clear that appropriate powertrain component sizing is crucial in the design of the powertrain. For example, the simulated powertrains require power from both the fuel cell and the ESS during the highest load peaks. This ultimately results in a fact that the powertrains cannot be used as plug-in powertrains where the power is supplied only from the ESS until the SoC of the ESS is dropped to a certain limit. In an addition to this, the regenerative braking peaks are much higher in practical applications and therefore require higher power sinking capability from the ESS or a brake resistor. A higher voltage ESS with high enough power-handling capability would solve these problems and make the converter design easier.

The three-way configuration has a number of advantages over the two-way configuration: i) the supercapacitor provides transient suppression making the battery current more steady. This has a positive effect on the battery lifetime at least in the case of Lead-acid batteries; [9] ii) the supercapacitor peak-power capability is very high. Thus, the battery power density does not need to be that high because the supercapacitor will provide the largest power transients. This enables battery design of higher specific energy and lifetime; and iii) the energy efficiency of supercapacitors is very high. On the other hand, the energy efficiency of Lead-acid batteries is only in the order of 60 %. [45] The supercapacitor can therefore increase the total energy efficiency when paralleled with the battery.

6. REACTANT STARVATION EXPERIMENT

The reactant starvation phenomenon was measured to assess the need for ramp-rate limitation for fuel cell output current. This chapter presents the obtained results.

The experiment was performed on Nedstack P8 fuel cell stack which can deliver approximately 8 kW of power and its voltage and current ranges are approximately 36 – 48 V and 0 – 250 A, respectively. The fuel cell voltage and current was measured while current transients were applied at the output. Figure 6.1 describes the experimental setup as a block diagram and Figure 6.2 presents a photo of the actual experimental setup.

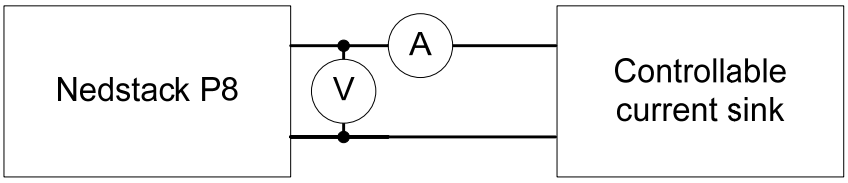

Figure 6.1. *Reactant starvation measurement setup*

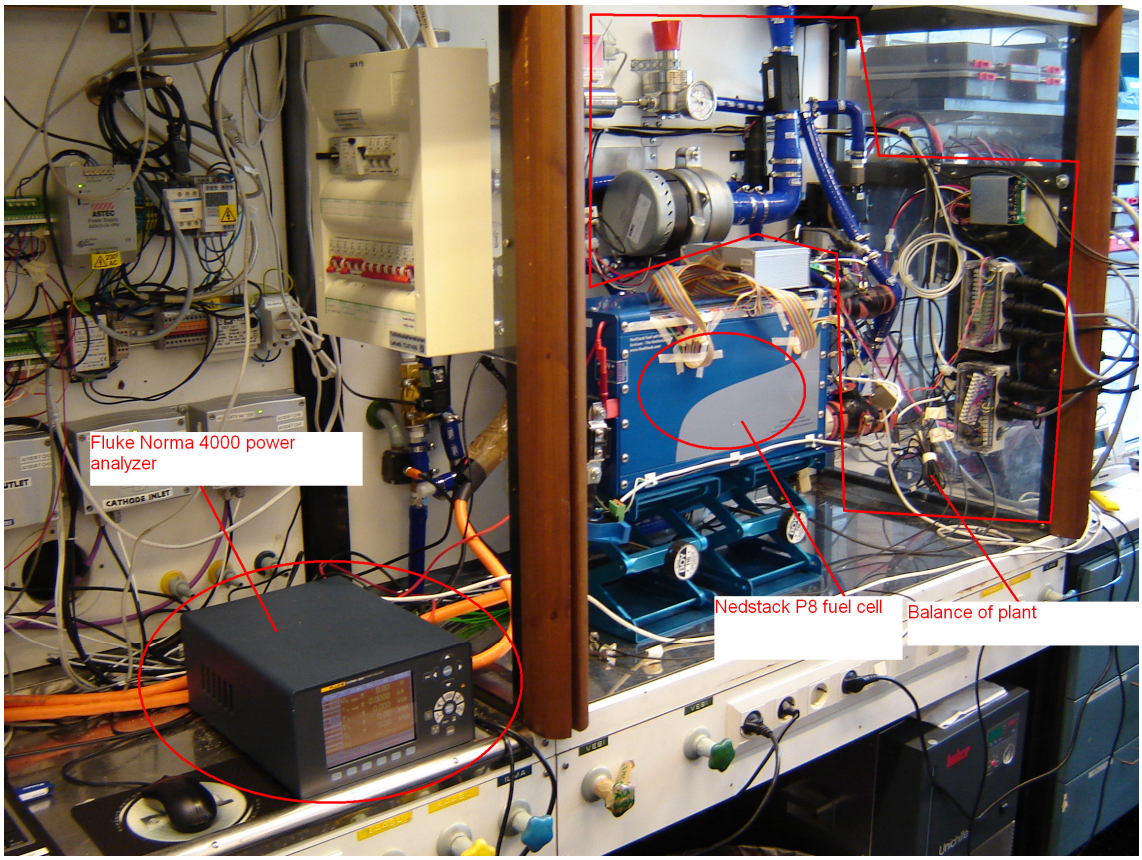

Figure 6.2. *Experimental setup for the reactant starvation measurement*

The measurement device, fuel cell and a portion of BoP can be seen in Figure 6.2. The programmable constant current sink load is excluded from the figure. Fluke Norma 4000 power analyzer was used to measure the fuel cell voltage and current. This was done at approximately 2.7 kHz sampling rate. The load was programmed to provide transients of different magnitudes. The first test was performed without a ramp-rate limitation and the second with 400 A/s ramp-rate.

The fuel cell was first warmed up to nominal operating temperature before applying the transients. A 300 A, 60 mV shunt resistor was used to measure the current. The fuel cell uses hydrogen recirculation and has a purge valve which opens periodically to expel inert gases which accumulate over time. Care was taken for the purge valve to stay closed over the whole measurement period because purge has an effect on the fuel cell voltage.

6.1. Measurement Results

Figure 6.3 presents the reactant starvation experiment without the ramp-rate limitation. In this case, the reactant is air. Hydrogen starvation was avoided by performing a long purge before the measurement.

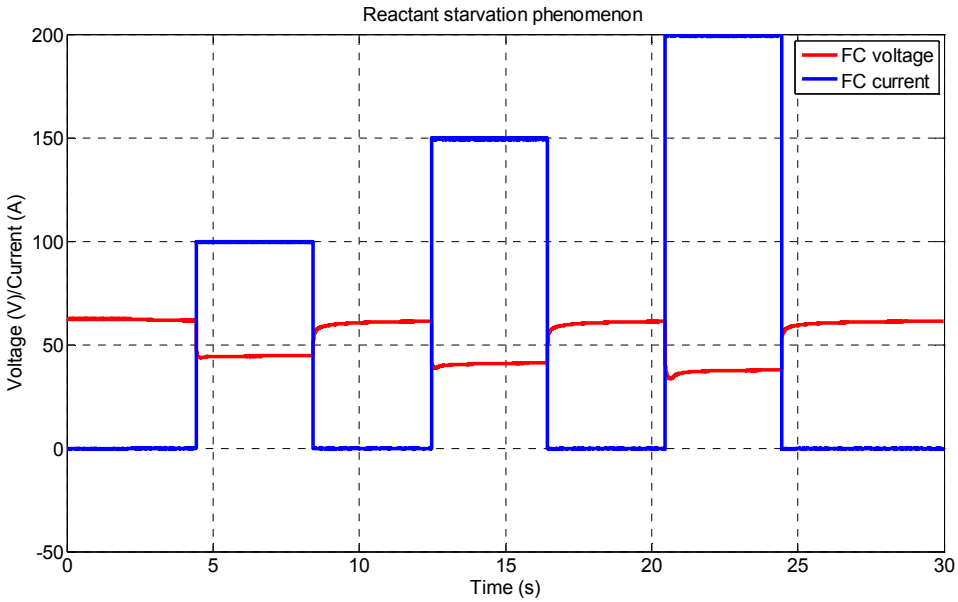

Figure 6.3. *Reactant starvation experiment*

The reactant starvation is best visible after the 0 to 200 A transient as can be concluded from Figure 6.3. It can be also concluded that the reactant starvation phenomenon is present only during the positive transients. Therefore, the ramp-rate limitation should be implemented only to the positive direction. It follows that the fuel cell output current can be decreased without restrictions.

Figure 6.4 describes the 0 to 200 A transient.

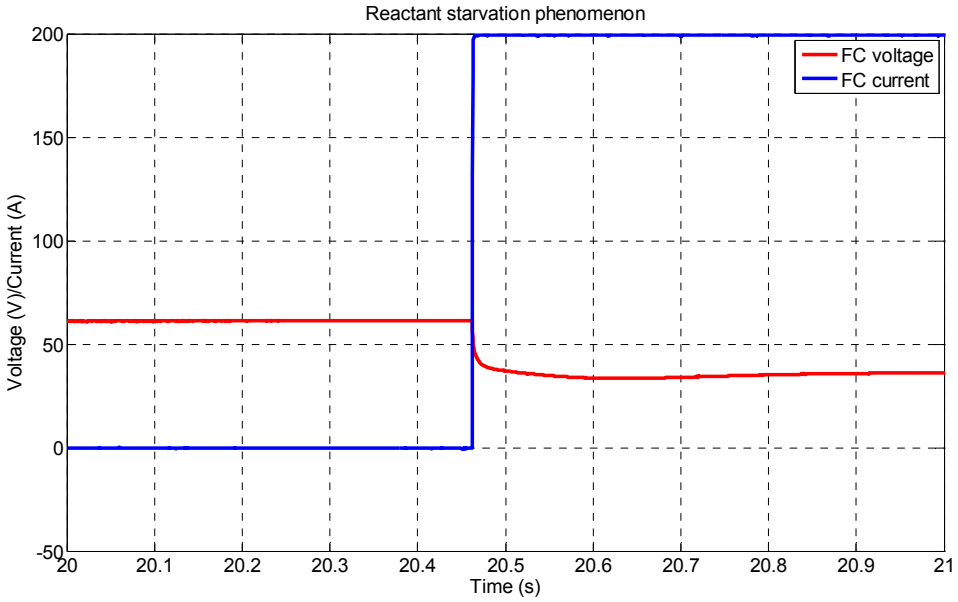

Figure 6.4. *0 to 200 A transient*

The reactant starvation phenomenon is clearly visible in Figure 6.4. Its effect is an additional voltage drop before the reactant supply systems can respond and stabilize the

voltage into a final value. From Figure 6.4, it can be concluded that the voltage drops from 61.2 V to the minimum of 33.5 V and then stabilizes to 37.7 V. The reactant starvation is very harmful to the fuel cell lifetime as was explained in Subsection 3.1.1. A ramp-rate limitation should be implemented into the downstream converter in order for the reactant supply to be able to respond to the changed output current demand. Figure 6.5 describes the 0 to 200 A current transient with a 400 A/s ramp-rate.

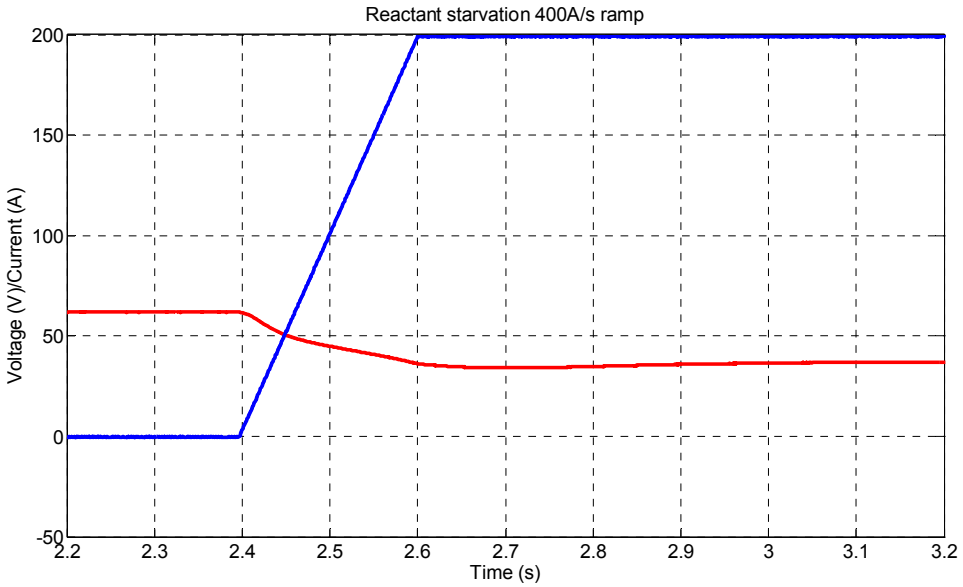

Figure 6.5. *0 to 200 A with 400 A/s ramp-rate*

According to Figure 6.5, the reactant starvation phenomenon still remains but the minimum voltage is now 34.1 V which is 600 mV higher than the minimum voltage without the ramp-rate. Also, the voltage drop occurs much more slowly. Limiting the ramp-rate further can remove the reactant starvation phenomenon completely. Unfortunately, it was not possible to test this because the load could not provide smaller ramp-rates than 400 A/s. However, based on the fuel cell operational experiences, approximately 100 A/s should be sufficient.

7. CONCLUSION

The goal of this thesis has been to study the aspects of power electronics in hybrid fuel cell powertrains and to bring knowledge of those aspects to the VTT fuel cells team. From the simulations, it is easy to conclude that it is possible to construct a very stable and properly working hybrid fuel cell powertrain provided that attention has been paid on wide variety of issues. However, as the models were not verified, a practical powertrain needs to be built to verify the results and to study the problems associated with the construction.

The results indicate, that in order to construct a stable and properly operating hybrid powertrain, several issues have to be carefully considered such as: i) correct powertrain configuration; ii) correct sizing of the energy source components based on load profiles; iii) proper selection of voltage levels; iv) implementation of proper DC/DC topologies; v) careful design of converter control loops; and vi) implementation of proper power management strategies. In addition to these, it is clear that the practical implementation would yield more issues to be treated and solved.

7.1. Suggestions for Future Work

It is clear that the implementation of power electronics in hybrid fuel cell powertrains is a very wide topic. This thesis has only scratched the surface of the issues that have to be taken into account when designing such powertrains.

One of the issues, that has not been discussed at all in this thesis, is scalability of the powertrain. Scalability is a very important aspect because powertrains can be constructed in many power levels. Smaller powertrains should not be a problem in terms of power electronics but scaling up the power levels can be a different matter. Examining the simulation results obtained in this thesis, it is clear that it is easy to increase the power levels by increasing the voltage levels of the various energy sources. Unfortunately, this can be done only up to a certain limit, which eventually leads to a fact that current levels have to be increased in order to increase power levels even further. This can cause problems in implementing the practical converters. However, there is a possibility of paralleling converters or increasing the number of converter legs in case of the interleaved converters. This can also have the advantage of increasing the overall reliability of the powertrain because the powertrain could be designed to operate at partial power during failure of one or more converters/converter legs. In any case, further work should be made on this subject.

REFERENCES

1. Thounthong, P., Davat, B., Rael, S. & Sethakul, P. Fuel cell high-power applications. Industrial Electronics Magazine, IEEE 2009, Vol. 3, No. 1, pp. 32-46. ISSN 1932-4529.

2. Karimäki, H. Ajoneuvokäytön polttokennoteholähteen hybridisointi – teoreettinen je kokeellinen tarkastelu. Master of Science ed. Tampere University of Technology: 2009.

3. Burke, A.F. Batteries and Ultracapacitors for Electric, Hybrid, and Fuel Cell Vehicles. Proceedings of the IEEE 2007, Vol. 95, No. 4, pp. 806-820. ISSN 0018-9219.

4. Borup, R.L., Davey, J.R., Garzon, F.H., Wood, D.L. & Inbody, M.A. PEM fuel cell electrocatalyst durability measurements. Journal of Power Sources 2006, 12/7, Vol. 163, No. 1, pp. 76-81. ISSN 0378-7753. doi: DOI: 10.1016/j.jpowsour.2006.03.009.

5. Bernard, J., Delprat, S., Buchi, F.N. & Guerra, T.M. Fuel-Cell Hybrid Powertrain: Toward Minimization of Hydrogen Consumption. Vehicular Technology, IEEE Transactions on 2009, Vol. 58, No. 7, pp. 3168-3176. ISSN 0018-9545.

6. Bauman, J. & Kazerani, M. A Comparative Study of Fuel-Cell–Battery, Fuel-Cell–Ultracapacitor, and Fuel-Cell–Battery–Ultracapacitor Vehicles. Vehicular Technology, IEEE Transactions on 2008, Vol. 57, No. 2, pp. 760-769. ISSN 0018-9545.

7. Al Sakka, M., Van Mierlo, J., Gualous, H. & Lataire, P. Comparison of 30KW DC/DC converter topologies interfaces for fuel cell in hybrid electric vehicle. Power Electronics and Applications, 2009. EPE '09. 13th European Conference on. 2009. Pp. 1.

8. A123 Systems Technical data from A123 Systems web page, 2010, Available: http://www.a123systems.com/a123/technology [2010, 8/24] .

9. Bentley, P. & Stone, D.A. The parallel combination of a valve regulated lead acid cell and supercapacitor for use as a hybrid vehicle peak power buffer. Power Electronics and Applications, 2005 European Conference on. 2005. Pp. 10 pp. .

10. Bernard, J., Delprat, S., Guerra, T.M. & Büchi, F.N. Fuel efficient power management strategy for fuel cell hybrid powertrains. Control Engineering

Practice 2010, 4, Vol. 18, No. 4, pp. 408-417. ISSN 0967-0661. doi: DOI: 10.1016/j.conengprac.2009.12.009.

11. Li, X., Xu, L., Hua, J., Lin, X., Li, J. & Ouyang, M. Power management strategy for vehicular-applied hybrid fuel cell/battery power system. Journal of Power Sources 2009, 6/15, Vol. 191, No. 2, pp. 542-549. ISSN 0378-7753. doi: DOI: 10.1016/j.jpowsour.2009.01.092.

12. Johnson Matthey Platinum Today, the worlds leading authority on platinum group metals, 2010, Available: http://www.platinum.matthey.com/ [2010, .

13. Spendelow, J., Martin, K.E. & Papageorgopoulos, D. Platinum Group Metal Loading. [Online], . Available from: http://www.hydrogen.energy.gov/pdfs/9018_platinum_group.pdf.

14. Ballard Integration of heavy-duty PEM fuel cell systems, 2008, (17.9.2008-last update). Available: http://akseli.tekes.fi/opencms/opencms/OhjelmaPortaali/ohjelmat/Polttokennot/fi/Dokumenttiarkisto/Viestinta_ja_aktivointi/Seminaarit/17.9.2008_Finland-Germany_workshop/Straub.pdf [2010, 5/12] .

15. Shen, Q., Hou, M., Liang, D., Zhou, Z., Li, X., Shao, Z. & Yi, B. Study on the processes of start-up and shutdown in proton exchange membrane fuel cells. Journal of Power Sources 2009, 4/15, Vol. 189, No. 2, pp. 1114-1119. ISSN 0378-7753. doi: DOI: 10.1016/j.jpowsour.2008.12.075.

16. U.S. Department of Energy Fuel Cell Handbook (Seventh Edition). U.S Department of Energy, Office of Fossil Energy, 2004. 427. http://www.netl.doe.gov/technologies/coalpower/fuelcells/seca/pubs/FCHandbook7.pdf;.

17. Ordonez, M., Sonnaillon, M.O., Quaicoe, J.E. & Iqbal, M.T. An Embedded Frequency Response Analyzer for Fuel Cell Monitoring and Characterization. Industrial Electronics, IEEE Transactions on 2010, Vol. 57, No. 6, pp. 1925-1934. ISSN 0278-0046.

18. Laffly, E., Pera, M.-. & Hissel, D. Dynamic Model of a Polymer Electrolyte Fuel Cell Power Device. IEEE Industrial Electronics, IECON 2006 - 32nd Annual Conference on. 2006. Pp. 466. ISBN 1553-572X.

19. Fontes, G., Turpin, C., Astier, S. & Meynard, T.A. Interactions Between Fuel Cells and Power Converters: Influence of Current Harmonics on a Fuel Cell Stack. Power Electronics, IEEE Transactions on 2007, Vol. 22, No. 2, pp. 670-678. ISSN 0885-8993.

20. Gemmen, R.S. Analysis for the Effect of Inverter Ripple Current on Fuel Cell Operating Condition. Journal of Fluids Engineering 2003, May 2003, Vol. 125, No. 3, pp. 576-585. doi: 10.1115/1.1567307. http://link.aip.org/link/?JFG/125/576/1.

21. Wahdame, B., Girardot, L., Hissel, D., Harel, F., Francois, X., Candusso, D., Pera, M.C. & Dumercy, L. Impact of power converter current ripple on the durability of a fuel cell stack. Industrial Electronics, 2008. ISIE 2008. IEEE International Symposium on. 2008. Pp. 1495.

22. Changrong Liu & Jih-Sheng Lai Low Frequency Current Ripple Reduction Technique With Active Control in a Fuel Cell Power System With Inverter Load. Power Electronics, IEEE Transactions on 2007, Vol. 22, No. 4, pp. 1429-1436. ISSN 0885-8993.

23. Shireen, W., Kulkarni, R.A. & Arefeen, M. Analysis and minimization of input ripple current in PWM inverters for designing reliable fuel cell power systems. Journal of Power Sources 2006, 6/1, Vol. 156, No. 2, pp. 448-454. ISSN 0378-7753. doi: DOI: 10.1016/j.jpowsour.2005.06.012.

24. Linden, D. & Reddy, T.B. Handbook of Batteries (3rd Edition). McGraw-Hill, 2002.

25. ANL/ESD/08-1. Patil, P.G. Developments in lithium-ion battery technology in the Peoples Republic of China. Argonne National Laboratory, IL (USA), 2008.

26. Dürr, M., Cruden, A., Gair, S. & McDonald, J.R. Dynamic model of a lead acid battery for use in a domestic fuel cell system. Journal of Power Sources 2006, 10/27, Vol. 161, No. 2, pp. 1400-1411. ISSN 0378-7753. doi: DOI: 10.1016/j.jpowsour.2005.12.075.

27. Tenno, A., Tenno, R. & Suntio, T. Battery impedance and its relationship to battery characteristics. Telecommunications Energy Conference, 2002. INTELEC. 24th Annual International. 2002. Pp. 176.

28. Ruddell, A.J., Dutton, A.G., Wenzl, H., Ropeter, C., Sauer, D.U., Merten, J., Orfanogiannis, C., Twidell, J.W. & Vezin, P. Analysis of battery current microcycles in autonomous renewable energy systems. Journal of Power Sources 2002, 11/14, Vol. 112, No. 2, pp. 531-546. ISSN 0378-7753. doi: DOI: 10.1016/S0378-7753(02)00457-3.

29. Schindall, J. The Charge of the Ultra-Capacitors. IEEE spectrum November 2007, .

30. NREL: National Renewable Energy Laboratory Ultracapacitors, 2009, (September 30, 2009-last update). Available: http://www.nrel.gov/vehiclesandfuels/energystorage/ultracapacitors.html [2010, 5/4] .

31. Maxwell Technologies DATASHEET 48 V MODULESAvailable: http://www.maxwell.com/ultracapacitors/datasheets/DATASHEET_48V_series_1009365.pdf [2010, 5/5] .

32. Maxwell Technologies Datasheet, K2 Series 650F - 3,000F Ultracapacitors. Maxwell Technologies, .

33. Maxwell Technologies Cell Balancing in Low Duty Cycle Applications.

34. Maxwell Technologies Maxwell Active Cell Voltage Management Electronics. 2007.

35. Rafik, F., Gualous, H., Gallay, R., Crausaz, A. & Berthon, A. Frequency, thermal and voltage supercapacitor characterization and modeling. Journal of Power Sources 2007, 3/20, Vol. 165, No. 2, pp. 928-934. ISSN 0378-7753. doi: DOI: 10.1016/j.jpowsour.2006.12.021.

36. Basu, S. & Undeland, T.M. Voltage and current ripple considerations for improving lifetime of Ultra-Capacitors used for energy buffer applications at converter inputs. Applied Power Electronics Conference and Exposition (APEC), 2010 Twenty-Fifth Annual IEEE. 2010. Pp. 244. ISBN 1048-2334.

37. Yu, X., Starke, M.R., Tolbert, L.M. & Ozpineci, B. Fuel cell power conditioning for electric power applications: a summary. Electric Power Applications, IET 2007, Vol. 1, No. 5, pp. 643-656. ISSN 1751-8660.

38. Thounthong, P., Sethakul, P., Rael, S. & Davat, B. Modeling and control of a fuel cell current control loop of a 4-phase interleaved step-up converter for DC distributed system. Power Electronics Specialists Conference, 2008. PESC 2008. IEEE. 2008. Pp. 230. ISBN 0275-9306.

39. Junhong Zhang, Rae-young Kim & Jih-Sheng Lai High-Power Density Design of a Soft-Switching High-Power Bidirectional DC-DC Converter. Power Electronics Specialists Conference, 2006. PESC '06. 37th IEEE. 2006. Pp. 1. ISBN 0275-9306.

40. Averberg, A. & Mertens, A. Design considerations of a voltage-fed full bridge DC-DC converter with high voltage gain for fuel cell applications. Power Electronics and Applications, 2007 European Conference on. 2007. Pp. 1.

41. Jih-Sheng Lai & Nelson, D.J. Energy Management Power Converters in Hybrid Electric and Fuel Cell Vehicles. Proceedings of the IEEE 2007, Vol. 95, No. 4, pp. 766-777. ISSN 0018-9219.

42. Suntio, T. Dynamic Profile of Switched-Mode Converter: Modeling, Analysis and Control. WILEY-VCH, 2009. 369. ISBN 978-3-527-40708-8.

43. Jung-Min Kwon, Eung-Ho Kim, Bong-Hwan Kwon & Kwang-Hee Nam High-Efficiency Fuel Cell Power Conditioning System With Input Current Ripple Reduction. Industrial Electronics, IEEE Transactions on 2009, Vol. 56, No. 3, pp. 826-834. ISSN 0278-0046.

44. Toyota Toyota Prius eBrochure [Homepage of Toyota], [Online]Available: http://www.toyota.com/prius-hybrid/specs.html [2010, 8/20] .

45. Hua, A.C. & Syue, B.Z. Charge and discharge characteristics of lead-acid battery and LiFePO4 battery. Power Electronics Conference (IPEC), 2010 International. 2010. Pp. 1478.

APPENDIX 1: BOOST CONVERTER DYNAMIC EQUATIONS

In this appendix, general dynamic equations will be derived for a boost converter using state-space representations. State-space method provides insight into the internal workings of a converter. It is very important to include parasitic elements in the dynamical analysis of DC/DC converters because they affect the dynamics of a converter.

A converter is a non-linear system with number of inputs which yield another set of outputs. A convenient way to model a converter is to use state space averaging (SSA). SSA gives excellent results for converters in CCM but has problems in DCM. Therefore only CCM analysis will be performed. A converter is analyzed in such a way that every sub circuit corresponding to different states is drawn. The input variables and state variable derivatives are expressed as output variables and state variables using Kirchhoff voltage and current laws. The results are equations for on- and off-time sub circuits. In order to stipulate the average behaviour of a converter, the sub circuit equations are multiplied by the duty ratio d and its complement d' and added together. The resulting averaged equation represents the nonlinear average behaviour of a converter. In order to it to be more useful, it needs to be linearized by taking proper partial derivatives, forming the small signal state space representation. When this small signal state space representation is converted into Laplace domain with zero initial conditions, the time-domain small signal state space is solved in frequency domain. This method yields a frequency dependent input-to-output description in the form of (A1.1).

$$y(s) = G(s)u(s) = \left[C(sI - A)^{-1}B + D\right]u(s) \qquad \text{(A1.1)}$$

In A1.1, y(s) is the output vector, u(s) the input vector, I is an identity matrix and -1 is a matrix inverse function. G(s) is called the transfer function matrix consisting of G- or Y-parameter representation. The G(s) becomes (A1.2) for voltage output type converters and (A1.3) for current output type converters. Though (4.2) and (4.3) may look similar for the most part, expect for the output impedance, the actual values of the parameters are very different for voltage and current output type converters.

$$G(s) = \begin{bmatrix} Y^{v}_{in-o} & T^{v}_{oi-o} & G^{v}_{ci} \\ G^{v}_{io-o} & -Z^{v}_{o-o} & G^{v}_{co} \end{bmatrix} \qquad \text{(A1.2)}$$

$$G(s)=\begin{bmatrix} Y^{i}_{in-o} & T^{i}_{oi-o} & G^{i}_{ci} \\ G^{i}_{io-o} & -Y^{i}_{o-o} & G^{i}_{co} \end{bmatrix} \quad \text{(A1.3)}$$

where

Y_{in-o} = input admittance
T_{oi-o} = reverse or output-to-input transfer function
G_{ci} = control-to-input transfer function
G_{io-o} = forward, input-to-output, line-to-output transfer function or audio-susceptibility
Z_{o-o} = output impedance
Y_{o-o} = output admittance
G_{co} = control-to-output transfer function

The G-parameter transfer function matrix (A1.2) is derived for VFVO boost converter depicted in Figure A1.1. It is important to include the parasitic elements of the different components in order to get accurate dynamic representations.

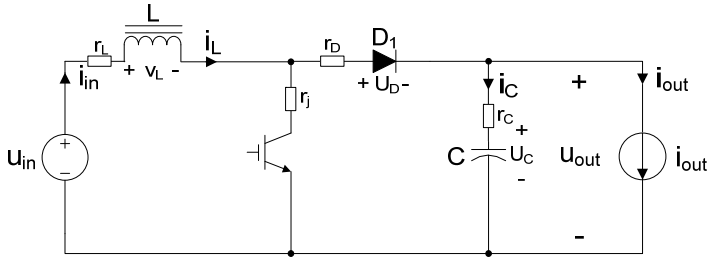

Figure A1.1. *A boost converter with parasitics*

The analysis starts from drawing the on- and off-time sub circuits described in Figures A1.2 and A1.3 respectively.

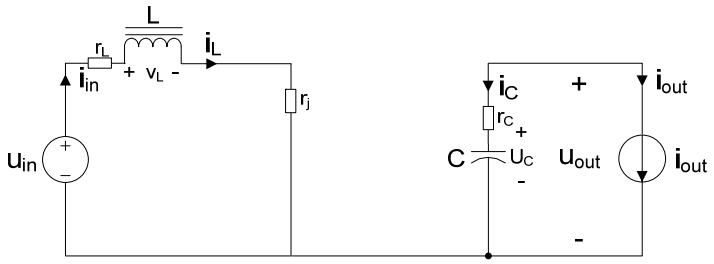

Figure A1.2. *Boost converter on-time sub circuit with parasitics*

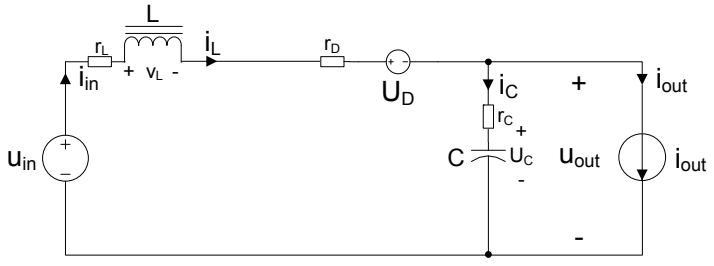

Figure A1.3. *Boost converter off-time sub circuit with parasitics*

The output variables and the associated derivatives of memory elements have to be derived as a function of input variables and state variables. In our case the respective variables are presented in Table A1.1.

Table A1.1. *Boost converter variables*

Output variables	Input variables	State variables
i_{in}	u_{in}	i_L
u_{out}	i_{out}	u_C

The memory element derivatives are formed from inductor and capacitor equations:

$$u_L = L\frac{di_L}{dt} => \frac{di_L}{dt} = \frac{u_L}{L} \tag{A1.4}$$

$$i_C = C\frac{du_C}{dt} => \frac{du_C}{dt} = \frac{i_C}{C} \tag{A1.5}$$

Using Kirchhoff voltage and current laws, we can form the expressions for the output variables and the state variable derivatives for the on-time sub circuit:

$$u_L = u_{in} - (r_L + r_j)i_L \tag{A1.6}$$

$$i_C = -i_{out} \tag{A1.7}$$

$$u_{out} = u_C + r_C i_C \tag{A1.8}$$

$$i_{in} = i_L \tag{A1.9}$$

Next the off-time sub circuit is analyzed. Applying Kirchhoff voltage and current law for the off-time sub circuit we get:

$$u_L = u_{in} - u_{out} - U_D - (r_L + r_D)i_L \tag{A1.10}$$

$$i_C = i_L - i_{out} \tag{A1.11}$$

$$u_{out} = u_C + r_C i_C \tag{A1.12}$$

$$i_{in} = i_L \tag{A1.13}$$

Combining the on-time and off-time equations with the state variable derivative Equations (A1.4-A1.5) and using the required formalism we get state space equations for on- and off-times.

On-time state space equations:

$$\frac{di_L}{dt} = -\frac{(r_L + r_j)i_L}{L} + \frac{u_{in}}{L} \tag{A1.14}$$

$$\frac{du_C}{dt} = -\frac{i_{out}}{C} \tag{A1.15}$$

$$i_{in} = i_L \tag{A1.16}$$

$$u_{out} = u_C - r_C i_{out} \tag{A1.17}$$

Off-time state space equations:

$$\frac{di_L}{dt} = -\frac{(r_L + r_D + r_C)i_L}{L} - \frac{u_C}{L} + \frac{u_{in}}{L} + \frac{r_C i_{out}}{L} - \frac{U_D}{L} \tag{A1.18}$$

$$\frac{du_C}{dt} = \frac{i_L}{C} - \frac{i_{out}}{C} \tag{A1.19}$$

$$i_{in} = i_L \tag{A1.20}$$

$$u_{out} = r_C i_L + u_C - r_C i_{out} \tag{A1.21}$$

SSA is formed when the on-time equations are multiplied with the duty ratio d and off-time equations with its complement d' and the resulting equations are added together. Remembering that d + d' = 1.

Averaged state space equations:

$$\frac{di_L}{dt} = -\frac{(r_L + dr_j + d'r_D + d'r_C)i_L}{L} - \frac{d'u_C}{L} + \frac{u_{in}}{L} + \frac{d' r_C i_{out}}{L} - \frac{d'U_D}{L} \tag{A1.22}$$

$$\frac{du_C}{dt} = \frac{d'i_L}{C} - \frac{i_{out}}{C} \tag{A1.23}$$

$$i_{in} = i_L \tag{A1.24}$$

$$u_{out} = d'r_C i_L + u_C - r_C i_{out} \tag{A1.25}$$

Next a small signal representation is formed by taking the proper partial derivatives. In this linearized state space, a hat over the variables represents small perturbation around the corresponding steady-state value and capital letters represent the steady-state values. It should be noted that a steady-state value of a capacitor voltage is the same as the steady state output voltage.

Small signal state space equations:

$$\frac{d\hat{i}_L}{dt} = -\frac{(r_L + Dr_j + D'r_D + Dr_C)\hat{i}_L}{L} - \frac{D'\hat{u}_C}{L} + \frac{\hat{u}_{in}}{L} + \frac{D'r_C\hat{i}_{out}}{L} + \frac{U_{out} + U_D + (r_D + Dr_C - r_j)I_L}{L}\hat{d} \quad \text{(A1.26)}$$

$$\frac{d\hat{u}_C}{dt} = \frac{D'\hat{i}_L}{C} - \frac{\hat{i}_{out}}{C} - \frac{I_L}{C}\hat{d} \quad \text{(A1.27)}$$

$$\hat{i}_{in} = \hat{i}_L \quad \text{(A1.28)}$$

$$\hat{u}_{out} = D'r_C\hat{i}_L + \hat{u}_C - r_C\hat{i}_{out} - r_C I_L\hat{d} \quad \text{(A1.29)}$$

The small signal state space Equations (A1.26-A1.29) are conveniently represented as matrices in a form of:

$$\begin{aligned} \dot{x}(t) &= Ax(t) + Bu(t) \\ y(t) &= Cx(t) + Du(t) \end{aligned} \quad \text{(A1.30)}$$

In (A1.30), x(t) is the state-variable vector, the dot over x(t) is the derivative of x(t), u(t) is the input vector, and y(t) is the output vector. The entries in the matrices A, B, C and D are scalars for the linearized system. Thus, the small signal state space (A1.26-A1.29) becomes:

$$\begin{bmatrix} \frac{d\hat{i}_L}{dt} \\ \frac{d\hat{u}_C}{dt} \end{bmatrix} = \begin{bmatrix} -\frac{r_L + Dr_j + D'(r_D + r_C)}{L} & -\frac{D'}{L} \\ \frac{D'}{C} & 0 \end{bmatrix} \begin{bmatrix} \hat{i}_L \\ \hat{u}_C \end{bmatrix} + \begin{bmatrix} \frac{1}{L} & \frac{D'r_C}{L} & \frac{U_{out} + U_D + (r_D + Dr_C - r_j)I_L}{L} \\ 0 & -\frac{1}{C} & -\frac{I_L}{C} \end{bmatrix} \begin{bmatrix} \hat{u}_{in} \\ \hat{i}_{out} \\ \hat{d} \end{bmatrix} \quad \text{(A1.31)}$$

$$\begin{bmatrix} \hat{i}_{in} \\ \hat{u}_{out} \end{bmatrix} = \begin{bmatrix} 1 & 0 \\ D'r_C & 1 \end{bmatrix} \begin{bmatrix} \hat{i}_L \\ \hat{u}_C \end{bmatrix} + \begin{bmatrix} 0 & 0 & 0 \\ 0 & -r_C & -r_C I_L \end{bmatrix} \begin{bmatrix} \hat{u}_{in} \\ \hat{i}_{out} \\ \hat{d} \end{bmatrix} \quad \text{(A1.32)}$$

Next, the matrices (A1.31) and (A1.32) are stated in Laplace domain to get an input-to-output description of:

$$y(s) = G(s)u(s) = \left[C(sI - A)^{-1}B + D\right]u(s) \quad \text{(A1.33)}$$

From (A1.33), we can derive the transfer function matrix G(s):

$$G(s)=\begin{bmatrix} Y^{v}_{in-o} & T^{v}_{oi-o} & G^{v}_{ci} \\ G^{v}_{io-o} & -Z^{v}_{o-o} & G^{v}_{co} \end{bmatrix}=$$

$$\frac{\begin{bmatrix} \frac{s}{L} & \frac{D'(1+sr_CC)}{LC} \\ \frac{D'(1+sr_CC)}{LC} & \frac{(r_L+Dr_j+D'r_D+DD'r_C+sL)(1+sr_CC)}{LC} \end{bmatrix} \begin{bmatrix} \frac{D'I_L}{LC}(1+s(\frac{U_{out}+U_D}{D'I_L}+\frac{r_D+Dr_C-r_j}{D'})C) \\ \frac{(D'(U_{out}+U_D)-(r_L+r_j+D'^2r_C)I_L-sLI_L)(1+sr_CC)}{LC} \end{bmatrix}}{s^2+s\frac{r_L+Dr_j+D'(r_D+r_C)}{L}+\frac{D'^2}{LC}} \qquad \text{(A1.34)}$$

(A4.34) contains the set of symbolical dynamic equations representing the dynamical behaviour of a VFVO boost converter.

APPENDIX 2: TWO-WAY HYBRID FUEL CELL POWERTRAIN MODEL

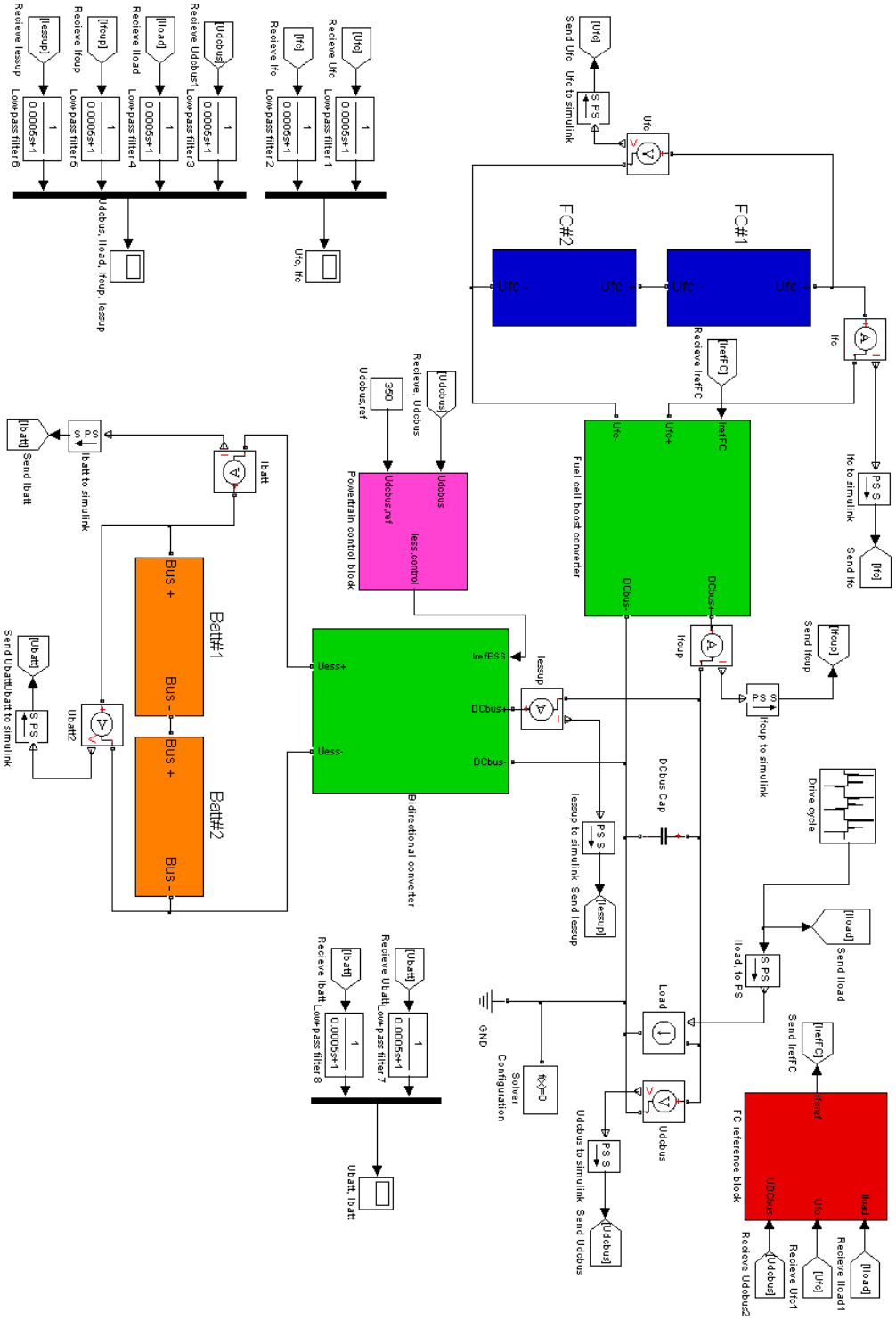

APPENDIX 3: THREE-WAY HYBRID FUEL CELL POWERTRAIN MODEL